

الجمهورية الجزائرية الديمقراطية الشعبية

People's Democratic Republic of Algeria

وزارة التعليم العالي والبحث العلمي

Ministry of Higher Education and Scientific Research

University Mohamed Khider – Biskra

Faculty of Sciences & Technology

Department : Civil Engineering &

Hydraulique

Ref :



جامعة محمد خيضر بسكرة
كلية العلوم و التكنولوجيا
قسم: الهندسة المدنية و الري
المرجع :

Thesis presented with a view to obtaining
LMD Doctorate in: Civil Engineering

Specialty (Option): Numerical Modelling in Civil Engineering

**3D Numerical Analysis of the Interaction of Back-to-Back
Reinforced Soil Walls**

**Analyse Numérique Tridimensionnelle de l'Interaction des Murs de
Soutènement à Parements Opposés en sols Renforcés**

Presented by:

BROUTHEN Abdelaziz

Publicly defended on: June 30th, 2022

Before the jury composed of:

Prof. BLOUNAR Lamine	Professor	Chair	University of Biskra
Prof. HOUHOU Mohamed Nabil	Professor	Supervisor	University of Biskra
Dr. Ivan Puig DAMIANS	Associate Professor & Researcher	Co-supervisor	Universitat Politècnica de Catalunya (UPC- BarcelonaTech)
Prof. BENMEBAREK Sadok	Professor	Examiner	University of Biskra
Prof. ABBECHE Khelifa	Professor	Examiner	University of Batna 2

ACKNOWLEDGMENTS

I would like to express my gratitude first and foremost to ALLAH the Almighty.

I'm specially and sincerely grateful to my Supervisor and Co-supervisor: Prof. HOUHOU Mohamed Nabil & Dr. Ivan Puig DAMIANS.

Prof. HOUHOU Mohamed Nabil, I would like to thank him for having given me his full confidence in carrying out this research work.

Dr. Ivan Puig DAMIANS, I'll never forget his support and kindness. He taught me many things in the field of numerical modelling. Many directions and advice in my research field. He has my deepest thanks.

I would also like to thank Prof. BELOUNAR Lamine of the University of Biskra for having done me a great honour by accepting to chair the jury of my thesis.

I also thank Prof. BENMEBAREK Sadok (University of Biskra), Prof. ABBACHE Khelifa (University of Batna 2), First and foremost for the time and attention they showed in my research by agreeing to evaluate it.

I would like to grateful the support provided by the Algerian Ministry of Education and Scientific Research (Exceptional National Program). Furthermore, I would like to thank the Department of Civil and Enviromental Engineering-Universitat Politècnica de catalunya (UPC-BarcelonaTech) welcoming me during my internship.

Finally, I would like to thank my dear mother who has been a great support for me during all these years of preparation of my thesis, also my father, my brothers and sisters.

To all members of MN2I2S Laboratory.

ABSTRACT

Back-to-back Reinforced Soil Walls are among complex geometry structures and are commonly used in ramp ways, rock fall protection systems, earth dams, levees, noise barriers and especially for bridge abutment approach. However, available design guidelines for this type of walls system are limited. Advanced computational models based on finite element and/or finite difference methods allow researchers to gain a better knowledge of these systems and anticipate the opposite side walls performance under operational conditions.

Firstly, a Two-dimensional (2D) modelling by the finite element (FE) code PLAXIS of the quantitative influence of problem geometry, strip pre-tensioning, strip type, and surcharging on horizontal displacements, development of soil shear and plastic zones, lateral earth pressure, and maximum reinforcement loads compared with the analytical international codes (i.e., NF, AASHTO Simplified Method and AASHTO Simplified Stiffness Method). The numerical results demonstrate how this type of reinforced soil walls perform jointly at a certain distance of interaction between the two opposite walls. The walls of the two opposing sides clearly interact with each other when they are close enough and with an overlapping reinforcement layout. Pre-tensioning load can contribute to achieving vertical wall-facing alignment at the end of construction. Using perforated/holed strips, the tensile loads at the end of construction were reduced by about 30% due to the improved polymeric–soil interface strength and stiffness.

Secondly, a Three-dimensional (3D) modelling by code PLAXIS to investigate the behaviour of back-to-back reinforced soil walls in case connected to bridge abutment at end of construction and under bridge load application, by comparing the predicted results of the 3D-FE analysis in terms of wall displacement, Lateral earth pressure, reinforcement loads and potential failure surface with those predicted using the 2D-FE analysis. The 3D results indicated that the farther away from the abutment wall (i.e., the corner), the nearest the 2D results at end of construction and under bridge load application. The 3D results at near the corner are more conservative than 2D under bridge load application due to the dead loads (i.e., bridge seat & bridge deck load) which is not taken into account in 2D simulations.

Keywords: Back-to-back walls; Numerical modelling; Geosynthetics; Reinforced soil; Two-dimensional; Three-dimensional.

ملخص

تعد جدران التربة المقواة المتتالية من بين الهياكل الهندسية المعقدة وتستخدم بشكل شائع في طرق المنحدرات وأنظمة الحماية من سقوط الصخور والسدود الترايبية والسدود وحواجز الضوضاء وخاصة لدعامة الجسر. ومع ذلك ، فإن إرشادات التصميم المتاحة لهذا النوع من أنظمة الجدران محدودة. تسمح النماذج الحسابية المتقدمة القائمة على العناصر المحدودة و / أو طرق الفروق المحدودة للباحثين باكتساب معرفة أفضل بهذه الأنظمة وتوقع أداء الجدران الجانبية المتعكسة في ظل ظروف التشغيل.

أولاً ، نمذجة ثنائية الأبعاد (2D) بواسطة رمز العنصر المحدود PLAXIS للتأثير الكمي للمشكل الهندسي ، والشد المسبق ، ونوع الشريط ، والشحن الإضافي على عمليات الإزاحة الأفقية ، وتطوير قص التربة والمناطق البلاستيكية ، وضغوط التربة الأفقية وأحمال التعزيز القصوى مقارنة مع الأكواد التحليلية الدولية (مثل المعايير الفرنسية NF و الكود الأمريكي AASHTO ذو الطريقة المبسطة و AASHTO ذو طريقة الصلابة المبسطة). توضح النتائج العددية كيف يعمل هذا النوع من جدران التربة المقواة بشكل مشترك على مسافة معينة من التفاعل بين الجدارين المتقابلين. تتفاعل الجدران الجانبية المتعارضة بشكل واضح مع بعضهما البعض عندما تكون قريبة بدرجة كافية وبتخطيط تقوية متداخل. يمكن أن يساهم حمل الشد المسبق في تحقيق المحاذاة الرأسية المواجهة للجدار في نهاية البناء. باستخدام الشرائط المتقبة / المتقوبة ، تم تقليل أحمال الشد في نهاية البناء بحوالي 30٪ بسبب تحسن قوة وصلابة البوليمر-التربة.

ثانياً ، نمذجة ثلاثية الأبعاد (3D) بواسطة الكود PLAXIS للتحقيق في سلوك جدران التربة المقواة المتتالية في حالة توصيلها بدعامة الجسر في نهاية البناء وتحت تطبيق تحميل الجسر ، من خلال مقارنة النتائج المتوقعة ل 3D عن طريق إزاحة الجدار وضغط الأرض الجانبي وأحمال التعزيز و سطح الانهيار المحتمل مع تلك المتوقعة باستخدام تحليل 2D. أشارت النتائج ثلاثية الأبعاد إلى أنه كلما كان بعيداً عن جدار الدعامة (أي الركن) ، كانت أقرب إلى النتائج ثنائية الأبعاد في نهاية البناء و تحت تطبيق تحميل الجسر . النتائج ثلاثية الأبعاد بالقرب من الزاوية أكثر تحفظاً من 2D تحت تطبيق تحميل الجسر و هذا نظراً لتأثير الأحمال الميئة (مثل حمل مقعد الجسر وحمل سطح الجسر) والتي لا تؤخذ في الاعتبار في عمليات المحاكاة ثنائية الأبعاد.

الكلمات المفتاحية: الجدران المتتالية المتعكسة ، نمذجة العددية ، الجيوسانتيك ، تعزيز التربة ، ثنائي الأبعاد ، ثلاثي الأبعاد.

TABEL OF CONTENT

FIGURES LISTE	
TABLES LISTE	

INTRODUCTION	1
---------------------	----------

PART I: Literature Review

CHAPTER ONE: Generalities about the Reinforced Soil Walls

1.1. General	5
1.2. Reinforced soil concept	6
1.3. Reinforced earth structure elements	7
1.4. Implementation of reinforced earth walls	9
1.5. Dimensioning of the reinforced earth walls	11
1.5.1. Structure dimensions	11
1.5.1.1. French Norm (NF 94-270: 2009)	11
1.5.1.2. British standard (BS 8006-1: 2010)	14
1.5.1.3. LRFD Bridge Design Specifications (AASHTO 2020)	18
1.5.2. External stability	19
1.5.2.1. Lateral earth pressure	19
1.5.2.2. Bearing capacity	24
1.5.3. Internal stability (Maximum reinforcement loads T_{max})	25
1.5.3.1. Coherent gravity method	25
1.5.3.2. Stiffness method	27

CHAPTER TWO: Back-to-Back Reinforced Soil Walls

2.1. Definition	32
2.2. Studies on Back-to-Back Walls	33
2.2.1. Analytical studies	34
2.2.1.1. Elias and Christopher (1997)	34
2.2.1.2. Berg et al (2009)	35
2.2.2. Numerical studies	36
2.2.2.1. Han and Leshchinsky (2010)	36
2.2.2.2. El-Sherbiny et al. (2013)	37
2.2.2.3. Benmebarek et al. (2016)	37
2.2.2.4. Djabri and Benmebarek (2016)	38

2.2.2.5. Sarvanam et al. (2016)	39
2.2.2.6. Benmebarek and Djabri (2017)	40
2.2.2.7. Sarvanam et al. (2019)	41
2.2.2.8. Sarvanam et al. (2020a)	42
2.2.2.9. Sarvanam et al. (2020b)	42
2.2.2.10. Yang et al. (2020a)	43
2.2.2.11. Rajagopal and Thiyyakkandi (2021)	44
2.2.2.12. Xu et al (2021)	45
2.2.3. Experimental studies	45
2.2.3.1. Won and Kim (2007)	45
2.2.3.2. Yang et al. (2020b)	46

PART II: Numerical Analysis

CHAPTER THREE: 2D Finite Element Analysis

3.1. Introduction	48
3.2. Finite Element modelling	49
3.2.1. General	49
3.2.2. Soil and road pavement	49
3.2.3. Facing: Precast Panels and Bearing Pads	50
3.2.4. Reinforcements	51
3.2.5. Interface Properties and Boundary Conditions	51
3.3. Numerical modelling verification	53
3.4. Numerical Results and Discussion	56
3.4.1. General	56
3.4.2. Effect of the Interaction Distance (D_i) between Back-to-Back Walls	56
3.4.3. Effect of the pre-tensioning (T_i)	69
3.4.4. Effect of the soil-polymeric interaction (R_i)	72
3.5. Conclusions	74

CHAPTER FOUR: 3D Finite Element Analysis

4.1. Introduction	77
4.2. FE Numerical Modelling	77
4.3. Verification on FE model	79
4.3. Results of Analyses	82
4.3.1. General	82
4.3.2. Wall displacement	82
4.3.3. Lateral earth pressure	83
4.3.4. Reinforcement loads	85

4.3.5. Potential failure surface	89
4.4. Conclusions	89

CONCLUSIONS	91
--------------------	----

REFERENCES	93
-------------------	----

FIGURES LISTE

Figure 1.1. Type of reinforced soil walls and abutments (source: BS 8006-1 2010)	6
Figure 1.2. State of stress in reinforced soil (McKittrick 1978)	7
Figure 1.3. General elements of a reinforced earth structure	9
Figure 1.4. Schematic diagram of a reinforced earth wall	9
Figure 1.5. Installation and pose the concrete panels (Soletanche Freyssinet ©)	10
Figure 1.6. Installation of the reinforcements (Soletanche Freyssinet ©)	10
Figure 1.7. Backfilling and compacting (Soletanche Freyssinet ©)	11
Figure 1.8. Definition of mechanical height	12
Figure 1.9. Common proportions of a vertical or sloping reinforced structure	12
Figure 1.10. Recommended minimum dimensions and length changes for vertical or sloping reinforced structures with strip or grid reinforcements	13
Figure 1.11. The length and spacing of the lower layers may be important for the stability of the mix	13
Figure 1.12. Definition of the embedment according to NF 94-270: 2009	14
Figure 1.13. Initial sizing of reinforced earth structures	15
Figure 1.14. Sizing of reinforced earth wall with various geometries	16
Figure 1.15. The embedment, D_m according to BS 8006-1: 2010	17
Figure 1.16. Coulomb earth pressure distribution for reinforced earth wall	20
Figure 1.17. Rankine earth pressure distribution for reinforced earth wall	22
Figure 1.18. Calculation of the earth thrust behind the reinforced earth wall	23
Figure 1.19. Pressure distribution along the base of the reinforced soil wall	24
Figure 1.20. Variation of coefficient of earth pressure with depth – Coherent gravity method	26
Figure 1.21. Illustration of D_{\max} factor	28
Figure 1.22. Comparison of AASHTO simplified and stiffness method equation (Allen and Bathurst 2015)	31
Figure 2.1. Back-to-back walls (French Ministry of Transport, 1979)	32
Figure 2.2. T-Rex Rapid Transit, Denver, CO $H = 14.0$ m, $W = 10.1$ m, $L = 9.8$ m, $W/H = 0.72$ and $L/H = 0.7$ (Anderson et al 2018)	32
Figure 2.3. Manhan Rail Trail over SR 10, Easthampton, MA $H = 9.77$ m, $W = 5.48$ m, $L = 4.88$ m overlapping $W/H = 0.56$, $L/H = 0.50$ (Anderson et al 2018)	33
Figure 2.4. Structures subject to low thrust (French Ministry of Transport, 1979)	33
Figure 2.5. Definition of back-to-back wall: (a) case 1 and (b) case 2 (Elias and Christopher 1997)	34
Figure 2.6. Definition of back-to-back wall: (a) case 1 and (b) case 2 (Berg et al., 2009)	35
Figure 2.7. Basic model for the case $W/H = 2$ (Han and Leshchinsky 2010)	36

Figure 2.8. Dimensions and parameters of the models studied (Benmebarek et al., 2016)	38
Figure 2.9. Dimensions of back-to-back GRS wall base case $W/H = 2$ (Djabri and Benmebarek 2016).	39
Figure 2.10. Modelling scheme of back-to-back MSE wall (Sarvanam et al., 2016)	39
Figure 2.11. The geometry of baseline case $L_R = 0.3H$ (Benmebarek and Djabri 2017)	40
Figure 2.12. FLAC model of back-to-back wall with mesh and surcharge application (Sarvanam et al., 2019)	41
Figure 2.13. FLAC model of back-to-back wall with mesh: (a) connected (b) unconnected walls (Sarvanam et al., 2020a)	42
Figure 2.14. Illustration showing: (a) A full-length panel facing MSE single wall representing the lateral deformation (b) unconnected walls (Sarvanam et al., 2020b)	43
Figure.2.15. Plaxis model of back-to-back geogrid reinforced soil walls (Yang et al., 2020a)	44
Figure 2.16. Proposed hybrid back-to-back wall (Rajagopal and Thiyyakkandi 2021)	44
Figure 2.17. Back-to-back MSE wall model schematic diagram (Xu et al., 2021)	45
Figure 2.18. The geosynthetic reinforced soil (GRS) walls of Won and Kim 2007	46
Figure 2.19. Back-to-back GRS walls near Rongcheng station (Yang et al., 2020b)	46
Figure 3.1. On-site polymeric strip installation examples: (a) back-to-back wall case, (b) longitudinal bar back anchorage and pegs, and (c) trench and triangle anchorage. (Photographs courtesy of VSL Construction Systems—VSoL® Retained Earth System)	48
Figure 3.2. Detail of the FEM model and mesh for the base case with $D_i = 0.6H$. Note: foundation soil zone has dimensions of 50 m wide and 10 m deep	49
Figure 3.3. Polymeric strip products from GECCO : (a) FASTEN FS and (b) FW (perforated), and (c) typical load-extension behaviour of grade 30 strip	51
Figure 3.4. Real and Schematic of instrumented MSE wall used for validation. (Jayakrishnan 2013)	54
Figure 3.5. Detail of the FEM model and mesh of experimental wall used for calibration	55
Figure 3.6. Comparison between the FE model results and the experimental data (Jayakrishnan 2013) : (a) maximum reinforcement axial force per strip, and (b) distribution of axial force along reinforcement strip	56
Figure 3.7. Facing displacements at the end of construction (EoC) for different interaction distances (D_i) between the back of the reinforced soil zone for opposite walls: (a) $D_i > 0$ and $D_i = 0$, and (b) $D_i < 0$	57
Figure 3.8. Shear strain contours at end of construction (EoC) for walls with different interaction distance (D_i) between the back of the reinforced soil zones for opposite walls. Note: results ranging from 0 to 1%	60

Figure 3.9. Shear strain contours at failure with ϕ - c reduction at end of construction (EoC) for walls with different interaction distance (D_i) between the back of the reinforced soil zones for opposite walls. Note: results ranging from 0 to 1%	61
Figure 3.10. Plastic zones (Mohr–Coulomb points) in the soil at the end of construction (EoC) for walls with different interaction distances. (D_i) between the back of the reinforced soil zones for opposite walls. (Note: white zones on top of the models represent the location of tension cut-off points)	62
Figure 3.11. Plastic zones (Mohr–Coulomb points) in the soil at failure with the ϕ - c reduction method at end of construction (EoC) for walls with different interaction distance (D_i) between the back of the reinforced soil zones for opposite walls. (Note: white zones on top of the models represent the location of tension cut-off points)	63
Figure 3.12. Lateral earth pressure at the facing at the end of construction (EoC) for different interaction distances (D_i) between back-to-back reinforced soil walls: (a) $D_i > 0$, (b) $D_i = 0$, and (c,d) $D_i < 0$	64
Figure 3.13. Lateral earth pressure at 1 m from the back of the facing at the end of construction (EoC) for different interaction distances (D_i) between back-to-back reinforced soil walls: (a) $D_i > 0$, (b) $D_i = 0$, and (c,d) $D_i < 0$	65
Figure 3.14. Lateral earth pressure behind the reinforcements (i.e., at L-distance from facing) at the end of construction (EoC) for different interaction distances (D_i) between back-to-back reinforced soil walls: (a) $D_i > 0$ and (b) $D_i = 0$	65
Figure 3.15. Total earth pressure at the facing, at 1 m from the facing, and behind the reinforcements (i.e., at L-distance from the facing) at the end of construction (EoC) for different interaction distances (D_i) between back-to-back reinforced soil walls	66
Figure 3.16. Reinforcement loads at end of construction (EoC) for walls with different interaction distances (D_i) between the back of the reinforced soil zones for opposite walls: (a) $D_i > 0$ and $D_i = 0$, and (b) $D_i < 0$	68
Figure 3.17. Numerical maximum tensile load for walls with different interaction distances (D_i) between the back of the reinforced soil zones for opposite walls: (a) $D_i > 0$ and $D_i = 0$, and (b) $D_i < 0$, and both cases compared with maximum tensile loads computed using AASHTO ($\times 2$) and NF design codes.	69
Figure 3.18. Facing displacements for $D_i = 0.6H$ case at the end of construction (EoC) and different pre-tensioning scenarios	70
Figure 3.19. Shear strain contours and plastic (failure) zones in the soil at the end of construction for the $D_i = 0.6H$ case. Strip pre-tension loads: (a) $T_i = 0.5$ kN/strip and (b) 1 kN/strip. Note: results range from 0–1% for shear strain contours, and white zones on top of the models represent the location of tension cut-off points for soil plastic zones).	71
Figure 3.20. Horizontal earth pressure at the facing for the $D_i = 0.6H$ case at the end of construction (EoC): (a) no tension case and (b) different pre-tensioning loads	71

Figure 3.21. Reinforcement loads for $D_i = 0.6H$ case at the end of construction (EoC) and different pre-tensioning loads	72
Figure 3.22. Facing displacements computed at the end of construction (EoC) using different polymeric–soil interface strengths and stiffness (R_i -factor) for the $D_i = 0.6H$ case with no pre-tensioning	73
Figure 3.23. Plastic zones (Mohr-Coulomb points) at end of construction for $D_i = 0.6H$ case with no pre-tensioning and polymeric–soil interface factor assumptions: (a) $R_i = 0.93$ (constant), and (b) $R_i =$ from 1.19 to 1.77 (variable). (Note: white zones on top of the models represent tension cut-off points location)	73
Figure 3.24. Horizontal earth pressure at the facing for the $D_i = 0.6H$ case at the end of construction (EoC) using different polymeric–soil interface strengths and stiffness (R_i -factor) for the $D_i = 0.6H$ case with no pre-tensioning	74
Figure 3.25. Reinforcement loads at end of construction (EoC) using different polymeric–soil interface strengths and stiffness (R_i -factor) for the $D_i = 0.6H$ case with no pre-tensioning	75
Figure 4.1. FE mesh of back-to-back MSE walls connected bridge abutment baseline case ($D_i = 0.6H$): 3D-FE mesh at EoC (a), Details of the reinforcements arrangement (b) and 3D-FE mesh under surface loading (c)	79
Figure 4.2. Numerical model geometry for 3D FE model simulations: 3D-FE mesh (a), Details of the reinforcements arrangement in 3D-FE model	80
Figure 4.3. Comparison of experimental data and numerical results of distribution of axial force along reinforcement strips	81
Figure 4.4. Comparison of experimental data and numerical results of maximum reinforcement axial force per strip	82
Figure 4.5. Lateral facing displacement comparison of 2D and 3D-FE analysis at EoC (a) and under service loading (b)	83
Figure 4.6. Lateral earth pressure at the facing (a), at 1 m from the facing (b), and behind the reinforcements (c) at the end of construction (EoC) by 2D & 3D simulation	84
Figure 4.7. Lateral earth pressure at the facing (a), at 1 m from the facing (b), and behind the reinforcements (c) under bridge loads application (EoC) by 2D & 3D simulation	85
Figure 4.8. Tensile reinforcement loads in selected reinforcement layers of 2D and 3D analysis at EoC	86
Figure 4.9. Tensile reinforcement loads in selected reinforcement layers of 2D and 3D analysis under bridge loading	87
Figure 4.10. Maximum reinforcement loads at end of construction (a) and under bridge loading (b) by 2D and 3D analysis comparison with maximum tensile loads computed using AASHTO Simplified and Stiffness Method, and NF design codes	88
Figure 4.11. Potential failure surface at end of construction (EoC) and under bridge loading by 3D analysis (a) and 2D analysis (b)	89

TABLES LISTE

Table 1.1. Recommended maximum vertical spacing of reinforcements for conventional reinforced earth structures made of class fill 1 or 2	13
Table 1.2. Ratio D_m / q_{ref} as a function of the slope β_p of the downstream land	14
Table 1.3. Calculated of the minimum embedment as a function of the mechanical height H in metres and the factored bearing pressure q_r in kN/m^2	17
Table 1.4. Minimum embedment depth	19
Table 1.5. Distribution of active pressures for different backfill	21
Table 3.1. Model properties for backfill, foundation soil, and pavement materials	50
Table 3.2. Precast concrete panel and bearing pad (joint) properties	51
Table 3.3. Interface material properties	53
Table 3.4. Soil properties (taken from Jayakrishnan 2013)	55

INTRODUCTION

i. Problematic

Among the recent methods of soil improvement is the technique of reinforcement with geosynthetics. This technique has been developed in many geotechnical structures, including flexible retaining walls.

Currently, back-to-back reinforced soil walls are frequently used in earth dams, dykes, railway constructions and especially bridge approaches.

The increasing use of this type of retaining technique is due to a number of factors, namely economy, aesthetics, simple and rapid construction techniques. As a result, it performs well in comparison to rigid walls.

These types of structures are often calculated by classical methods, based on the limit equilibrium of the soil, or methods using the Winkler hypothesis (reaction modulus method). However, available design guidelines for this wall system are limited. The distance between two opposing walls is a key parameter used for determining the analysis methods in FHWA guideline (Berg et al. 2009): Two extreme cases are identified: (1) reinforcements from both sides meet in the middle or overlap, and (2) the walls are far apart, independent of each other.

For this type of problem, the classical methods used in all the standards and technical guides have difficulties in analysing complex geometries. In addition, the interactions of back-to-back reinforced soil walls, especially those caused by reinforcement layers, can only be taken into account in a very approximate way. In another hand, an investigation that consider 3D effects are needed to better understand the static response of back-to-back walls in case integrated to bridge abutments.

Faced with the limitations of these methods, it is necessary to invest in numerical calculation methods (finite element methods). However, these approaches need to be calibrated by tests on a reduced model or in-situ.

ii. Objective

In structures with complex geometries such as bridge approach structures, it is always difficult to separate the internal from the external stability, as the critical failure surface can pass through both reinforced and unreinforced sections of the structure. For this reason, a global stability analysis is generally required for this type of structure, and only the numerical approach that would allow an accurate estimation of the global safety factor.

Previous studies show that this type of retaining structure is a delicate soil-structure interaction problem that involves the complex construction phasing, the stiffness of the reinforcing elements, the soil-structure interface, the mechanical behaviour of soils and the three-dimensional effects of the structure.

In this context, the present research theme focuses on the numerical study of the interaction of back-to-back reinforced soil retaining walls.

In recent years, the stability analysis of back-to-back reinforced soil walls has been studied by various researchers (Han and Leshchinsky 2010; Benmebarek et al. 2016, Benmebarek and Djabri 2017; Sarvanam et al. 2020a...etc.), some of them focused on the distance factor, which is a key factor in monitoring the behaviour of this type of structure, but it still needs more in-depth study because of its many probabilities. All previous studies used numerical methods in plane strain, but the experimentation shows that this type of structure has a particularly marked three-dimensional character when they are near to the abutment wall (Zheng et al 2022).

The objective of this research work is to contribute to the numerical analysis, using PLAXIS 2D & 3D software, of the influence of the geometry of the structure (the interaction distance between opposite sides walls, length of the primary faces in relation to the secondary face), the length of the reinforcement layers (possibility of the overlapping), the rigidity characterising the flexibility of the reinforcements, the soil-reinforcement interaction.

This analysis aims to evaluate the behaviour of the structure in terms of: horizontal displacements of the facings, development of reinforcement tensile loads, lateral earth pressures, critical failure surface. As well as highlighting the three-dimensional effects of the structure.

iii. Outline

The outline for this dissertation is as following:

PART I: Literature Review

CHAPTER ONE: Generalities about the Reinforced Soil Walls

Presents the literature review about reinforced soil earth walls generalities and its sizing according to the French norm (NF 94-270), British standard (BS 8006-1) and Load Resistance Factor Design (LRFD) Bridge Design Specifications (AASHTO).

CHAPTER TWO: Back-to-Back Reinforced soil Walls

Presents the definition of the back-to-back reinforced soil walls and the previous works on this type of structures (i.e., analytical, numerical and experimental).

PART II: Numerical Analysis

CHAPTER THREE: 2D Finite Element Analysis

Presents the 2D Finite Element (FE) Analysis of the effect of the interaction distance, the polymeric strips pre-tensioning, and the soil–polymeric interaction on the performance of back-to-back reinforced soil walls.

CHAPTER FOUR: 3D Finite Element Analysis

Presents the 3D Finite Element Analysis of the back-to-back reinforced soil walls connected bridge abutment and showdown with 2D.

We complete the thesis with a conclusion summarising all the results thus obtained.

iv. Scientific production obtained from the study

The journal papers published and conference papers presented over the course of (and related to) the Thesis study are listed below:

Journal paper (s):

a) Brouthen, A., Houhou, M.N., Damians, I.P., 2022. Numerical Study of the Influence of the Interaction Distance, the Polymeric Strips Pre-Tensioning, and the Soil–Polymeric Interaction on the Performance of Back-to-Back Reinforced Soil Walls. *Infrastructures* 7(2), 22.

Conference paper (s):

a) Brouthen A., Houhou, M.N., 2018. FEM to investigate of the reinforcement lengths effect on the performance of Geosynthetic-Reinforced Soil Walls. *Proceedings of the International Seminar in Civil Engineering (SIGC 2018)*, Oran, Algeria.

b) Brouthen, A., Houhou, M.N., 2018. Effect the embankment friction angle on the behavior of Gesynthetic-Reinforced Soil Walls. *Workshop on geotechnics between the state of the art and practice*, Biskra, Algeria.

c) Brouthen, A., Damians, I.P., Houhou, M.N., 2019. FEM and analytical methods to investigate the influence of facing batter angle on the performance of back-to-back mechanically stabilized segmental earth walls. *Proceedings of the The 1st International Congress on Advances in Geotechnical Engineering and Construction Management (ICAGECM'19)*, Skikda, Algeria.

d) Brouthen, A., Damians, I.P., Bathurst, R.J., Houhou, M.N., 2022. FE analysis of the effect of soil-reinforcement interaction and reinforcement pre-tensioning on the behaviour of back-to-back polymeric strip reinforced soil walls. *Proceedings of the 7th European Geosynthetics Conference (EuroGeo7)*, Warsaw, Poland.

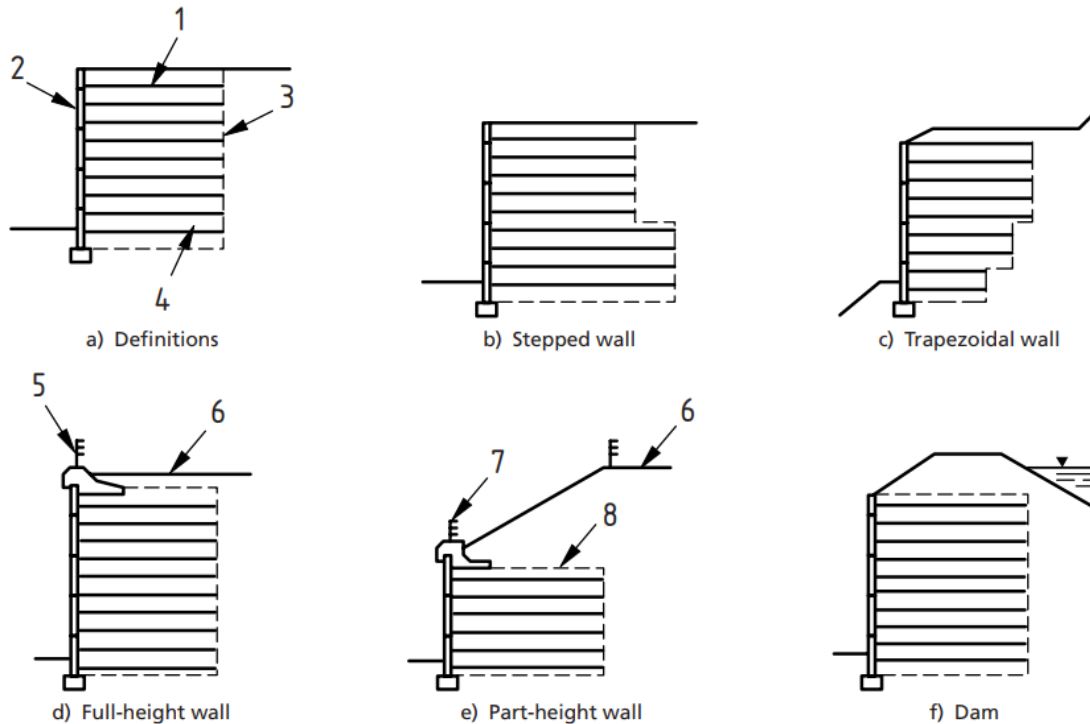
PART I
Literature Review

CHAPTER ONE

Generalities about the Reinforced Soil Walls

1.1. General

Soil masses are usually stabilized by either building a retaining structure, which is a structural process, or by adding reinforcing components to the soil. The latter process belongs to the field of geotechnics. However, certain technologies, such as reinforced soil massifs, exploit both of these areas at the same time. These are retaining structures made by strengthening the earth. One of the first types of works in this genre was the "Terre Armée". (Vidal 1966), an engineer and architect devised this building procedure from 1960 onwards, marking a watershed moment in the design of support and more broadly in soil reinforcement by allowing the earth to fully participate in the structure's stability. The structures built using the "Terre Armée" technique are essential of two types: earth retaining walls and load-bearing structures such as bridge abutments (see Figure 1.1). The reinforcements generally used in these two types of structures are metal strips. However, in aggressive environments, these metallic reinforcements are replaced by non-corrodible geosynthetics, which have higher extensibility.



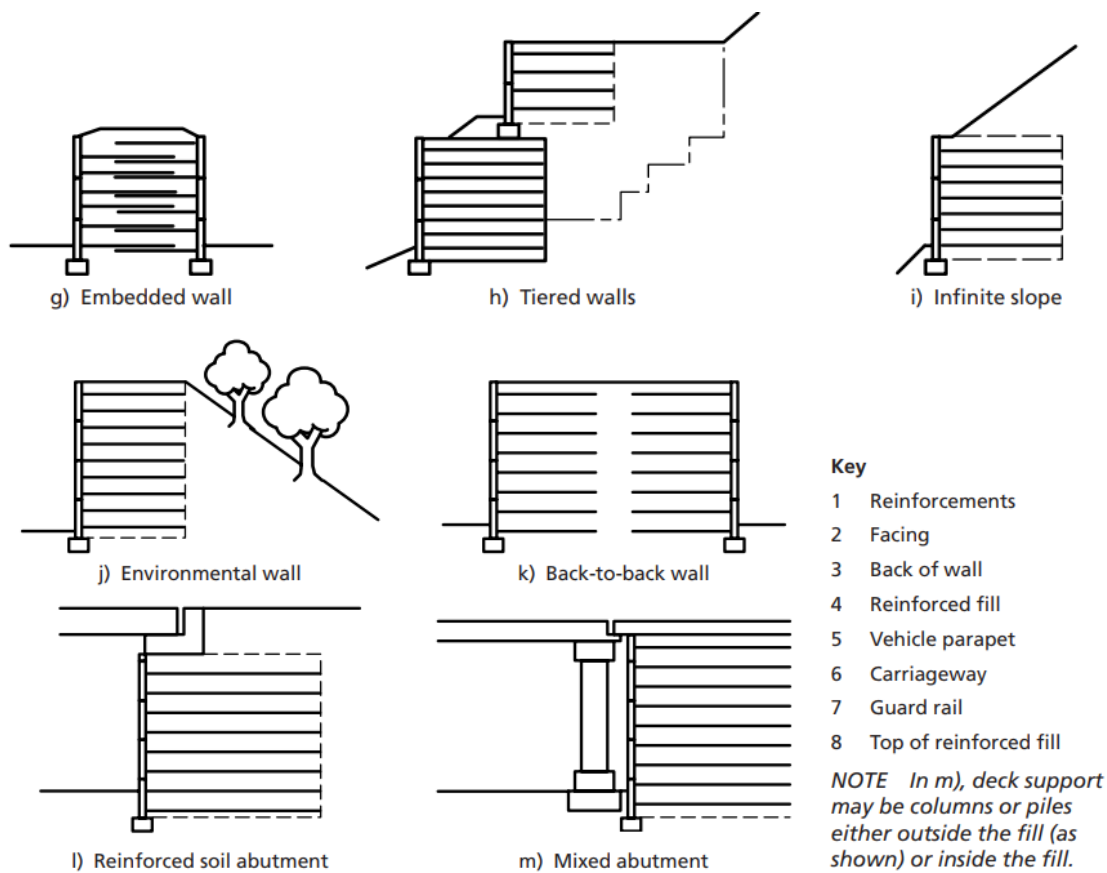


Figure 1.1. Type of reinforced soil walls and abutments (source: BS 8006-1 2010).

1.2. Reinforced soil concept

"The basic mechanics of Reinforced Earth were well understood by (Vidal 1966) and were detailed in-depth in his early books," writes (McKittrick 1978). Figure 1.2 depicts a simplified version of these fundamental principles. Axial stress on a sample of granular material causes lateral expansion in dense materials, as seen in Figure 1.2a. The lateral strain is more than one-half of the axial strain due to dilatation. However, if inextensible horizontal reinforcing elements are placed within the soil mass, as shown in Figure 1.2b, these reinforcements will prevent lateral strain due to friction between the reinforcing elements and the soil, and the behaviour will be the same as if the element had been subjected to a lateral restraining force or load. The equivalent lateral load on the soil element is equal to the earth pressure at rest ($K_o \sigma_v$), and this lateral stress acts on each element of the soil mass. As a result, the horizontal restraining stresses or lateral forces increase in exact proportion to the vertical stresses. The stress circle sits significantly below the rupture curve at all sites for any value of the angle of internal friction, ϕ , which is generally associated with granular soils. Only loss of friction between the soil and the reinforcements or tensile failure of the reinforcements can cause failure. This fundamental premise was investigated and found to

be true (Schlosser and Long 1969, Hausmann 1976 and others). Theoretical correlations were established between reinforcement spacing and tensile resistance, as well as an increase in "anisotropic pseudo cohesion" of reinforced materials.

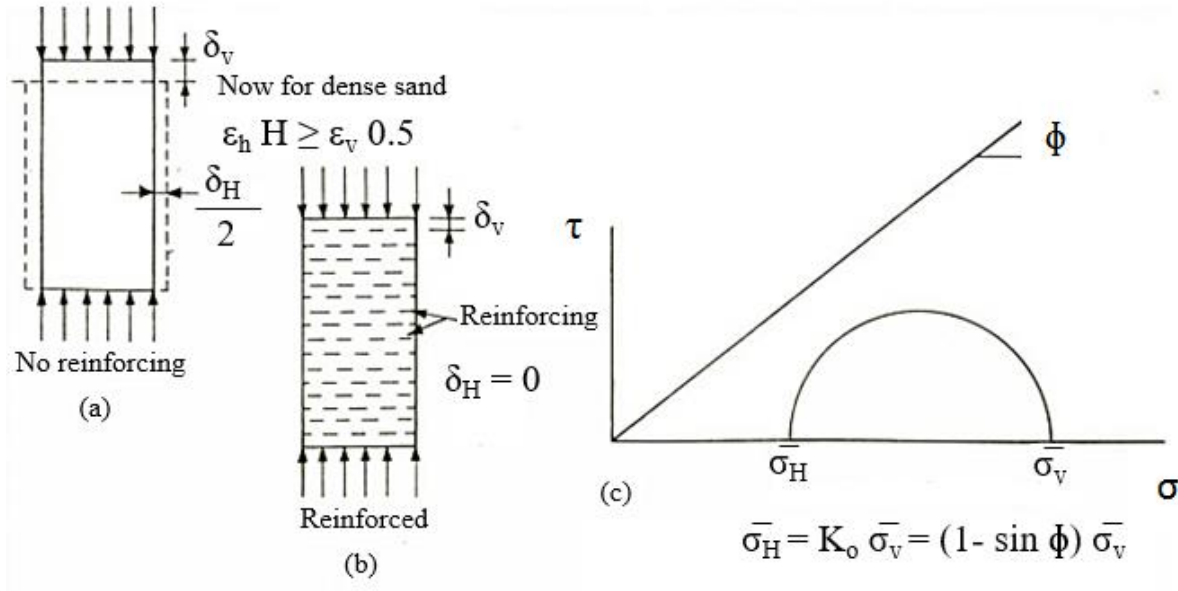


Figure 1.2. State of stress in reinforced soil (McKittrick 1978).

1.3. Reinforced earth structure elements

The main components of reinforced earth structures (see Figure 1.3) are listed below:

- **Panels:** are concrete square or cruciform of about 850 kg and 1.5m wide and high and have a minimum thickness of 140 mm. When they are put in place, they are nested one inside the other by a system of vertical dowels intended to facilitate assembly and ensure continuity of installation. The whole gives the facing vertical flexibility of the same order as that of the metal elements in the form of thin curved plates initially designed by Vidal 1966. The possibilities of rotation around the dowels make it possible to create curved walls with standard scales. The shape, texture and colour of the outer surface of the panels can be changed to give architectural looks different for each wall. In all panel joints, geotextiles sheets must be installed on the inward panel side to prevent erosion of the fill material in drainage.
- **Reinforcements:** are mainly linear elements (bars, strips, plates, meshes, grids, sheets, etc.), with little or no bending resistance, but providing sufficient friction through shear and pullout strength with soil interaction, with additional passive strength in the case of ribbed or gridded reinforcing shapes. Depending on the application, they can be made up of:

- **Metallic:** the deformation of metallic reinforcements at failure is much less than the deformation of the soil. They are characterised by a high modulus of rigidity (i.e., the maximum tensile strength is mobilised by a small deformation, about 2% to 3%).
 - **Geosynthetic:** the deformation of geosynthetics reinforcements at failure is comparable to or even greater than the deformation of the soil. They are characterised by their much lower stiffness compared to inextensible reinforcements. Namely, the maximum tensile strength is mobilised by a deformation greater than 4%.
- **Reinforced fill:** The backfill material can be either natural soil or material of industrial origin. It must not contain topsoil, putrescible material (which can rot) or domestic waste. All the recommendations (AASHTO, FHWA, NCMA, LCPC, SETRA, etc.) indicate purely granulometric criteria necessary to ensure adequate soil-reinforcement friction, satisfactory mechanical behaviour in the short and long term and sufficient drainage capacities. In the Load Resistance Factor Design (LRFD) Bridge Design Specifications (AASHTO 2014), soil gradation shall not be upgraded and must satisfy well-graded classification (in accordance with the Unified Soil Classification System in the American Society for Testing Materials - ASTM D2487 2011), which implies, for a sand soil (SW), required Coefficient of Uniformity ($C_u = D_{60}/D_{10}$) greater than 6 ($C_u > 6$), and a Coefficient of curvature (curve-shape parameter, defined by $C_c = (D_{30})^2/(D_{60} \times D_{10})$) from 1 to 3 ($1 < C_c < 3$). For gravel to be classified as well-graded (GW) the following criteria must be met: $C_u > 4$, and $1 < C_c < 3$. AASHTO (2014) do not recommend using an angle of internal friction of more than 40° .

Other components (aside from the geotextile joint sheets already described) may be less crucial in terms of final structural stability, but it is just as important for correct structure assembly and behavior under working stress-operational situations. These are listed as follows:

- **Bearing pads:** are compressible pieces that are put at all horizontal facing panel joints to guarantee facing flexibility while avoiding differential settlements between the backfill and the facing. Bearing pads may have enough compression strength to withstand the vertical stresses originating from the facing and avoid concrete-concrete contact, despite being plainly softer than the concrete panels. Bearing pads are often made of polymeric materials with adequate hardness and strength (rubber, neoprene, polyethylene, etc.)
- **Leveling pad:** It is an unreinforced concrete footing. The geometry of the leveling pad is about 15 cm in depth and 30 cm in width. The sole mission of the leveling pad

is to obtain a flat and smooth surface, which facilitates the support and the assembly of the first row of panels. Its implementation in the longitudinal, horizontal transverse directions must be extremely careful and good, it is the basis of a good subsequent assembly.

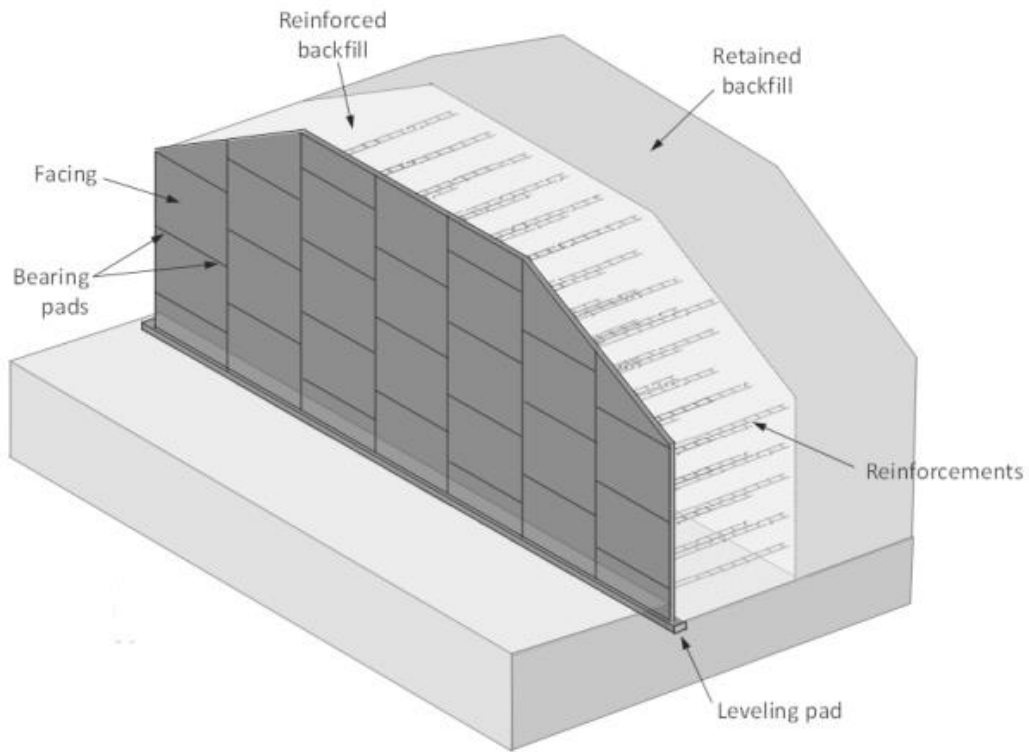


Figure 1.3. General elements of a reinforced earth structure.

1.4. Implementation of reinforced earth walls

The implementation of reinforced earth wall, similar to a classic backfill, is quick and easy (Figure 1.4).

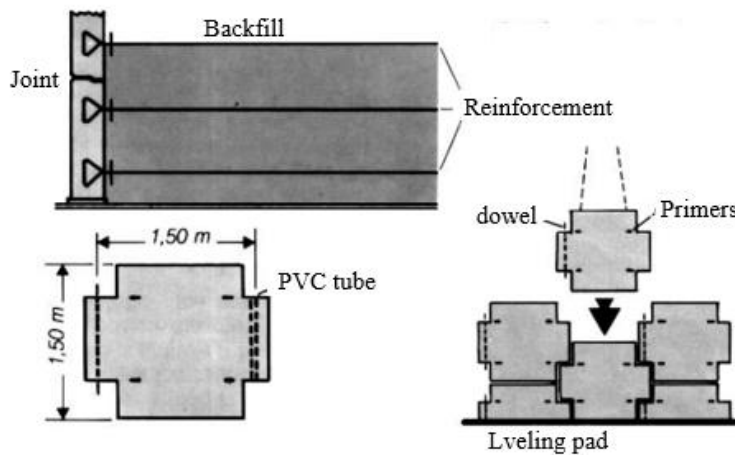


Figure 1.4. Schematic diagram of a reinforced earth wall.

There are 3 distinct stages in the construction of an reinforced earth wall:

➤ **Mounting the facing panels**

Once the first row of panels has been placed on a smooth and well-levelled concrete levelling pad to ensure the correct initial positioning, the rows of panels can be levelled to ensure correct initial positioning; the upper rows of panels are installed as the backfill progresses. In the case of concrete facing panels, elastomeric bearing pads are installed within the horizontal joints between the panels to provide the facing with flexibility and compressibility (Figure 1.5).



Figure 1.5. Installation and pose the concrete panels (Soletanche Freyssinet ©)

➤ **Installation of the reinforcement**

The reinforcement layers are spaced 70-80 cm apart, which is generally about two times the thickness of the backfill layers. They are placed on top of the compacted backfill layer and are connected to the facing panels by bolting in the case of steel reinforcement, or are threaded through sheaths embedded in the facing in the case of synthetic reinforcement (Figure 1.6).



Figure 1.6. Installation of the reinforcements (Soletanche Freyssinet ©)

➤ **Backfilling and compacting**

In addition to the typical earthmoving equipment required for backfill placement, a light crane is required to handle the panels, which weigh between 0.8 and 1.2 tonnes for normal 14 cm thick panels. Machinery should not be allowed to travel directly over the reinforcement and prohibit heavy machines from approaching the panels within 1.50 m (which could affect their verticality). At any point in the reinforced soil mass, the compaction rate must be more than or equal to 95 per cent of the Normal Proctor Optimum. Compaction should be identical to that of the appropriate road embankments in the case of road structures in particular (Figure 1.7). However, the backfill located within 1 m to 1.50 m of the facing will be compacted using a small vibrating roller. The rest of the installation continues with the same requirements as those indicated for the first row of panels.



Figure 1.7. Backfilling and compacting (Soletanche Freyssinet ©)

1.5. Dimensioning of the reinforced earth walls

1.5.1. Structure dimensions

1.5.1.1. French Norm (NF 94-270: 2009)

a) Cross-sectional profile geometry

The mechanical height h_m of the construction is frequently used to determine the proportions. The mechanical height, as shown in Figure 1.8, is a fictitious height that permits certain design criteria for structures without a head slope to be applied to structures with more complex geometry. It also establishes the reference level from which the reinforcement layer depths z are measured.

The transverse dimension of a vertical reinforced wall or sloping wall is often around $0.7 h_m$ (see Figure 1.9).

For vertical or sloping structures with strip or grid reinforcements, this objective is generally considered to be met when (Figure 1.10):

- ✓ The length of the reinforcements is greater than or equal to $0.4 h_m$ at the toe and 2.50 m at any level;
- ✓ Changes in length are less than $0.15 h_m$;
- ✓ No reinforcement end falls below line AB.

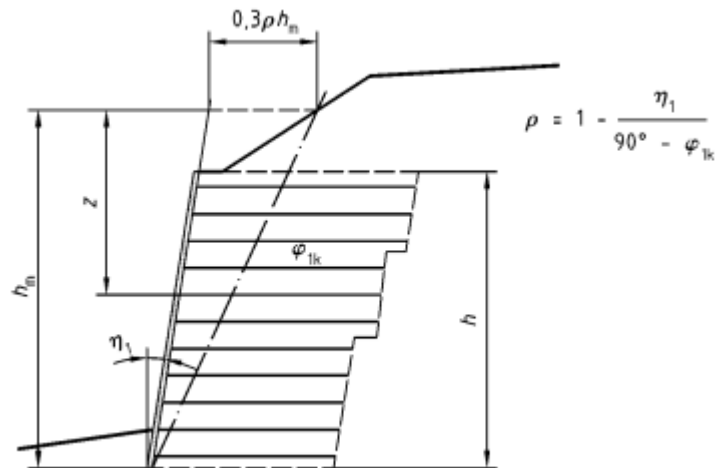


Figure 1.8. Definition of mechanical height (NF 94-270: 2009).

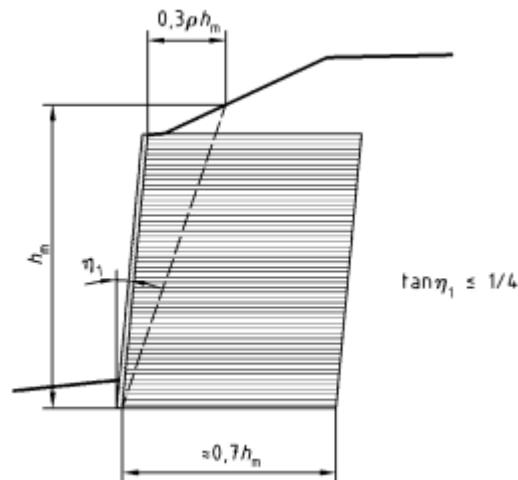


Figure 1.9. Common proportions of a vertical or sloping reinforced structure (NF 94-270: 2009).

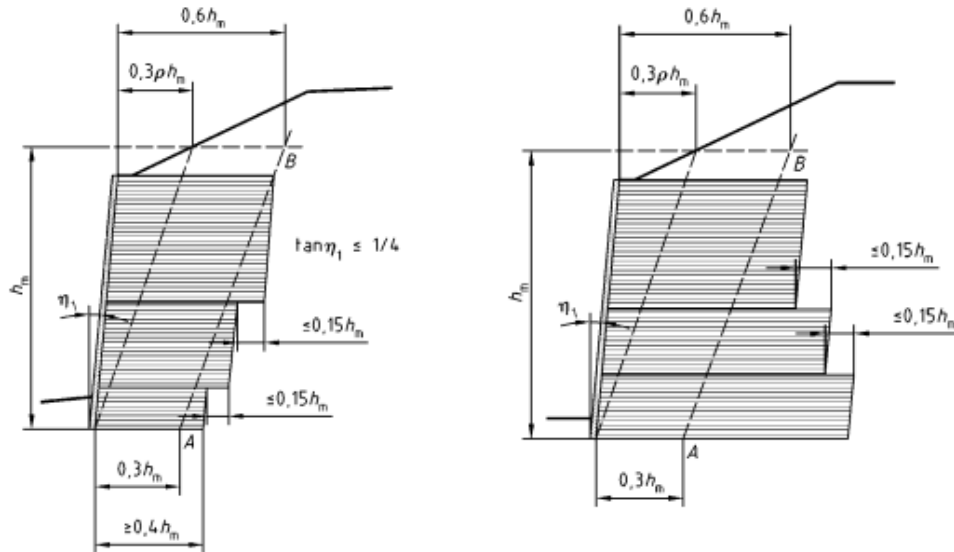


Figure 1.10. Recommended minimum dimensions and length changes for vertical or sloping reinforced structures with strip or grid reinforcements (NF 94-270: 2009).

The vertical spacing s_v is usually in the range of 0.20 m to 0.80 m (Figure 1.11).

As an indication, Table 1.1 gives, as a function of the ratio L_{inf} / h_m , the maximum relative spacing's s_v/h_m that are recommended for conventional reinforced earth structures made of class fill 1 or 2.

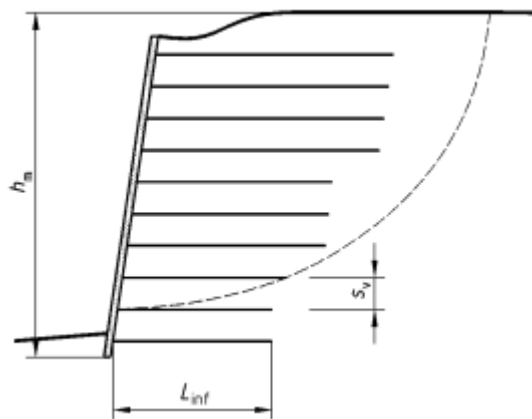


Figure 1.11. The length and spacing of the lower layers may be important for the stability of the mix (NF 94-270: 2009).

Table 1.1. Recommended maximum vertical spacing of reinforcements for conventional reinforced earth structures made of class fill 1 or 2 (taken from NF 94-270: 2009).

Relative length of reinforcements L_{inf} / h_m	Maximum relative vertical spacing s_v / h_m
$L_{inf} / h_m \leq 0.55$	$\leq 1/8$
$0.55 < L_{inf} / h_m \leq 0.65$	$\leq 1/6$
$0.65 < L_{inf} / h_m \leq 0.75$	$\leq 1/4, 5$
$0.75 < L_{inf} / h_m$	-

b) Embedment

A reinforced earth structure should have an embedment D (Figure 1.12) and its depth should be greater than the value D_m defined in Table 1.2 as a function of the reference bearing pressure q_{ref} , with a minimum value of 0.40 m.

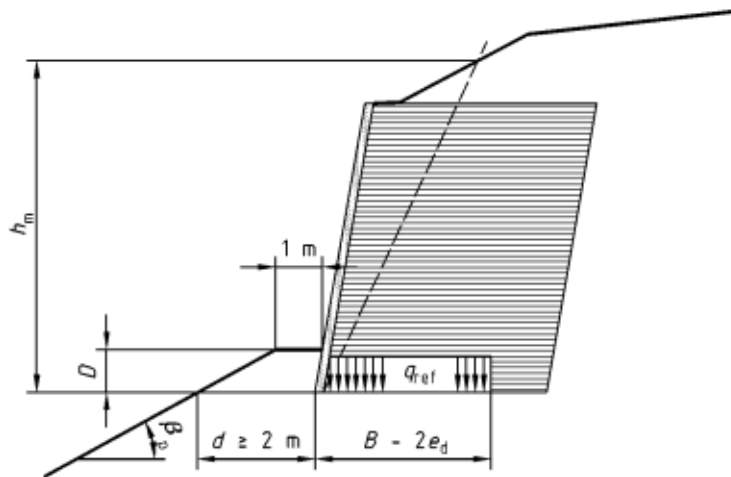


Figure 1.12. Definition of the embedment according to NF 94-270: 2009.

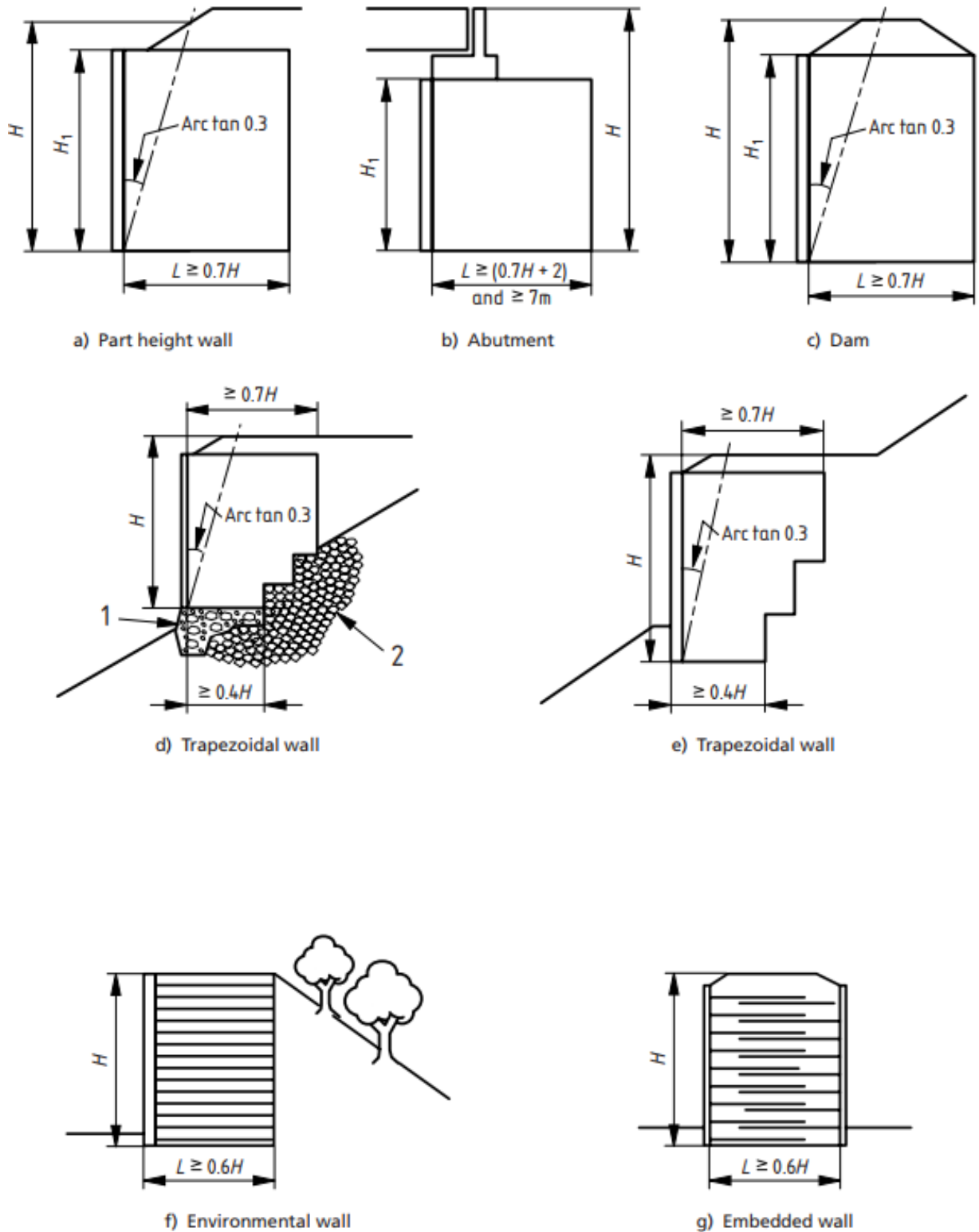
Table 1.2. Ratio D_m/q_{ref} as a function of the slope β_p of the downstream land (taken from NF 94-270: 2009)

slope β_p of the downstream land	D_m/q_{ref} (m/kPa)
0	1.5×10^{-3}
18° ($\tan \beta_p = 1/3$)	$3,0 \times 10^{-3}$
27° ($\tan \beta_p = 1/2$)	4.5×10^{-3}
34° ($\tan \beta_p = 2/3$)	6.5×10^{-3}

1.5.1.2. British standard (BS 8006-1: 2010)

a) Cross-sectional profile geometry

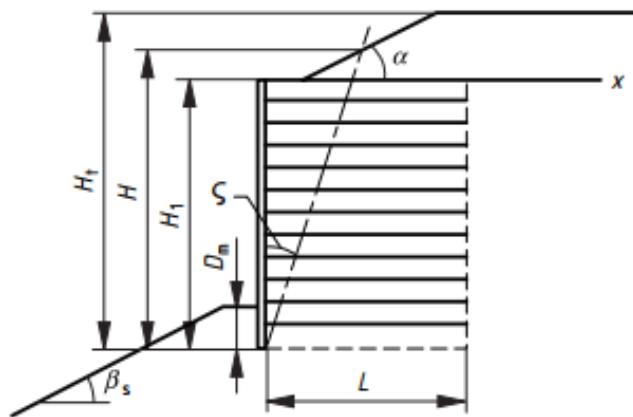
The mechanical height H of a structure is defined as the vertical distance from the structure's toe to the point where an arc tan 0.3 to the vertical outcrops the upper ground line above the wall. The initial size of the reinforced earth structures is shown in detail in Figures 1.13 and 1.14.



Key

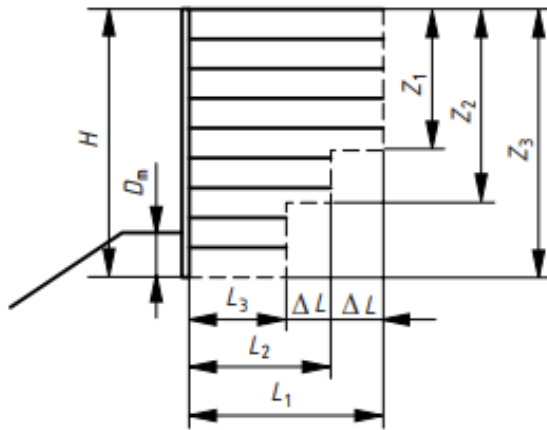
- 1 Concrete
- 2 Rock

Figure 1.13. Initial sizing of reinforced earth structures (BS 8006-1 2010).



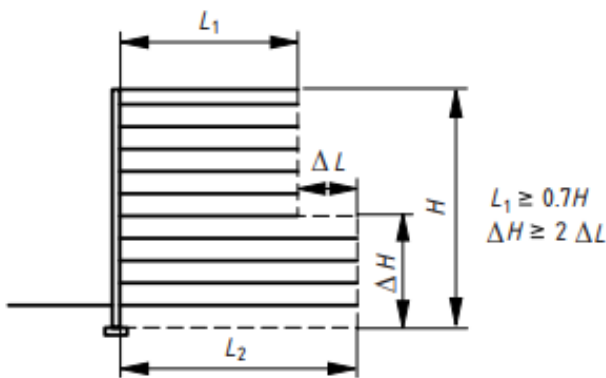
a) Rectangular cross section

H = Mechanical height
 H_1 = Facing height
 H_t = Total height
 ζ = Arc tan 0.3
 L = Reinforcement length
 D_m = Embedment depth
 $L \geq 0.7H$



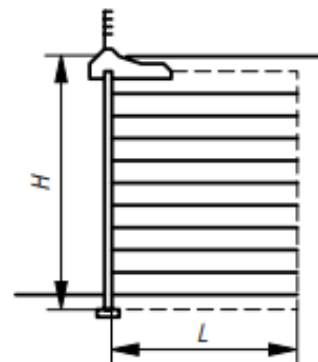
b) Trapezoidal cross section

$z_1 = 0.5H$
 $z_2 = 0.75H$
 $z_3 = H$
 $L_1 = 0.7H$
 $L_2 = 0.55H$
 $L_3 = 0.4H$ and ≥ 3 m
 NOTE 1 No reinforcements to end within shaded zone.
 NOTE 2 Horizontal steps ΔL to be $\leq 0.15H$.



c) Stepped cross section

$L_1 \geq 0.7H$
 $\Delta H \geq 2 \Delta L$



d) Walls with parapets

Figure 1.14. Sizing of reinforced earth wall with various geometries (BS 8006-1 2010).

b) Embedment

An embedment depth greater than the minimum of 0.45 m (Figure 1.15).

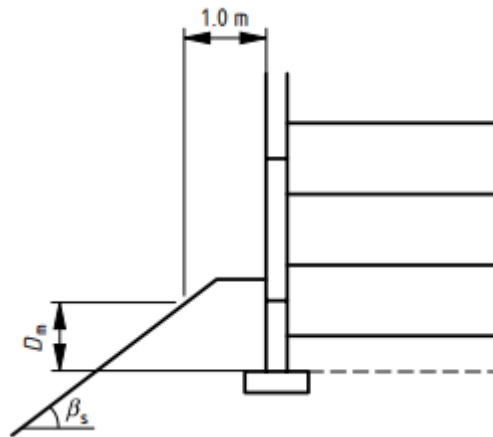


Figure 1.15. The embedment, D_m according to BS 8006-1: 2010.

The minimum embedment should not be less than that shown in Table 1.3, which is based on a structural slenderness ratio of $L/H = 0.7$ and good ground conditions. Greater embedment should be considered on sites where the foundation is weak or soft. The minimal embedment depth indicated in terms of the wall's mechanical height in Table 1.3 is a cautious number that should be applied in most cases. To give a more rigorous solution, the minimum embedment depth defined in terms of the calculated bearing pressure at the base of the wall might be used.

Anti-scour measures, rip-rap, or gabion mattresses should be supplied for structures vulnerable to river or sea water activity to ensure stability.

Table 1.3. Calculated of the minimum embedment as a function of the mechanical height H in metres and the factored bearing pressure q_r in kN/m^2 (taken from BS 8006-1: 2010) .

Slope of the ground at toe β_s	Structure type	Minimum embedment D_m (m)	Minimum embedment factor $D_m/q_{ref}(\text{m}^3/\text{kN})$
$\beta_s = 0$	Walls	$H/20$	1.35×10^{-3}
$\beta_s = 0$	Abutments	$H/10$	1.35×10^{-3}
$\beta_s = 18^\circ$ ($\cot \beta_s = 3/1$)	Walls	$H/10$	2.7×10^{-3}
$\beta_s = 27^\circ$ ($\cot \beta_s = 2/1$)	Walls	$H/7$	4.0×10^{-3}
$\beta_s = 34^\circ$ ($\cot \beta_s = 3/2$)	Walls	$H/5$	5.9×10^{-3}

1.5.1.3. LRFD Bridge Design Specifications (AASHTO 2020)

a) Minimum length of reinforcement

The minimum soil reinforcement length for sheet, strip, and grid-type reinforcement is 70% of the wall height measured from the levelling pad. Surcharges and other external stresses, as well as fragile foundation soils, will require additional reinforcement length. Unless substantiating data is supplied to suggest that variation in length is acceptable, the reinforcement length must be constant across the height of the wall.

Only after reliable, site-specific assessments of the strength of the unreinforced fill and the foundation soil can significant shortening of the reinforcement elements below the minimum suggested ratio of $0.7H$ be contemplated. The results of Christopher et al. (1990) strongly show that shorter reinforcing length to height ratios, i.e., $0.5H$ to $0.6H$, significantly increase horizontal deformations.

Under the following conditions, a no uniform reinforcement length may be considered:

- ✓ Extending the highest reinforcement layers beyond $0.7H$ in order to achieve pull-out criteria or address seismic or impact loading.
- ✓ Extending the lowermost reinforcing layers beyond $0.7H$ to meet overall (global) stability criteria based on the findings of a comprehensive global stability analysis.
- ✓ If the wall is supported by rock or exceptionally competent foundation soil, the lowest reinforcing layers can be reduced to less than $0.7H$ to reduce excavation requirements.

b) Embedment

Bearing resistance, settlement, and stability requirements determine the minimum embedment depth of the bottom of the reinforced soil mass.

Unless the reinforced soil wall is built on rock foundations, the embedment at the front face of the wall must be at least:

- ✓ A depth based on the prevailing depth of frost penetration and the external stability requirement, if the soil below the wall is frost susceptible.
- ✓ 2.0 ft on sloping ground ($4H: 1V$ or steeper) or where there is a risk of erosion or future excavation removing the soil in front of the wall toe, or 1.0 ft on level ground where there is no risk of erosion or future excavation removing the soil in front of the wall toe.

Reinforced soil walls built along rivers and streams must have embedment depths that are at least 2.0 ft below the probable scour depth.

According to AASHTO 2020, the minimum embedment criteria are listed in Table 1.4.

Table 1.4. Minimum embedment depth (taken from AASHTO 2020).

Slop in front of structure	Structure type	Minimum embedment depth
Horizontal	walls	H/20
	Abutments	H/10
3H/1V	walls	H/10
2/H/1V	walls	H/7
1.5H/1V	walls	H/5

1.5.2. External stability

1.5.2.1. Lateral earth pressure

a) Coulomb method

Coulomb (Coulomb 1776) was the first developed a method for estimating retaining walls. Today, Coulomb's method is universally used, especially in the United States, because of its theoretical and practical simplicity. Coulomb's theory is based on two hypotheses:

- ✓ The soil breaks up along a plane rupture surface;
- ✓ The force acting on the wall has a known direction. In other words, this means that the interface friction angle δ between soil and structure.

Under active pressure conditions, the thrust pressure on a reinforced soil earth wall with a geometry is obtained after the forces equilibrium (see Figure 1.16).

The active thrust on a wall supporting a cohesionless soil and lateral earth pressure coefficient can be expressed as follows:

$$P_A = \frac{1}{2} K_A \gamma H^2 \tag{1.1}$$

$$K_A = \frac{\cos^2(\phi - \theta)}{\cos^2 \theta \cos(\delta + \theta) \left[1 + \left(\frac{\sin(\phi + \delta) \sin(\phi - \beta)}{\cos(\delta + \theta) \cos(\beta - \theta)} \right)^{1/2} \right]^2} \tag{1.2}$$

Where:

ϕ : soil friction angle;

δ : soil-structure interface angle;

θ : inclination of the wall with vertical;

β : inclination of the soil surface above the wall with the horizontal.

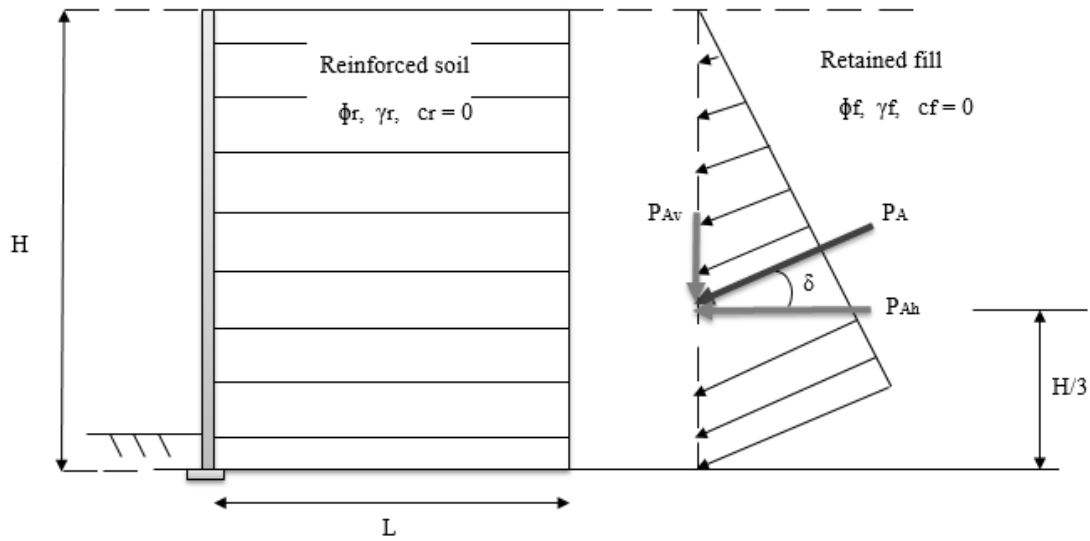


Figure 1.16. Coulomb earth pressure distribution for reinforced earth wall.

b) Rankine method

Rankine (Rankine 1857) developed the simplest method of calculating lateral earth pressures. He was able to make the lateral earth pressure problem deterministic and directly calculate the static pressure acting on retaining walls. By making the following hypotheses:

- ✓ The soil is homogeneous and isotropic.
- ✓ The wall does not change the orientation and repair of the vertical stresses in the soil.
- ✓ The friction angle between the wall and the soil is zero ($\delta = 0$).

For active conditions, Rankine expressed the active earth thrust and lateral earth pressure coefficient as follow:

$$P_A = \frac{1}{2} K_A \gamma H^2 \tag{1.3}$$

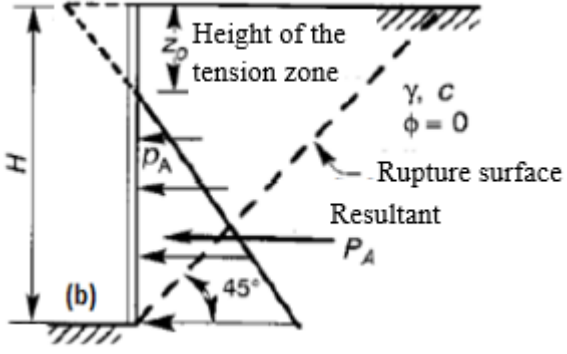
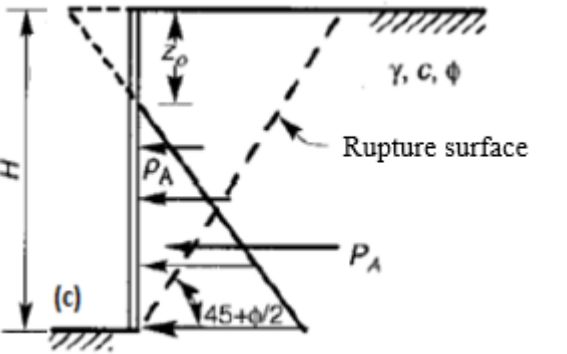
$$K_A = \frac{1 - \sin \phi}{1 + \sin \phi} = \tan^2 \left(45^\circ - \frac{\phi}{2} \right) \tag{1.4}$$

For the case of a granular backfill inclined by an angle β with respect to the horizontal, an infinite number of solutions can be used to calculate K_A (Terzaghi 1943; Taylor 1948), as :

$$K_A = \cos \beta \frac{\cos \beta - \sqrt{\cos^2 \beta - \cos^2 \phi}}{\cos \beta + \sqrt{\cos^2 \beta - \cos^2 \phi}} \tag{1.5}$$

The pressure distribution along the wall, depends on the relative magnitudes of the frictional and cohesive components of the soil resistance of the backfill (Kramer 1996) as shown in Table 1.5:

Table 1.5. Distribution of active pressures for different backfill.

Backfill type	The active earth pressure
Cohesive soil $(c \neq 0, \phi = 0)$	<div style="text-align: center;">  </div> $z_0 = 2c / \gamma \tag{1.6}$ $P_A = \gamma z - 2c \tag{1.7}$ $P_A = \left(\frac{\gamma H^2}{2} \right) - 2cH + \frac{2c^2}{\gamma} \tag{1.8}$
Cohesive and frictional soil $(c \neq 0, \phi \neq 0)$	<div style="text-align: center;">  </div> $z_0 = \left(\frac{2c}{\gamma} \right) \tan(45^\circ - \frac{\phi}{2}) \tag{1.9}$ $P_A = \gamma z \tan^2(45^\circ - \frac{\phi}{2}) - 2c \tan(45^\circ - \frac{\phi}{2}) \tag{1.10}$ $P_A = \left(\frac{\gamma H^2}{2} \right) \tan^2(\frac{\pi}{4} - \frac{\phi}{2}) - 2cH \tan(\frac{\pi}{4} - \frac{\phi}{2}) + \frac{2c^2}{\gamma} \tag{1.11}$

Under active pressure conditions, the thrust pressure on a reinforced soil earth wall by Rankine method as shown in Figure 1.17.

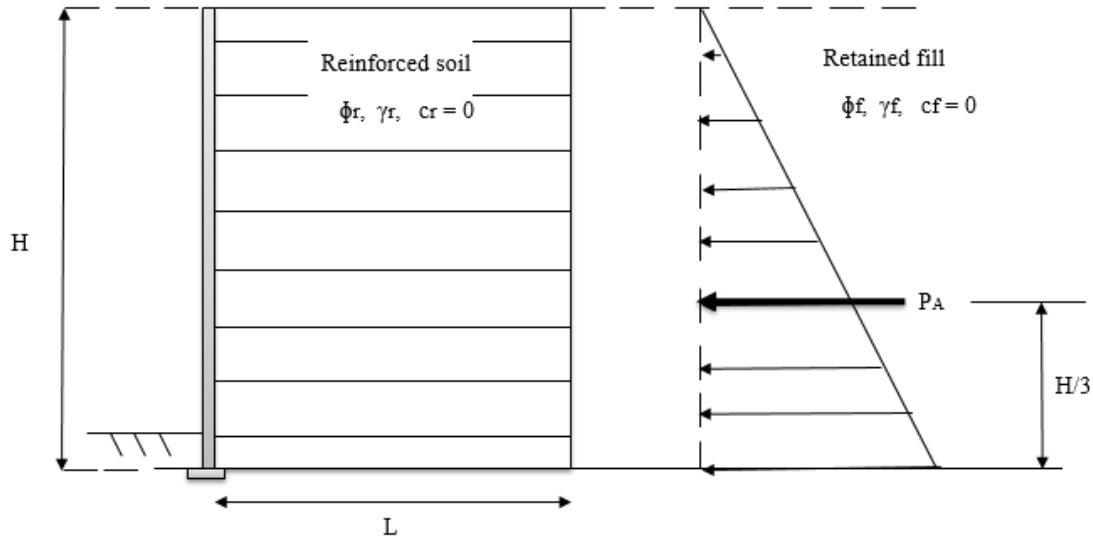


Figure 1.17. Rankine earth pressure distribution for reinforced earth wall.

c) French Norm (NF 94-270: 2009)

French Norm recommends an alternative method for a vertical wall, supporting a homogeneous cohesionless soil behind the reinforced backfill and founded on homogeneous soil. The thrust force due to the weight of the soil can be calculated as shown in Figure 1.18, considering the inclination δ_x of the thrust P_{ax} as follows:

$$\delta_x = \frac{2}{3} \phi_{2d} \tag{1.12}$$

$$\delta_y = 0.8 \left(1 - 0.7 \frac{L_m}{H_e} \right) \phi_{1d}$$

The thrust P_{ay} is inclined by δ_y such that :

$$\delta_y = 0.8 \left(1 - 0.7 \frac{L_m}{H_e} \right) \phi_{1d} \tag{1.13}$$

With:

$$l_m = \frac{S_r}{h_e} \tag{1.14}$$

Where:

ϕ_{1d} : is the calculated value of the friction angle of the material of the reinforced zone;

ϕ_{2d} : is the calculated value of the ground friction angle behind the reinforced zone;

l_m : is the average length of the reinforcement layers;

e) LRFD Bridge Design Specifications (AASHTO 2020)

In case there is a tilting in backfill and the wall face is battered the earth pressure coefficient calculated from the Coulomb wedge theory, and in the case of the absence of these two factors, it is calculated by Rankine method.

1.5.2.2. Bearing capacity

The reinforced soil wall transmits quasi-linear stresses to the foundation due to its own weight (W) and the effects of the surcharges and lateral thrusts which act on it.

The French norm (NF 94-270: 2009), the British standard (BS 8006-1: 2010) and the Load Resistance Factor Design (LRFD) Bridge Design Specifications (AASHTO 2020) are all based on Meyerhof's formula for calculation the typical bearing pressure q_r applied at the base of the wall (see Figure 1.19):

$$q_r = \frac{R_v}{L - 2e} \tag{1.18}$$

Where:

R_v : is the resultant of all factored vertical load components.

L : is the reinforcement length at the base of the wall;

e : is the eccentricity of resultant load R_v about the centre line of the base of width L .

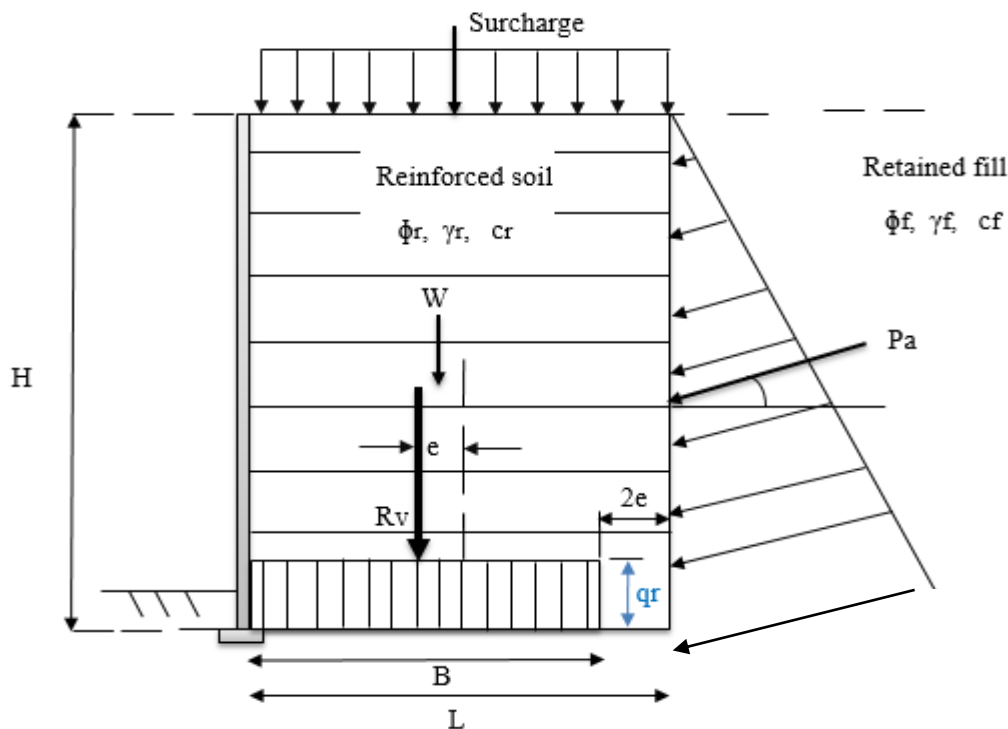


Figure 1.19. Pressure distribution along the base of the reinforced soil wall.

1.5.3. Internal stability (Maximum reinforcement loads T_{max})

1.5.3.1. Coherent gravity method

The maximum tensile load (T_{max}) in the proposed reinforcement layer per metre of face is calculated as follows:

$$T_{max} = \sigma_h s_v \quad (1.19)$$

where

s_v : is the vertical spacing between the reinforcement layers;

σ_h : is the total horizontal design stress in the backfill at the level of the reinforcement layer considered and at the line of maximum tension, equal to:

$$\sigma_h = K \sigma_v \quad (1.20)$$

Where:

σ_v : is the total vertical design stress in the backfill at the level of the considered reinforcement layer and at the line of maximum tension determined by the Meyerhof method;

K : is a proportionality coefficient determined empirically from the experimental results (it is the earth pressure coefficient internal to the massif).

The determination of the vertical stress $\sigma_v(z)$ at the depth z of the considered reinforcement layer is done by reducing the forces coming from everything above this bed (weight, surcharges, earth pressure at the back of the massif) and by distributing them over the reduced width $L(z) - 2e$:

$$\sigma_v(z) = \frac{R_v}{L(z) - 2e} \quad (1.21)$$

Where:

R_v : is the vertical component of the resultant force calculation per metre of facing;

$L(z)$: is the width of the reinforcement layer at depth z ;

e : is the eccentricity of the load resultant.

The coefficient K depends on the depth z of the considered reinforcement layer (Figure 1.20):

by NF 94-270:

If $z \leq z_0$:

$$K_{(z)} = \Omega_1 K_a \left[1.6 \left(1 - \frac{z}{z_0} \right) + \frac{z}{z_0} \right] \tag{1.22}$$

If $z > z_0$:

$$K_{(z)} = \Omega_1 K_a \tag{1.23}$$

Where:

z_0 : is a depth taken as 6 m;

K_a : is the active thrust coefficient of backfill massif, given by:

$$K_a = \tan^2 \left(\frac{\pi}{4} - \frac{\phi}{2} \right) \tag{1.24}$$

Ω_I : is a coefficient (≥ 1.0) related to the type of reinforcement, for metal or synthetic reinforcements in strip or sheet form, $\Omega_I = 1.0$. If the backfill material may have elements larger than $s_x / 2$ or $s_y / 2$, $\Omega_I = 1.25$ should be used

by BS 8006-1 & AASHTO:

If $z \leq z_0$:

$$K_{(z)} = K_o \left(1 - \frac{z}{z_0} \right) + \left(K_a \frac{z}{z_0} \right) \tag{1.25}$$

If $z > z_0$:

$$K_{(z)} = K_a \tag{1.26}$$

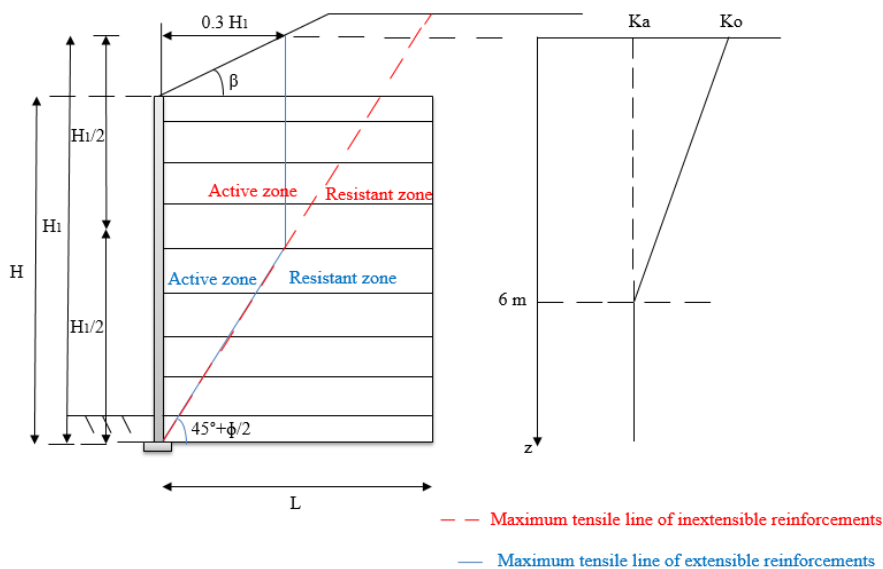


Figure 1.20. Variation of coefficient of earth pressure with depth – Coherent gravity method.

1.5.3.2. Stiffness method

The Stiffness method, like the Coherent gravity method, was created empirically to estimate MSE wall soil reinforcement loads under operational conditions, and it's applied only by (AASHTO 2020). As a result, it's critical to ensure that the reinforcement strains aren't large enough to allow a shear surface to fully develop through the reinforced wall backfill. Because the Stiffness Method produces a less conservative estimate of reinforcement loads, especially for somewhat extensible soil reinforcement, ensuring that the soil failure (Service Limit State) is not reached or exceeded as stipulated in (AASHTO 2020) is a crucial component of this method.

Using the Stiffness Method, T_{\max} should be calculated as follows:

$$T_{\max} = S_v \left[H \gamma_r D_{t_{\max}} + \gamma_f \left(\frac{H_{\text{ref}}}{H} \right) S \right] K_{avh} \Phi \quad (1.27)$$

Where:

S_v : is the tributary vertical reinforcement layer thickness ;

H : is the height of the wall;

H_{ref} : is the reference wall height and equal 6 m;

γ_r : is the unit weight of soil in wall reinforcement zone;

S : is the average soil surcharge thickness over reinforcement;

γ_f : is the unit weight of soil in wall in surcharge above wall;

$D_{t_{\max}}$: T_{\max} distribution factor;

K_{avh} : is the active ground pressure coefficient for a vertically facing wall;

Φ : is empirically determined influence factor that captures the effect that the soil reinforcement properties, soil cohesion, and wall geometry have on T_{\max} ;

Figure 1.21 shows the calculation of the T_{\max} distribution factor, $D_{t_{\max}}$. The wall height, H , has been used to normalize depths below the wall top in the figure. T_{\max} is the maximum value of $T_{\max_{\max}}$ in the wall section.

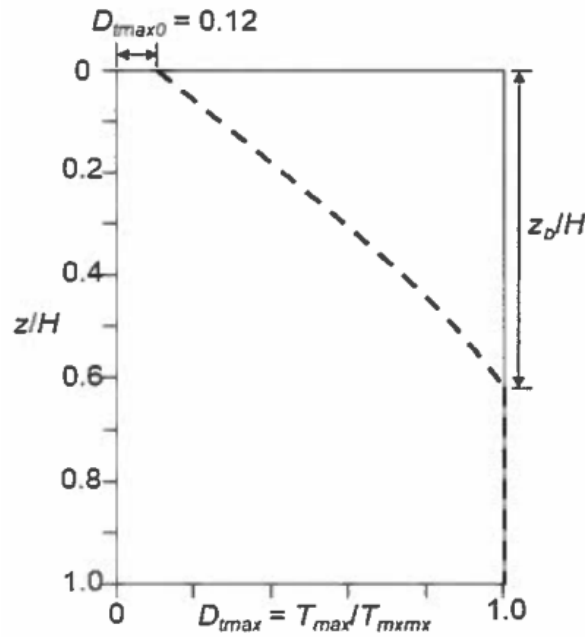


Figure 1.21. Illustration of D_{tmax} factor (source: AASHTO 2020).

D_{tmax} shall be determined as follows:

For $z < z_b$:

$$D_{tmax} = D_{tmax0} + (z/z_b) \times (1 - D_{tmax0}) \tag{1.28}$$

For $z \geq z_b$:

$$D_{tmax} = 1.0 \tag{1.29}$$

$$z_b = C_h \times (H)^{1.2} \tag{1.30}$$

Where:

z : is the depth of reinforcement layer below top of wall at wall face;

z_b : is the depth below top of wall at wall face where D_{tmax} becomes equal to 1.0 (and below which D_{tmax} equals 1.0);

D_{tmax0} : is T_{max} distribution factor magnitude at top of wall at wall face, equal to 0.12;

C_h : is the coefficient equal to 0.32 when H is in ft and 0.40 when H is in meters.

Φ shall be determined as described in Allen and Bathurst (2015 and 2018), as follows for vertical or near-vertical walls (i.e., a facing batter of 10 degrees or less from the vertical) with a single reinforcement strength and stiffness and cohesionless backfill soil (defined as having a plasticity index of 6 or less):

$$\Phi = \Phi_g \Phi_{fs} \Phi_{local} \Phi_{fb} \Phi_c$$

Where:

Φ_g : is the global stiffness factor;

Φ_{fs} : is the facing stiffness factor;

Φ_{local} : is the local stiffness factor;

Φ_{fb} : is the facing batter factor;

Φ_c : is the soil cohesion factor.

The global stiffness factor Φ_g shall be calculated as follows:

$$\Phi_g = 0.16 \left(\frac{S_{global}}{P_a} \right)^{0.26} \quad (1.31)$$

Where:

S_{global} : is the global reinforcement stiffness;

P_a : is the atmospheric pressure (101 kPa);

$$S_{global} = \frac{J_{ave}}{(H/n)} = \frac{\sum_{i=1}^n J_i}{H} \quad (1.32)$$

Where:

J_{ave} : is the average secant tensile stiffness of all n geosynthetic reinforcement layers;

n : is the number of reinforcement layers in wall section;

J_i : is the secant tensile stiffness of geosynthetic reinforcement at 2% strain and 1000 h on a per width of wall basis (layer i);

$$J_i = J2\% \times R_c \quad (1.33)$$

$J2\%$: is the secant tensile stiffness of geosynthetic reinforcement at 2% strain and 1000 h on a per unit width of reinforcement basis (obtained from laboratory testing);

R_c : is the reinforcement coverage ratio.

The facing stiffness factor Φ_{fs} shall be calculated as follows:

$$\Phi_{fs} = 0.57 \left[\left(\frac{S_{global}}{P_a} \right) F_f \right]^{0.15} \quad (1.34)$$

Where:

F_f : is the facing stiffness parameter;

$$F_f = \frac{1.5H^3 P_a}{Eb^3 (h_{eff} / H)} \quad (1.35)$$

Where:

b : is the thickness of the facing column;

E : is the elastic modulus of the “equivalent elastic beam” representing the wall face;

h_{eff} : is the equivalent height of an un-jointed facing column that is approximately 100% efficient in transmitting moment through the height of the facing column.

The local stiffness factor Φ_{local} shall be calculated as follows:

$$\Phi_{local} = \left(\frac{S_{local}}{S_{localave}} \right)^a \quad (1.36)$$

Where:

a : is a coefficient equal 0 when the reinforcement are steel and equal 0.5 when the reinforcement are geosynthetic and extensible steel grids;

S_{local} : is the local reinforcement stiffness;

$$S_{local} = J_i / S_v \quad (1.37)$$

$S_{localave}$: is the average local reinforcement stiffness;

$$S_{localave} = \frac{\sum_{i=1}^n J_i / S_v}{n} \quad (1.38)$$

The facing batter factor Φ_{fb} shall be calculated as follows:

$$\Phi_{fb} = \left(\frac{K_{abh}}{K_{avh}} \right)^{0.4} \quad (1.39)$$

Where:

K_{abh} : is the coefficient of active earth pressure, battered;

$$K_{abh} = \frac{\cos^2(\phi_r + \omega)}{\cos^3 \omega \left(1 + \frac{\sin \phi_r}{\cos \omega} \right)^2} \quad (1.40)$$

$$K_{avh} = K_a = (1 - \sin \phi_r) / (1 + \sin \phi_r) \quad (1.41)$$

where:

ϕ_r : is the friction angle of the reinforced soil backfill;

ω : is the wall face batter in clockwise direction from the vertical.

The soil cohesion factor Φ_c shall be calculated as follows:

$$\Phi_c = e^{-16(c/(\gamma_r H))}$$

(1.42)

Where:

c : is the soil cohesion;

γ_r : is the unit weight of the reinforced soil.

A comparison between the Simplified method and the complete Stiffness method, excluding traffic surcharge load, is provided in Figure 1.22. The Stiffness method was created by starting with the Simplified method, correcting the T_{max} distribution to more accurately reflect measurements in full-scale structures, and replacing the semi-empirical (k_r / k_a) term with a reinforcement stiffness-based term calibrated to full-scale structure measurements.

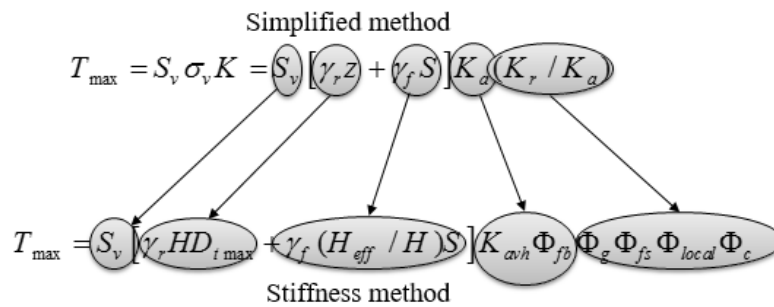


Figure 1.22. Comparison of AASHTO simplified and stiffness method equation (Allen and Bathurst 2015).

CHAPTER TWO

Back-to-Back Reinforced Soil Walls

2.1. Definition

A back-to-back reinforced earth wall is actually two reinforced earth walls with parallel faces, which may be separated by an embankment, joined or embedded in each other (Figure 2.1). Such walls are a unique design challenge that necessitates an understanding of the structure's wall geometry (height and width), reinforcement lengths (independent or overlapping), reinforcement type (inextensible or extendable), and backfill qualities on either side. Back-to-back mechanically stabilized earth walls are used in ramp ways, rock fall protection systems, earth dams, levees and noise barriers and especially in bridge approaches (see Figure 2.2 and 2.3).

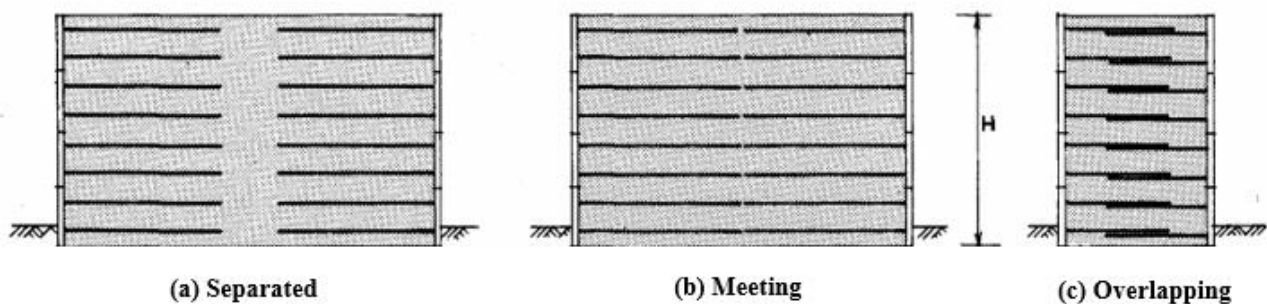


Figure 2.1. Back-to-back walls (French Ministry of Transport,1979).



Figure 2.2. T-Rex Rapid Transit, Denver, CO
 $H = 14.0$ m, $W = 10.1$ m, $L = 9.8$ m, $W/H=0.72$ and $L/H = 0.7$ (Anderson et al 2018)



Figure 2.3. Manhan Rail Trail over SR 10, Easthampton, MA

$H = 9.77$ m, $W = 5.48$ m, $L = 4.88$ m overlapping $W/H=0.56$, $L/H = 0.50$ (Anderson et al 2018).

In the early 1970s, Reinforced Earth was utilized to build the first back-to-back MSE walls, which have since been used for highways, railroads, defensive buildings, and dams. The notion of overlapping reinforcing strips was recognized as technically possible in 1979 in the French Rules and Recommendations of the Art (Ministry of Transport), which gave formal design direction (Figure 2.4).

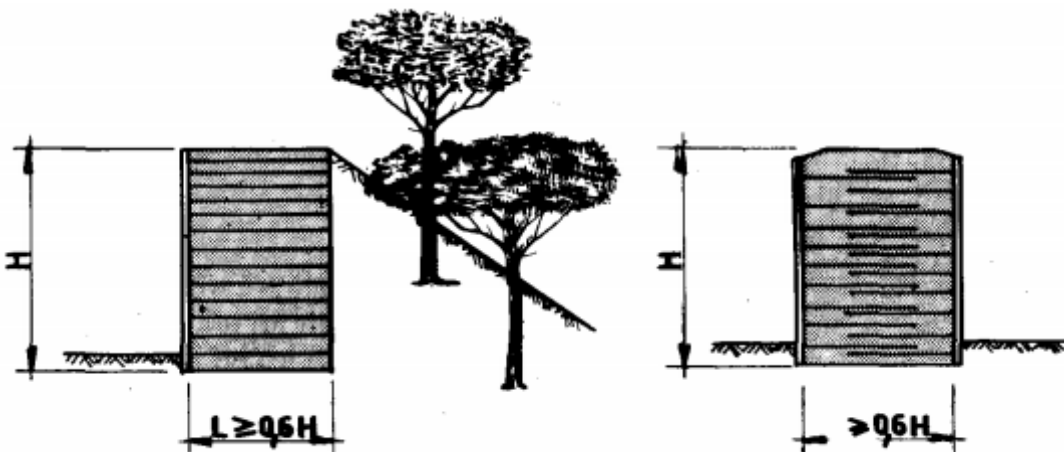


Figure 2.4. Structures subject to low thrust (French Ministry of Transport, 1979).

2.2. Studies on Back-to-Back Walls

Following the reported performance of back-to-back reinforced soil retaining walls under working stress, several researchers have investigated the influence of a number of parameters on their behaviour. They have used different analytical approaches, numerical analyses. On the other hand, experimental studies are almost non-existent for this type of structure and do not exceed one or two studies, even these two studies concern particular cases that are not very common in reality. We will cite most of them. As for studies under dynamic loading, they are almost non-existent compared to static studies (i.e., Benmebarek and Djabri 2017; Dram et al 2021; Samee et al 2021a; Samee et al 2021b; Yazdandoust et al 2022).

2.2.1. Analytical studies

2.2.1.1. Elias and Christopher (1997)

The former US Federal Highway Administration (FHWA 1997) indicate that the design of back-to-back walls is considered a special situation (Elias and Christopher 1997). According to these guides, This circumstance of two opposite sides wlls can result in a different backfill thrust value, which affects the external stability calculations. Two scenarios can be examined, as shown in Figure 2.5.

(a) Case 1:

(b) Case 2:

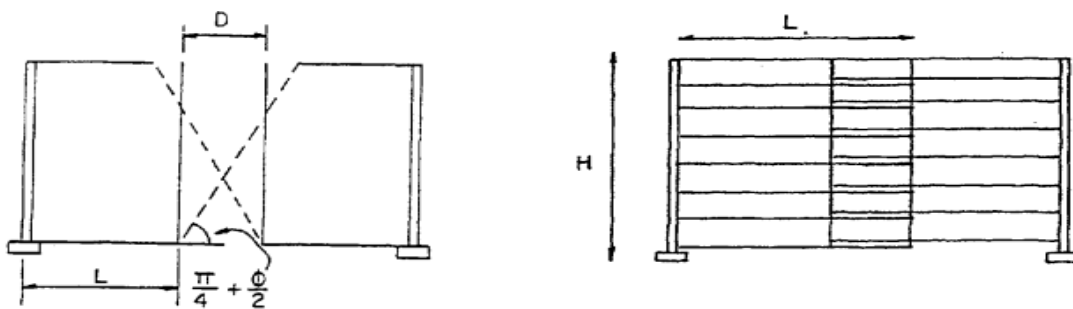


Figure 2.5. Definition of back-to-back wall: (a) case 1 and (b) case 2 (Elias and Christopher 1997).

- Case 1: each wall behaves and may be constructed separately because the overall base width is broad enough. There is no overlapping of reinforcements in particular. In theory, if the distance between the two walls, D , is less than:

$$D = H \tan(45^\circ - \phi / 2) \tag{2.1}$$

then the active wedges at the back of each wall cannot fully stretch out and the active thrust is reduced. However, it is assumed that for values of:

$$D > H \tan(45^\circ - \phi / 2) \tag{2.2}$$

full active thrust is mobilized.

- Case 2: there is an overlapping of the reinforcements so that the two walls interact. As a result, the two walls are built independently for internal stability using the same process as the single wall but assuming no active backfill thrust.

Some engineers could be tempted to use single reinforcements attached to both wall facings in this situation. This option radically alters the structure's strain patterns and results in greater reinforcement tensions, rendering the design process described in this manual obsolete. Furthermore, challenges with wall alignment may arise during construction, particularly if the walls are not in a tangent section.

2.2.1.2. Berg et al (2009)

In the latest FHWA guidelines, this type of retaining wall is classified as complex geometry. The active earth pressure behind the reinforced zone is modified and two cases are considered (Berg et al., 2009) (see Figure 2.6):

- Case 1: if the interaction distance D_1 between the back of the reinforced soil zone for opposite walls is less than the active zone:

$$D < H_1 \tan(45^\circ - \phi/2) \approx 0.5H_1 \quad (2.3)$$

Where H_1 is the maximum height of the parallel walls and ϕ is the friction angle of the backfill, then the failure surface cannot be fully developed, the lateral earth pressure is reduced and the two walls cannot be designed independently. However, for design, it is assumed that for values of:

$$D > H_1 \tan(45^\circ - \phi/2) \approx 0.5H_1 \quad (2.4)$$

then full active thrust is mobilized.

- Case 2: there is an overlapping of the reinforcement layers such that the two walls interact. When the overlap (L_R length) is greater than $0.3H_2$, where H_2 is the shorter of the parallel walls, no active earth thrust from the backfill needs to be considered for external stability calculations.
- For intermediate geometries between Cases 1 and 2, when:

$$0 < D < H_1 \tan(45^\circ - \phi/2) \quad (2.5)$$

FHWA recommends linearly interpolate between full active earth pressures in Case 1 and zero earth pressure in Case 2.

(a) Case 1:

(b) Case 2:

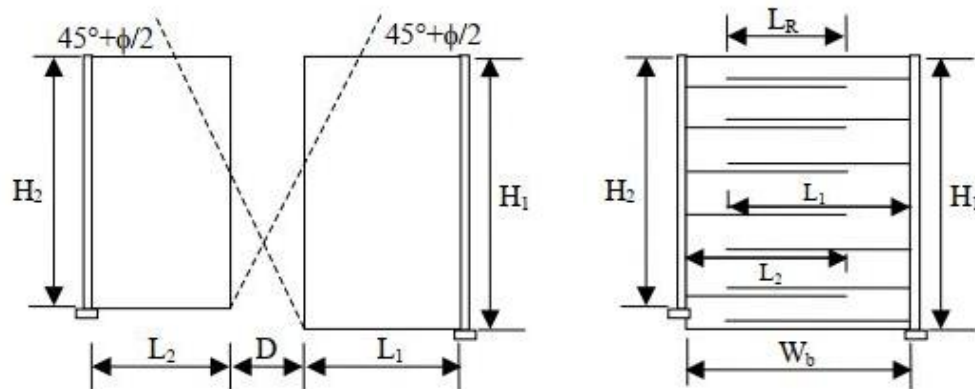


Figure 2.6. Definition of back-to-back wall: (a) case 1 and (b) case 2 (Berg et al., 2009).

For Case 2 geometries with overlaps (L_R) greater than $0.3H_2$, the following guidelines should be used:

- ✓ $L_1/H_1 \geq 0.6$ where L_1 and H_1 is the length of the reinforcement and height, respectively, of the taller wall.
- ✓ $L_2/H_2 \geq 0.6$ where L_2 and H_2 is the length of the reinforcement and height, respectively, of the shorter wall.
- ✓ $W_b/H_1 \geq 1.1$ where W_b is the base width as shown in Figure 1.28 and H_1 is the height of the taller wall.

The FHWA (Berg et al., 2009) guides are valid for static conditions as well as for seismic actions where the horizontal acceleration at the foundation is less than 0.05g.

Designers may be tempted to employ single layers of reinforcements that are connected to both wall facings for back-to-back walls. This option provides an unyielding structure with an at rest stress state (K_0) from top to bottom, resulting in substantially higher reinforcement tensions than the design method previously utilized in this manual. Increases in lateral stress must be factored into the tension determination in reinforcement and connection, as well as the design of facing elements. Compaction may also result in increased stress at the connection, which must be factored into the lateral earth pressure calculations. Furthermore, preserving wall alignment during construction may be challenging, especially if the walls are not in a tangent section.

2.2.2. Numerical studies

2.2.2.1. Han and Leshchinsky (2010)

Han and Leshchinsky (2010) adopted finite difference numerical methods based on Fast Lagrangian Analysis of Continua FLAC software for the study, as well as limit-equilibrium approaches. The objective was to investigate the effect of the wall width to height ratio (W/H) and the quality of the backfill material (friction angle ϕ) on the behavior of back-to-back reinforced soil walls under self-weight (Figure 2.7). The critical failure surface, the maximum required tensile force in the reinforcement as well as the active thrust behind the reinforced zone are selected as criteria for assessing the stability of the structure.

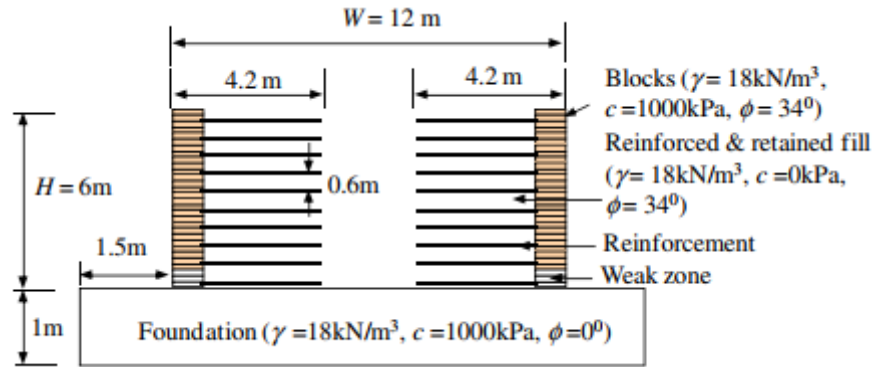


Figure 2.7. Basic model for the case $W/H=2$ (Han and Leshchinsky 2010).

The following results were obtained:

- ✓ The analysis of the failure surface shows that the two opposite walls are treated in an independent way when they are far apart, the case $W/H \geq 2$ ($D \geq 3.6$ m), and interact with each other when they are close.
- ✓ The FHWA design guideline underestimates the interaction distance.
- ✓ When the distance between the facings becomes very small ($W/H=1.4$), the lateral pressure of the earth behind the reinforced zone is still existing. The required maximum tensile force in the reinforcements decreases slightly.
- ✓ On the other hand, when the facings are very close together, connecting the reinforcements in the middle reduces the maximum tension required at the reinforcement.

2.2.2.2. El-Sherbiny et al. (2013)

A finite element analysis (PLAXIS software) was performed on a typical highway ramp comprising back-to-back MSE walls of height $H=5$ m (El-Sherbiny et al 2013). The structure was designed according to the FHWA (2009) guidelines. For each height, the ramp width (W) was adjusted so that the clear distance between the backs of the walls (D) varied from zero to the whole height of the wall. The wall's response with overlapping reinforcement and continuous reinforcement over the ramp was also tested. The overlap was limited to $0.3 H$ in length. Except where the reinforcement overlapped, the width of each back-to-back wall was set to the standard $0.7H$ value. In all simulations, the spacing between reinforcement layers was set at 0.45 m. The objective was to investigate the effect of distance between back-to-back reinforced soil walls and reinforcement length on the critical failure surface, tensile forces in the reinforcement, and lateral earth pressure behind the reinforced zone.

The following results were obtained:

- ✓ If the wall spacing to height ratio is greater than one, the back-to-back walls behave independently.

- ✓ The ratio (D/H) is less than one the two opposite sides walls interact with each other and the earth pressure behind the wall diminishes because the failure wedge behind the wall is not fully developed.
- ✓ When the distance (D) between the two walls is reduced, the tensile forces in the reinforcement diminish.
- ✓ When a single reinforcement layer is used instead of overlapping layers in very narrow walls, the tensile forces are reduced.

2.2.2.3. Benmebarek et al. (2016)

A FE numerical investigation, using the PLAXIS 2D code, on the behaviour of back-to-back mechanically stabilized earth walls (Benmebarek et al., 2016) (see Figure 2.8). The objective was to evaluate the effects of reducing the distance between the two opposite facings of the structure. The length of the reinforcement, the quality of the backfill material as well as the consequences of connecting the reinforcements in the middle, when the walls are joined, are also discussed.

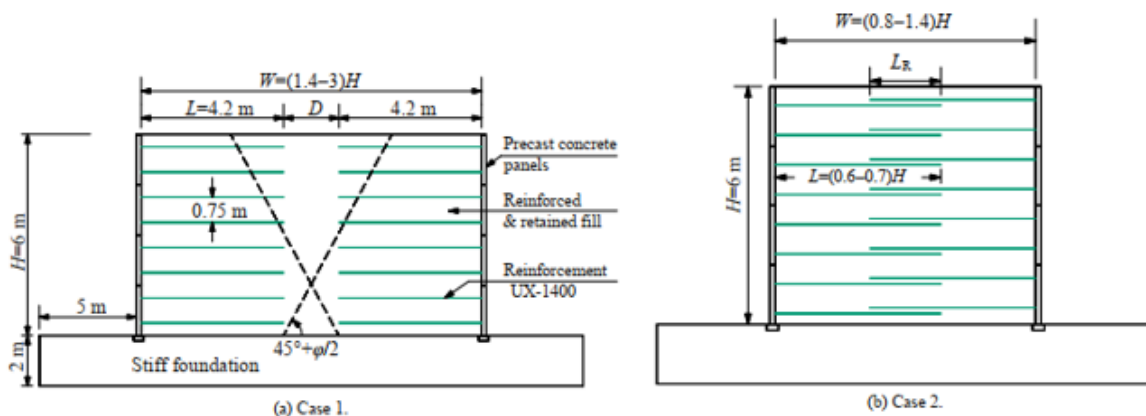


Figure 2.8. Dimensions and parameters of the models studied (Benmebarek et al., 2016).

The following results were obtained:

- ✓ If the distance of the embankment between back-to-back mechanically stabilized earth walls is bigger than the active zone, each side of the wall perform independently, and this is in keeping with the findings of the FHWA design guideline.
- ✓ When back-to-back walls interact, the FHWA design standard underestimates the lateral earth pressure.
- ✓ The maximum tensile force in the reinforcement is greatly overestimated by the FHWA design standard for closer back-to-back MSE walls.
- ✓ A little increase in embankment cohesion can result in large reductions in both lateral ground pressure and maximum tensile loads of reinforcement.
- ✓ The factor of safety is greatly improved by connecting reinforcement between back-to-back walls ($D = 0$).

2.2.2.4. Djabri and Benmebarek (2016)

The behavior of back-to-back geosynthetic reinforced soil retaining walls was studied using a Finite element approach implemented into the Plaxis software (Djabri and Benmebarek 2016) (see Figure 2.9). The objective of this research was to study the influence of the distance between the back-to-back walls on the shear zones, the lateral earth pressure behind the reinforced zone, the facing displacement and the required tensile strength of reinforcement under static loading.

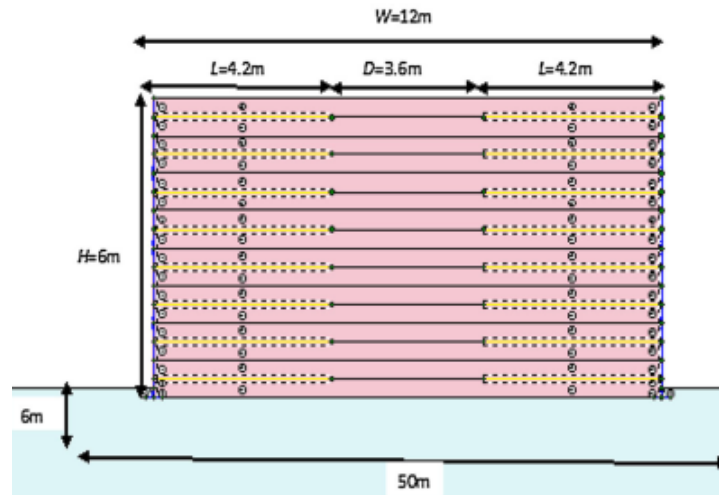


Figure 2.9. Dimensions of back-to-back GRS wall base case $W/H = 2$ (Djabri and Benmebarek 2016).

The following results were obtained:

- ✓ The back-to-back behaves independently when they are far apart and interact with each other when they are close together.
- ✓ The FHWA assumption leads to more cautious estimates regarding the distance between back-to-back walls, which equals 0.
- ✓ Due to the inability of analytical methods to evaluate two side walls, it is demonstrated that the finite element approach can be employed perfectly of back-to-back reinforced soil walls for static analysis.

2.2.2.5. Sarvanam et al. (2016)

A finite difference analysis (FLAC programme) was carried out on back-to-back retaining walls (Sarvanam et al., 2016) (see Figure 2.10). The goal was to look at how reinforcement tensile forces are mobilized at different levels within a back-to-back MSE wall under operating stress. Tensile forces in reinforcements connected in the middle are also measured. A parametric study was conducted to evaluate the influence of the stiffness of reinforcement ranging from 500 kN/m to 50000 kN/m and the ratio of width to wall height (W/H) ranging from 1.4 to 2.0 on tensile forces in every reinforcement layer. Charts depicting the change of maximum tensile forces along the height of the wall are also presented.

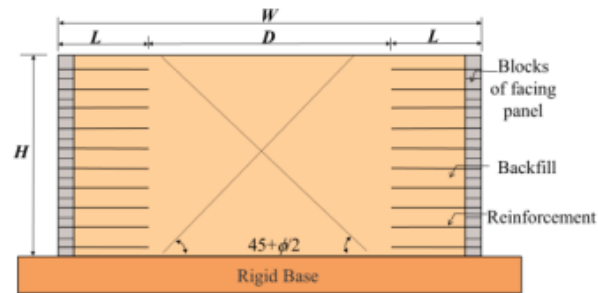


Figure 2.10. Modelling scheme of back-to-back MSE wall (Sarvanam et al., 2016).

The following results were obtained:

- ✓ The maximum tension in the reinforcement was reached at 0.9 m height from the bottom of the wall.
- ✓ When the reinforcing stiffness is large ($J = 50000$ kN/m), the maximum tension in the connected case is less than in the disconnected case. In the case of reinforcement with a low stiffness value ($J = 500$ kN/m), there was no significant difference between the connected and disconnected cases.
- ✓ When it comes to the magnitude of the maximum tension profile, the W/H ratio has no significant influence. However, when the distance between the two opposite walls grows, the location of the greatest tension along the reinforcing length shifts.

2.2.2.6. Benmebarek and Djabri (2017)

FEM to investigate the influence of overlapping reinforcement on the critical failure surface, the factor of safety, the facing displacement and the required tensile strength of reinforcement under static conditions using code PLAXIS has been published by Benmebarek and Djabri 2017 (see Figure 2.11).

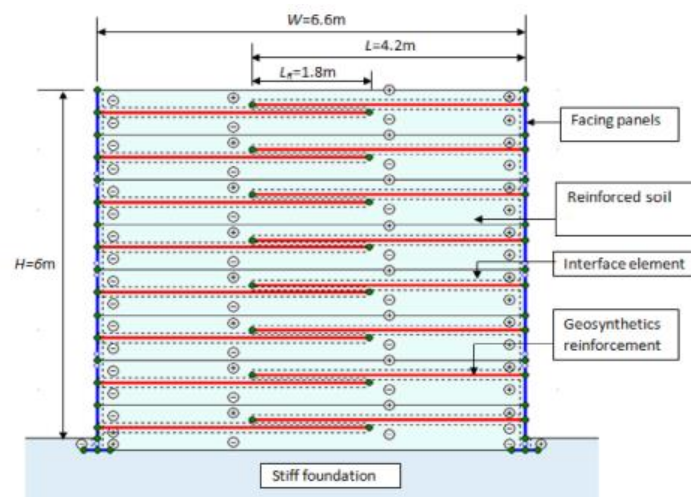


Figure 2.11. The geometry of baseline case $L_R = 0.3H$ (Benmebarek and Djabri 2017).

The following results were obtained:

- ✓ Increasing in the overlapping reinforcement length L_R lead to increase in the facing displacement and the factor of safety.
- ✓ When the L_R/H ratio is more than 0.3, overlapping of reinforcements has a major impact on internal stability.
- ✓ The conventional analytical calculation NFP 94-270 for maximum tensile loads in the reinforcement is more conservative than FE results.
- ✓ Reducing the length of overlapping reinforcements to $0.6H$ and this is somewhat less than the length allowed by the FHWA recommendations.
- ✓ The height and width of the wall has significant effect on external and internal stability of the walls.

2.2.2.7. Sarvanam et al. (2019)

Sarvanam et al. (2019) studied the effects of surcharge and compaction stresses on lateral pressures, lateral displacements and the maximum tensile forces in the reinforcements along the depth of back-to-back MSE walls using a finite difference method (FLAC 2D) (see Figure 2.12). The distance between walls to the height of the wall (W/H) ratio is varied between 1.4 and 2.0, and the reinforcing stiffness is varied between 500 and 50,000 kN/m.

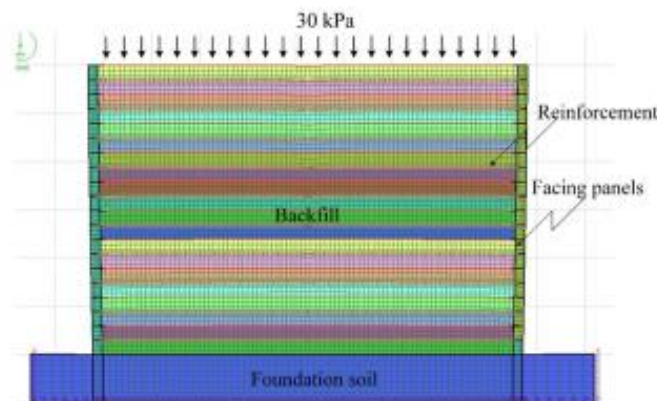


Figure 2.12. FLAC model of back-to-back wall with mesh and surcharge application (Sarvanam et al., 2019).

The following results were obtained:

- ✓ For all W/H ratios, the variation of lateral pressures with depth at the end of the reinforcement length are bilinear.
- ✓ The W/H ratio had no effect on lateral pressures at the facing.
- ✓ Critical depth, Z_c , at which lateral pressures rapidly increase with depth with increasing in the reinforcement stiffness J , and the W/H ratio, but it is virtually unaffected by loading conditions.
- ✓ Surcharge-induced lateral pressures fall considerably more with depth for small reinforcement stiffness, J , and W/H ratio than for high W/H ratio and reinforcement stiffness.
- ✓ Surcharge and compaction stress have an influence till to the bottom of the wall.

- ✓ Without any further changes to the design parameters, connected walls can be designed in the same way as unconnected walls.
- ✓ The FHWA's assumption of at-rest conditions for connected back-to-back walls can result in a very cautious design. In gravity loads, lateral pressures for connected and unconnected walls are nearly comparable in both extensible and inextensible cases. In compaction and surcharge stresses, the lateral pressures at the facing in connected walls are lower than those in unconnected walls.
- ✓ The lateral pressures at the end of the reinforcement zone are underestimated in FHWA guidelines for back-to-back walls, resulting in an overestimation of the factor of safety values in external stability calculations. As a result, the design becomes unsafe.

2.2.2.8. Sarvanam et al. (2020a)

A two-dimensional finite difference method based FLAC software was used to study the performance of connected and unconnected back-to-back MSE walls under working stresses by Sarvanam et al. (2020a) (see Figure 2.13). The objective of this study was to investigate the influence of reinforcement stiffness on tensile force, the maximum tensile force in the reinforcement, and lateral pressures and wall displacement for both unconnected and connected walls.

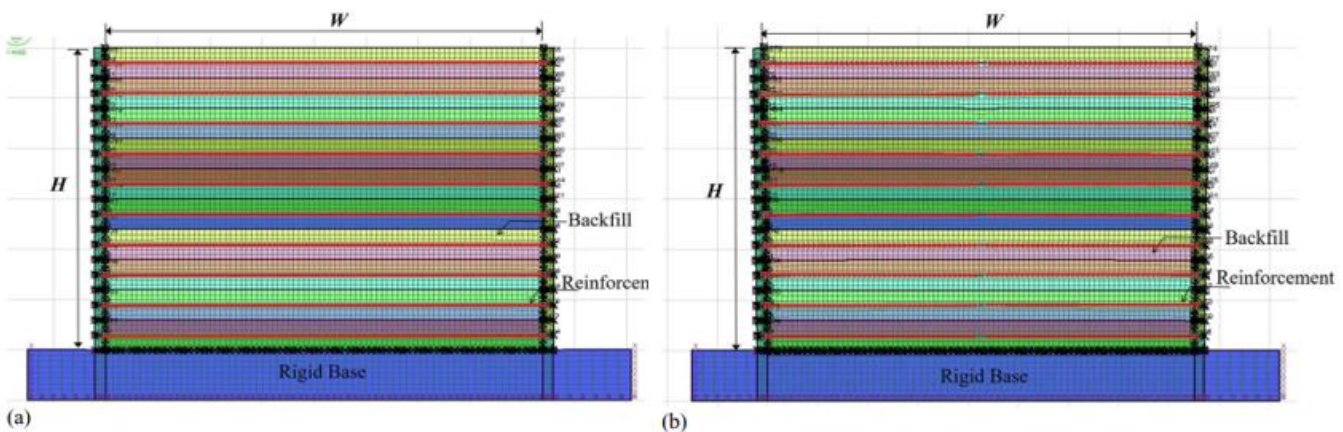


Figure 2.13. FLAC model of back-to-back wall with mesh: (a) connected (b) unconnected walls (Sarvanam et al., 2020a).

The following results were obtained:

- ✓ For the case of the unconnected back-to-back wall with somewhat extensible reinforcement, a well-defined potential failure surface was discovered.
- ✓ The lateral pressures at the facing in both cases are almost identical.
- ✓ The tensile force developed in the connected reinforcement layers case is uniform along its length (except at higher depths).

2.2.2.9. Sarvanam et al. (2020b)

Sarvanam et al. (2020b) studied the single and back-to-back connected walls with full-length panel facia using the finite difference based software (FLAC 2D) (see Figure 2.14). The goal of this research was to analysis the behavior of this both type of walls (single and double opposite faced walls) on Lateral pressures, vertical stresses, and lateral deformations at the facing for different reinforcement stiffness values are evaluated for both single and back-to-back walls under operational stresses. Reinforcement stiffness of 500 kN/m, 5000 kN/m, and 50,000 kN/m were taken into account.

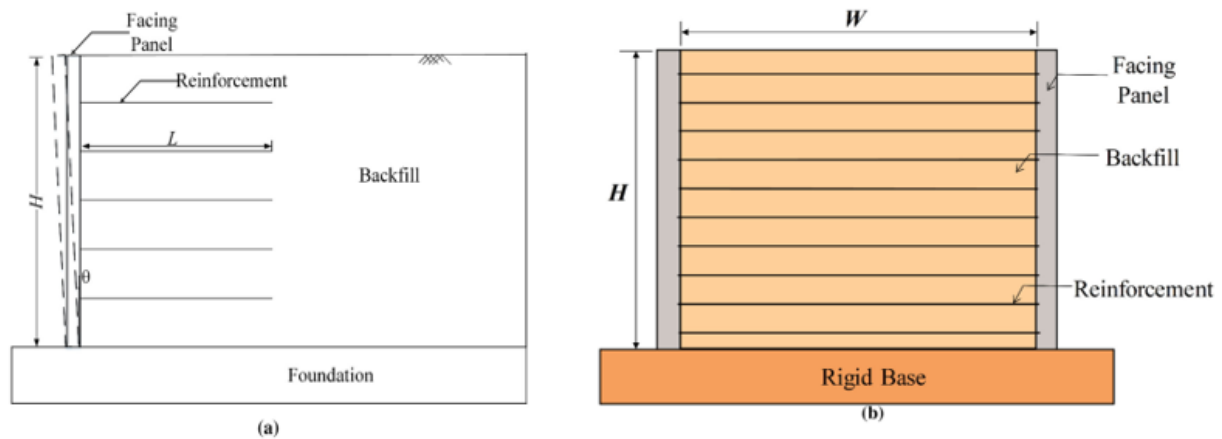


Figure 2.14. Illustration showing: (a) A full-length panel facing MSE single wall representing the lateral deformation (b) unconnected walls (Sarvanam et al., 2020b).

The following results were obtained:

- ✓ The lateral pressures at the facing of a single MSE wall with stiff reinforcement are higher than those for active earth pressure.
- ✓ Lateral facing displacement with low stiffness reinforcement are greater than those with high stiffness reinforcement.
- ✓ The horizontal facing displacement with high stiffness reinforcement is slightly inwards near the top of the wall in back-to-back walls.

2.2.2.10. Yang et al. (2020a)

Yang et al. (2020a) used the finite element approach to investigate the mutual effect range and influence mode of back-to-back geogrid reinforced soil walls (BBGRSW) with various panel widths and slope angles, and also the position of the potential slip surface in the non-reinforced zone of the Geosynthetics Reinforced Soil (GRS) wall using the slip line field theory of the non-associated flow rule. Figure 2.15 shows the Plaxis model of layout of back-to-back geogrid reinforced soil walls (BBGRSW).

The following results were obtained:

- ✓ The horizontal displacement of the wall is affected when the distance D between the reinforced sections on both sides of the BBGRSW is smaller than the wall height.
- ✓ The lateral earth pressure distribution at the end of the wall reinforcement is similar to the Rankine active earth pressure distribution.

- ✓ The deformation and distribution of earth pressure on the right wall can be affected by a change in the slope angle of the left wall.
- ✓ The fundamental reason for influencing the distribution of geogrid tensile force is that there is an embedded action region between the reinforcements on both sides.
- ✓ The active sliding surface of the soil behind the reinforced soil zone is sandwiched by the horizontal plane and the angle is roughly $45^\circ + \psi/2$, not the Rankine active fracture surface mentioned in the FHWA design guidance.

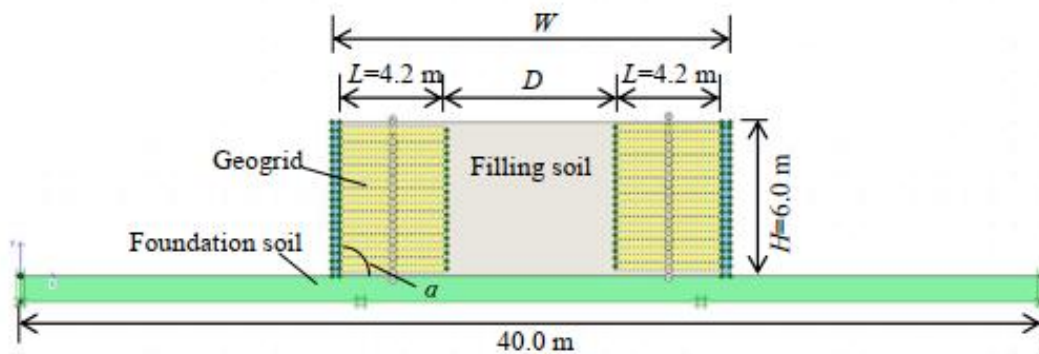


Figure 2.15. Plaxis model of back-to-back geogrid reinforced soil walls (Yang et al., 2020a).

2.2.2.11. Rajagopal and Thiyyakkandi (2021)

Rajagopal and Thiyyakkandi (2021) contrasted the overall performance of back-to-back MSE walls with a trapezoidal marginal fill zone surrounded by a near-optimal quantity of select fill (i.e., hybrid fill) as an alternative to a wall with a chosen fill. Finite element modelling was used to compare the behaviour of hybrid-fill walls at the termination of construction and during high rainfall infiltration with fully select fill and fully marginal fill walls (see Figure 2.16).

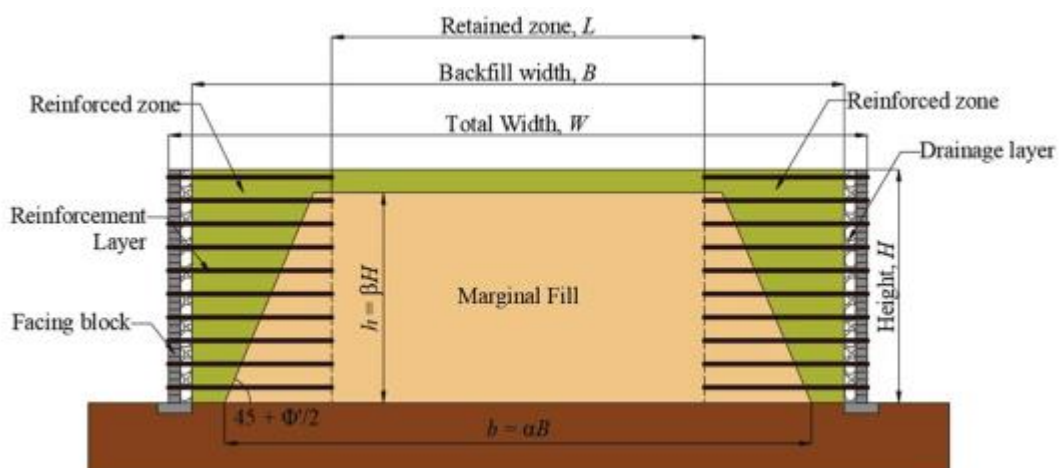


Figure 2.16. Proposed hybrid back-to-back wall (Rajagopal and Thiyyakkandi 2021).

The following results were obtained:

- ✓ The hybrid-fill wall with 31–47 per cent select fill outperforms a totally marginal fill wall in terms of overall performance (i.e., horizontal and vertical displacement, maximum reinforcement tensile loads, and factor of safety), notably under the severe rainfall penetration scenario.
- ✓ In areas where a significant quantity of well-graded soil is not readily accessible, the suggested hybrid-fill wall provides a stable and cost-effective alternative method.

2.2.2.12. Xu et al. (2021)

The upper-bound bearing capacity of footing on back-to-back MSE walls was investigated using finite element limit analysis (FELA) method employing the cutting-edge program OptumG2 by Xu et al. (2021) (see Figure 2.17). The study's goal is to look at how the distance between reinforced zones, wall height, reinforcement design, and footing width and position affect expected bearing capacity and failure mechanisms of back-to-back MSE walls.

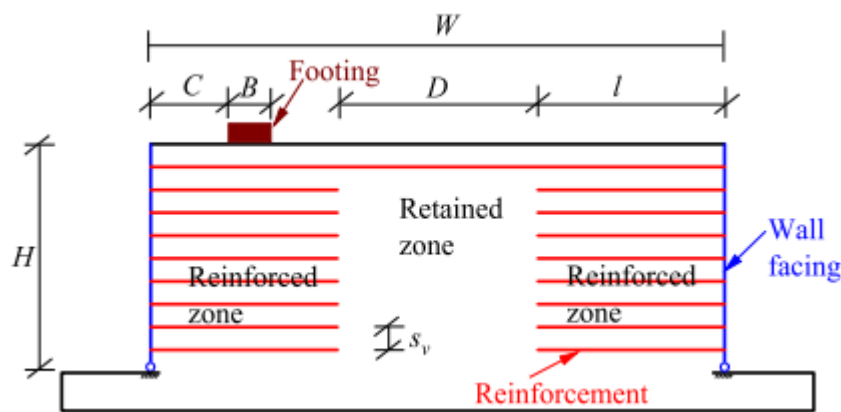


Figure 2.17. Back-to-back MSE wall model schematic diagram (Xu et al., 2021).

The following results were obtained:

- ✓ With increasing wall height, the influence of wall height on bearing capacity reduces.
- ✓ If the footing toe is on the top of the retained zone, a vertical slip plane might occur at the back of the reinforced zone in walls with tight reinforcement.
- ✓ The most effective approach of improving the bearing capacity of the structure subjected to footing load is to use a full length top reinforcement layer (rather than lower-level layers) to link the back-to-back walls.

2.2.3. Experimental studies

The experimental studies of back-to-back reinforced soil walls are very limited, where does not exceed one study (Yang et al., 2020b) in addition to Won and Kim 2007.

2.2.3.1. Won and Kim (2007)

To test the influence of the geosynthetic type on the wall's internal deformation, a full-scale back-to-back geosynthetic-reinforced wall was built by Won and Kim, 2007 (see Figure 2.18). No contact was seen from two sides of walls due to the huge distance $D (= 0.88H)$.



Figure 2.18. The geosynthetic reinforced soil (GRS) walls of Won and Kim 2007.

2.2.3.2. Yang et al. (2020b)

Yang et al.(2020b) conducted a 60-month long-term remote observation testing of the back-to-back geogrid reinforced retaining wall of the Qing-Rong passenger dedicated railway in Shandong Province (Figure 2.19). The goal of this research was to look at the performance of back-to-back reinforced retaining walls after they were built, as well as the lateral earth pressure on the reinforced soil wall. Pressure cells and flexible deformation gauges were used to monitor the vertical tension along the wall's base and the tensile force on the geogrid.



(a) Left side of the GRS wall



(b) Right side of the GRS wall

Figure 2.19. Back-to-back GRS walls near Rongcheng station (Yang et al., 2020b).

The following results were obtained:

- ✓ The pressure on the wall and its deformation were nearly constant.

- ✓ During the 60 months after construction, the lateral earth pressure on the back of the wall panel was estimated to be around 119.2 percent of the completion time.
- ✓ During the 60 months following construction, the reinforced soil retaining wall's vertical stress remained nearly constant.
- ✓ The strain of the geogrid in the wall showed stage-type variations.
- ✓ Only around 30% of the peak strain was accounted for the measured geogrids' maximum strain.
- ✓ The amount of displacement on the wall was minimal, indicating that both sides of the wall were in good shape.
- ✓ These findings can be used as a guide for optimizing the construction of reinforced soil retaining walls for high-speed railroads.

PART II
Numerical Analysis

CHAPTER THREE

2D Finite Element Analysis

3.1. Introduction

This study describes the results of a series of 2D finite element method simulations that were carried out on an idealized 6 m high wall with geometrical cases 1 and 2 shown in Figure 2.6 (see chapter Two). The reinforced soil wall is composed of precast concrete panel facing and polymeric strip reinforcements. The polymeric strips are made from bundled high-tenacity polyester yarns (providing tensile strength) that are encased in a polyethylene sheath (providing interface frictional strength, alignment, and protection of the inner yarns). The strips may be placed in a continuous wrapped arrangement (loops) as in Figure 3.1a, or placed as single strips (free tail ends). The strips ending at the back of the reinforced backfill (i.e., at L distance from facing) are fixed to the ground using different methods such as rear anchorage bars for the case of continuous strip loops (Figure 3.2b), using trenches that provide tension during backfilling and compaction (Figure 3.3c), or single steel triangles or plates attached or clamped to the strips and pegs drilled or staked into the backfill (for continuous and single strips). Prior to backfilling over each extensible reinforcement layer, the current construction practice is to apply some tension to the reinforcements with the purpose of removing any slack and to minimize any facing deformation during the mobilization of the reinforcement tensile forces (FHWA 2009 and EN 2006). To achieve this initial tight condition for polymeric strips, pre-tensioning the load by hand is typically enough. However, in some cases, a constant and uniform pre-tensioning load level may be required for all reinforcement strips in a layer.

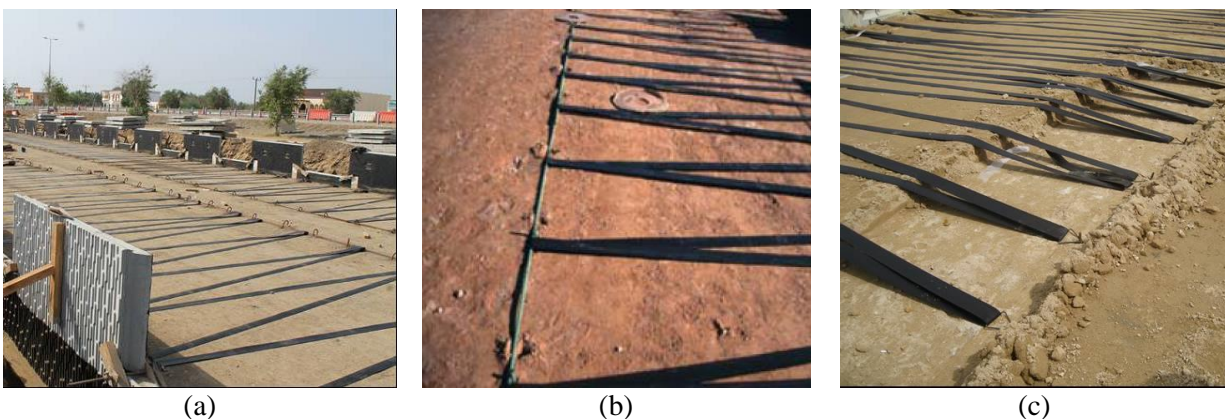


Figure 3.1. On-site polymeric strip installation examples: (a) back-to-back wall case, (b) longitudinal bar back anchorage and pegs, and (c) trench and triangle anchorage. (Photographs courtesy of VSL Construction Systems—VSoL® Retained Earth System).

In this study, single layers connected to both facing walls with ratio $W/H = L = 0.7H$, two different ratios of $L_R/H = 0.3$ and 0.6 , and three different ratios of $D_i/H = 0, 0.3,$ and 0.6 are considered together with no pre-tensioning and two different pre-tensioning loads applied to all reinforcement layers during construction. The influence of small uniform surcharge loads due to a thin pavement layer and traffic is also examined for the case with the largest interaction distance between opposing reinforced soil zones. The study also considers polymeric strip reinforcement with smooth and perforated sheathing treatments, which generate different soil-reinforcement interaction performance. A two-dimensional numerical analysis of a back-to-back reinforced soil wall is carried out using the finite element method (FEM) commercial software PLAXIS 2D.

3.2. Finite Element modelling

3.2.1. General

The 2D PLAXIS FEM program was used to model the construction and post-construction performance of back-to-back reinforced soil wall simulations. The FEM mesh including geometry details for the baseline model used in this study is shown in Figure 3.2. The assumed foundation soil was 10 m deep and 50 m long. The height of both wall facings (H) was kept constant and equal to $H = 6$ m, with toe embedment depth of 0.6 m (i.e., equal to $0.1H$). The walls were assumed to comprise eight reinforcement layers within the structural height (i.e., vertical reinforcement spacing of 0.75 m). The length of the polymeric strip reinforcement elements was taken as $L = 0.7H$ (typical minimum value recommended in many international codes in the Design of Mechanically Stabilized Earth Walls and Reinforced Slopes (FHWA), the Load Resistance Factor Design (LRFD) Bridge Design Specifications (AASHTO), and the Code of Practice for Strengthened/Reinforced Soils and Other Fills (BSI)). The soil zones were modelled using 15-node triangular elements (69,737 nodes from 7891 elements). The element areas were reduced to 0.005 m² at soil-facing and soil-reinforcement interfaces, and to 0.0001 m² adjacent to the horizontal panel joints where elastomeric bearing pads are modelled. In order to achieve a better wall performance in terms of horizontal facing displacements, staged construction was modelled using a sequence of 0.375 m thick layers. Compaction effects were not modelled directly but the soil modulus was modified in the vicinity of the facings to at least partially account for the compaction method, as discussed later. Panel installation was performed using temporary stiff beam element connections (see Figure 3.2—panel clamp detail). During construction, these beam elements were prevented from rotating to simulate the panel clamp and/or propping devices typically used in practice to temporarily sustain and provide the required panel unit alignment (Damians et al., 2015).

3.2.2. Soil and road pavement

The material properties for the soil material zones (i.e., backfill and foundation) and road pavement are summarized in Table 3.1. For simplicity, the soil was modelled as linear elastic perfectly plastic with Mohr–Coulomb failure criterion. The thin pavement layer was

modelled as a linear-elastic material to avoid any unexpected and non-relevant behaviour (for the scope of this study) at that location. A lower soil elastic modulus within 1 m distance of the wall facing was used to model the influence of lighter compaction equipment typically used close to the facing.

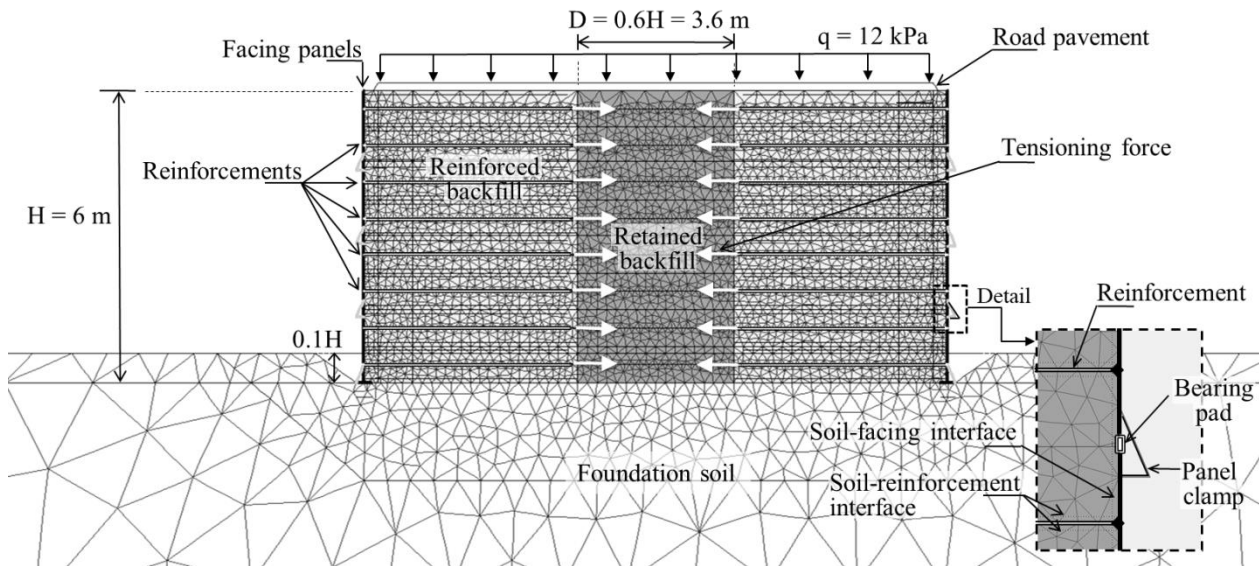


Figure 3.2. Detail of the FEM model and mesh for the base case with $D_1 = 0.6H$. Note: foundation soil zone has dimensions of 50 m wide and 10 m deep.

Table 3.1. Model properties for backfill, foundation soil, and pavement materials.

Parameter	Backfill		Foundation	Road Pavement (20 cm Thick)
	(Distance from Face ^(a)): >1 m	<1 m		
Unit weight, γ (kN/m ³)	18	18	20	23
Friction angle ^(b) , ϕ (°)	44	44	40	-
Dilatancy angle, ψ (°)	14	14	10	-
Cohesion, c (kPa)	1	1	10	-
Elastic modulus, E (MPa)	50	25	1000 ^(c)	3500
Poisson's ratio, ν (-)	0.3	0.3	0.3	0.35

^(a) Backfill properties were assumed to vary due to lower compaction effort near the facing. ^(b) Peak friction angle assuming plane-strain boundary conditions (equivalent to about 36–37° under triaxial conditions by Damians et al. 2016). ^(c) Foundation assumed to be rigid enough to not generate undesired/out of this paper's scope instabilities. Extended sensitivities regarding foundation stiffness variations can be found in Damians et al., 2013; Damians et al., 2014; Damians et al., 2016.

3.2.3. Facing: Precast Panels and Bearing Pads

The wall facing was modelled assuming discrete panels of 1.5 m height. Panels and bearing pads were simulated using linear-elastic beam elements. Material properties for the precast

concrete facing panels and the high-density polyethylene (HPDE) bearing pads are summarized in Table 3.2. Bearing pads are typically installed in the horizontal joints between adjacent vertical panels. They have the practical function to smoothly distribute vertical loads between the facing panels and to prevent concrete-to-concrete panel contact by accommodating differential facing–backfill settlements (Damians et al., 2013 and Damians et al., 2016) In the present study, two units of 20 mm thick high density polyethylene (HDPE) bearing pads were assumed at each horizontal joint between 1.5 m wide panels.

Table 3.2. Precast concrete panel and bearing pad (joint) properties.

Parameter	Facing Panels (Concrete)	Bearing Pads (HPDE)
Axial stiffness, EA (MN/m)	6000	1.1
Bearing stiffness, EI (kN/m ² /m)	11,000	2.1
Weight, w (kN/m/m)	4.5	0.1
Poisson’s ratio, ν (-)	0.15	0.40

3.2.4. Reinforcements

Polymeric strips were modelled using “geogrid” PLAXIS elements. In 2D representation, the 1D discrete strip elements are simplified and converted to equivalent continuous sheets. In this study, the equivalent linear-elastic axial stiffness (EA) of the polymeric strip reinforcements was computed as follows.

$$(EA)_{\text{polymeric strips}} = \frac{F^*}{\epsilon} \left(\frac{n_{\text{strips}}}{L_{\text{panel}}} \right) \tag{3.1}$$

where F^* is the ultimate tensile load capacity of the strip, ϵ is the strain at nominal ultimate load F^* ($\epsilon \approx 0.10$ – 0.12 from Figure 3.3c), and n_{strips} is the number of strips per panel width L_{panel} (i.e., $n_{\text{strips}} = 6$ units matching the 3 connections for each $L_{\text{panel}} = 1.5$ m); hence $(n_{\text{strips}} / L_{\text{panel}}) = 4$ strips/m corresponds to the number of strips per plane-strain model meter. In this study, the polymeric strips are Grade 30 kN-type, with different strip sheathing shapes (regular-smooth and with center-line perforations); see Figure 3.3a,b, respectively, with a resulting linear-elastic axial stiffness of $(EA)_{\text{polymeric strips}} = 1$ MN/m.

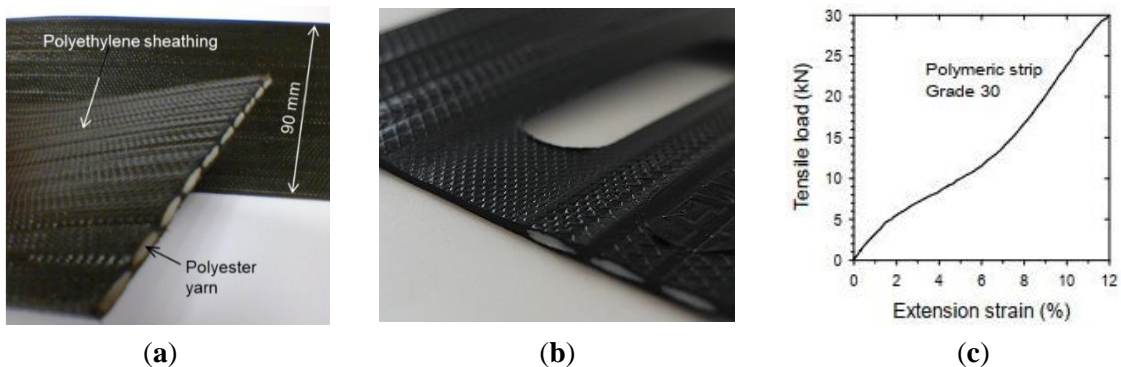


Figure 3.3. Polymeric strip products from GECO : (a) FASTEN FS and (b) FW (perforated), and (c) typical load-extension behaviour of grade 30 strip.

3.2.5. Interface Properties and Boundary Conditions

Facing and reinforcement elements transfer load to the surrounding soil through interface shear. The key parameter quantifying the interaction between the soil and the interface material is the strength–stiffness reduction factor ($R_i \leq 1.0$). It may be applied to the properties of the adjacent soil (default option in PLAXIS) or, as in this study, for a more accurate approach, by defining the interface as a separate “interface” material with the following properties (Equations (3.2)–(2.5)):

$$c_i = R_i c_{\text{soil}} \quad (3.2)$$

$$\phi_i = \tan^{-1}(R_i \tan \phi_{\text{soil}}) \quad (3.3)$$

$$\psi_i = \begin{cases} 0 & R_i < 1.0 \\ \psi_{\text{soil}} & R_i \geq 1.0 \end{cases} \quad (3.4)$$

$$G_i = R_i^2 G_{\text{soil}} \quad (3.5)$$

where: c_{soil} and c_i are the cohesion of the soil and the interface, respectively; ϕ_{soil} and ϕ_i are the friction angle of soil and the interface; ψ_{soil} and ψ_i are the dilatancy angle of the soil and the interface; G_{soil} and G_i are the shear modulus of the soil and the interface, respectively; and $\nu_i = 0.45$ (i.e., assuming oedometric conditions at the interface). In this study, an interface reduction factor of $R_i = 0.3$ was assumed for the soil-facing interface, which is in alignment with values computed from an instrumented field structure (Runser et al., 2001) and numerical analyses reported in the literature (Damians et al., 2015b and Yu et al., 2014). From Equation (3.6) and elastic stiffness relations, Young’s modulus of the interface can be computed as follows:

$$E_i = 2G_i (1 + \nu_i) \quad (3.6)$$

For the soil-strip reinforcement interface considering the 3D to 2D conversion for the strip reinforcement elements, the parameter R_i for each “geogrid” reinforcement layer was computed using the following equation:

$$R_i = \frac{1}{A_{\text{layer}}} \left(\left(C_{i(\text{soil})} A_{\text{soil/layer}} \right) + \left(C_{i(\text{strip})} A_{\text{strip/layer}} \right) \right) \quad (3.7)$$

where: A_{layer} is the total surface area of each reinforcement layer equal to the panel width ($L_{\text{panel}} = 1.5$ m) multiplied by the strip length ($L_{\text{strip}} = 0.7H = 4.2$ m); $A_{\text{strip/layer}}$ is the soil-strip contact area (which depends on the number of strips per metre $n_{\text{strips}}/L_{\text{panel}}$, the strip width (90 mm) and the strip length); $A_{\text{soil/layer}}$ is the soil-soil contact area per layer (i.e., $A_{\text{layer}} - A_{\text{strip/layer}}$); C_i refers to the coefficient of interaction defined as $C_i = \tan \phi_i / \tan \phi_{\text{soil}}$. Therefore, $C_{i(\text{soil})}$ corresponds to the soil-soil interaction coefficient ($C_{i(\text{soil})} = 1$) and $C_{i(\text{strip})}$ is the soil-

reinforcement interaction coefficient, assumed equal to 0.8 as per product default specifications for the smooth strip case. However, according to pull-out tests performed on high adherence perforated strips (FASTEN FW product; see Fig. 3.3b) and with the same or similar soil, an additional case with variable values of $C_{i(\text{strip})}$ from 1.51 (bottom layer) to 3.15 (top layer) was assumed. These values are much higher than the typical values for smooth soil-polymeric strip interaction assuming frictional/shear strength only (i.e., $C_{i(\text{strip})} \leq 1$). However, the perforated strip materials generate significant additional interface strength through bearing capacity due to granular particle interlock in the perforations (similar to the passive soil resistance developed by the transverse members in steel ladders and grids). Nevertheless, no design recommendations are currently available to account for this additional capacity. The assumptions made in this paper for the perforated strips are for preliminary purposes only and to demonstrate potential improvement in wall performance using these materials. The corresponding interface property values assumed for soil-facing and soil-reinforcements are shown in Table 3.3 for both smooth and perforated strip types.

Table 3.3. Interface material properties.

Parameters	Soil-Facing Interface	Soil-Reinforcement Interface:			
		Smooth Strip		Perforated Strip	
		(Distance from Back of the Facing):			
		>1 m	<1 m	>1 m	<1 m
Cohesion, c_i (kPa)	0.3	0.93		1.19 to 1.77	
Friction angle, ϕ_i (°)	16	42		49 to 60	
Dilatancy angle, ψ_i (°)	0	0		14	
Shear modulus, G_i (MPa)	0.9	8.4	16.7	27.0–60.4	13.5–30.2
Elastic modulus, E_i (MPa)	2.5	24	48	78.3–175.2	39.2–87.6
Interface strength-stiffness reduction factor, R_i (Equation (2.7))	0.3	0.93		variable: from 1.19 (bottom) to 1.77 (top)	

3.3. Numerical modelling verification

In order to develop confidence with 2D PLAXIS finite element modelling, a comparison with a representative 6.0 m high full-scale model was performed. The full-scale monitored structure considered for this purpose was the one reported by Jayakrishnan 2013 (see previous reference for full details). Note that the single-faced reinforced soil wall data was used in this study as no experimental study results on representative back-to-back reinforced soil walls were found available in the literature. This reinforced soil wall was constructed using polymeric strip reinforcements with a vertical spacing of 0.75 m and a horizontal spacing of 0.76 m placed in the backfill and connected to 1.48 m square concrete facing panels. The length of the polymeric strips changed according to the depth from 4.08 m at the lower levels to 5.08 m at the top. The value of the ultimate tensile load (i.e., strips grade) was about 45 kN per strip, while the strain at failure was 12%. The axial stiffness (EA) for a single geostrip is about 375 kN and the equivalent axial stiffness $EA_{\text{equivalent}}$ is about 1 MN. The soil properties used for verification modelling were the same as the experimental data

(see Table 3.4). Detailed information of the field instrumentation can be found in Jayakrishnan 2013 and Capelleri 2019. Figure 3.4 shows the full-scale and schematic of instrumented MSE wall. Figure 3.5 shows details of the FE numerical model and mesh generated for the full-scale reinforced soil wall comparison and verification purposes.

Figure 3.6 presents reinforcement tensile load results comparison between the calculated FE model and experimental data measurements from the experimental full-scale test from Jayakrishnan 2013. As can be seen, both maximum and tensile reinforcement axial loads distribution comparisons with the calculated results were consistent, which verified the reliability of the modelling methodology and modelling assumptions involved using PLAXIS 2D.

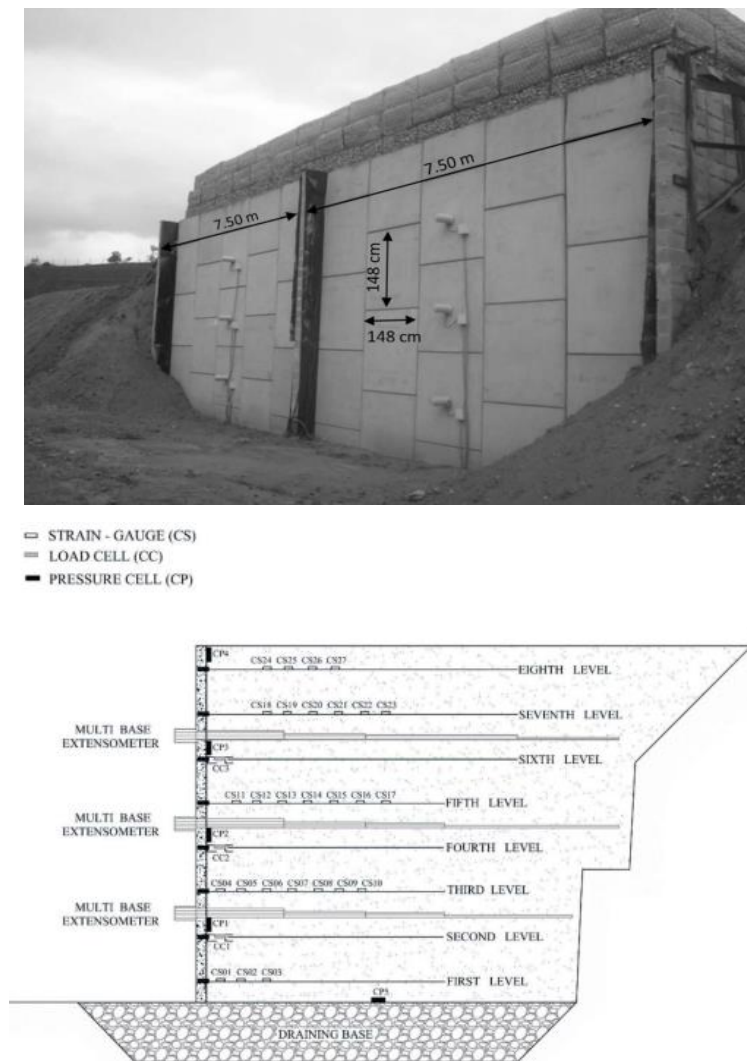


Figure 3.4. A full-scale and Schematic of instrumented MSE wall used for validation. (Jayakrishnan 2013).

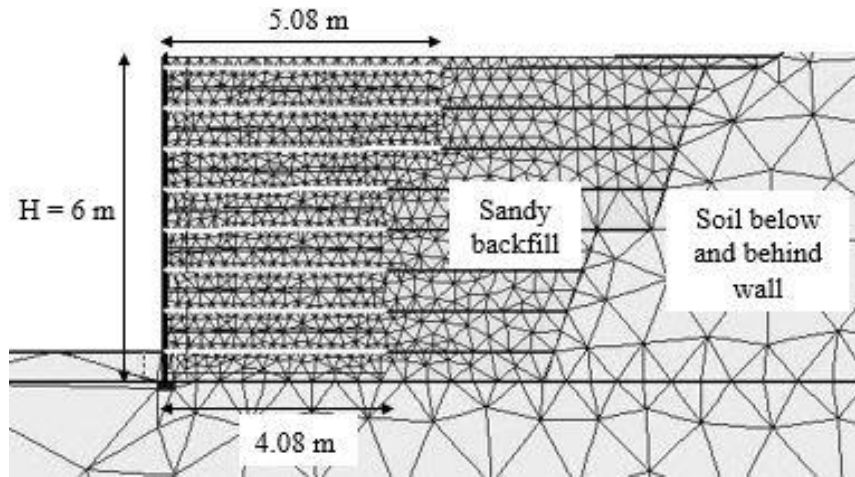
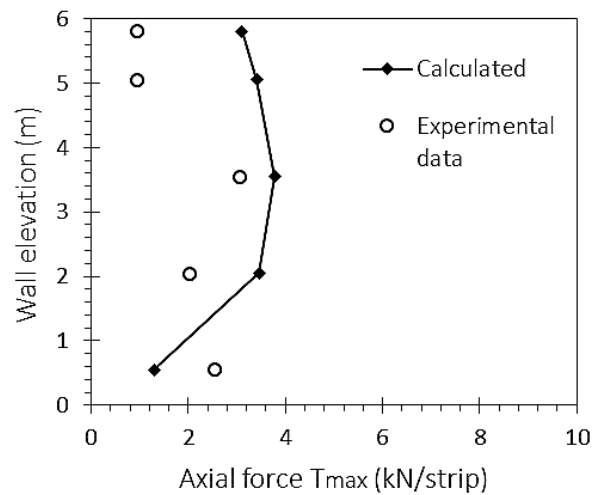


Figure 3.5. Detail of the FEM model and mesh of experimental wall used for calibration.

Table 3.4. Soil properties (taken from Jayakrishnan 2013).

Parameter	Sandy Backfill	Soil below and behind the Wall
Material model	Mohr-Coulomb	Mohr-Coulomb
Unit weight, γ (kN/m ³)	17	18.5
Elastic modulus, E (MPa)	50	60
Poisson's ratio, ν (-)	0.3	0.3
Cohesion, c (kPa)	0	20
Friction angle, ϕ (°)	42	38

(a)



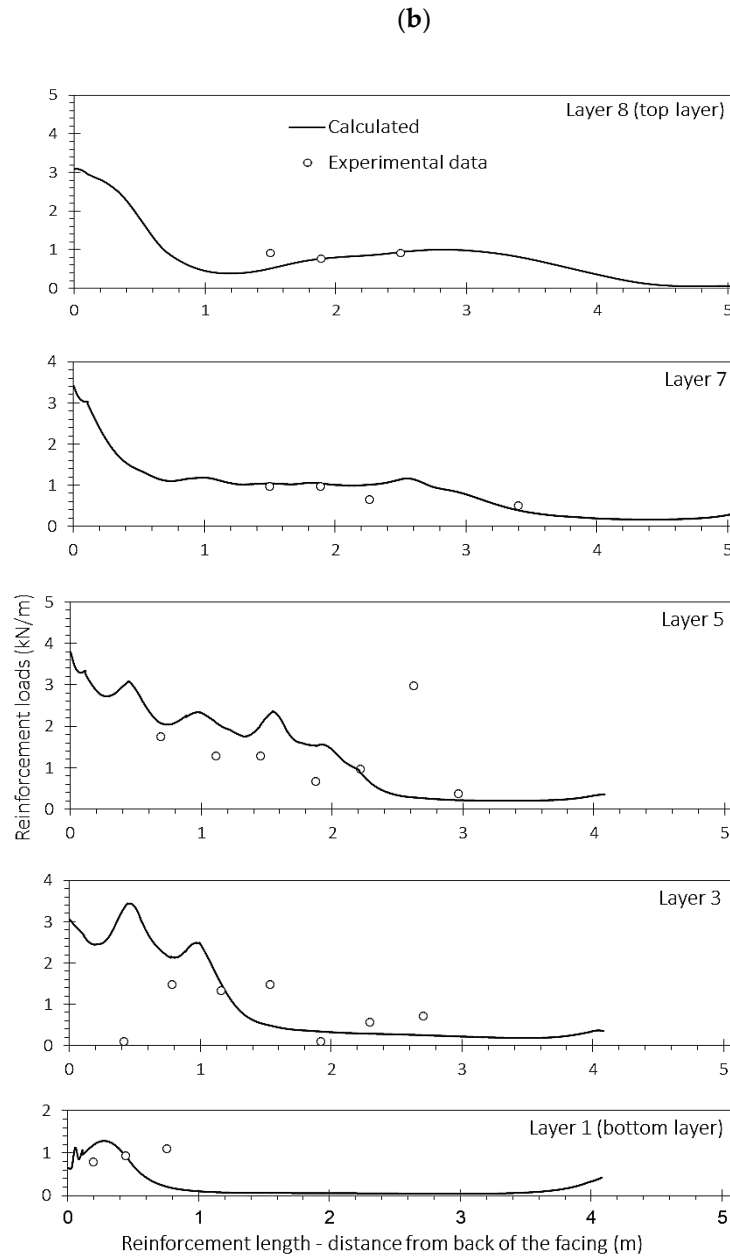


Figure 3.6. Comparison between the FE model results and the experimental data (Jayakrishnan 2013) : (a) maximum reinforcement axial force per strip, and (b) distribution of axial force along reinforcement strip.

3.4. Numerical Results and Discussion

3.4.1. General

Facing displacement, lateral earth pressure, and reinforcement tensile load distributions were computed for cases with different interaction distance between the back of the reinforced soil zone for opposite walls (base case $D_i = 0.6H$, $D_i = 0.3H$, $D_i = 0$; continuous or discontinuous strips from one wall face to the opposite wall face), different overlapping distance ($L_R = 0.3H$, $L_R = 0.6H$), and single layers connected to both walls facing ($W = L = 0.7H$). The magnitude of pre-tensioning load (no-tension, 0.5 kN/strip, and 1 kN/strip), and

soil-reinforcement interaction (R_i constant or variable; see Table 3.3). The unconnected strip reinforcement case ($D_i = 0$) was generated assuming a 10 cm distance between the opposite tail ends. Due to the symmetry of the general problem, results are presented for the left half of the problem domain. In addition to the facing displacements, lateral earth pressure and reinforcement loads, shear strain contours and plastic (failure) zones are also given for some cases when relevant. The results of sensitivity analyses were performed around the base case scenario with $D_i = 0.6H$ geometry at the end of construction (EoC), without pre-tensioning and constant R_i (i.e., smooth strips). As noted in the introduction, construction method and quality (e.g., panel placement and alignment, and soil placement and compaction) will influence wall performance. These factors cannot be captured in numerical models of the type used here.

3.4.2. Effect of the Interaction Distance (D_i) between Back-to-Back Walls

Figure 3.7 presents computed horizontal facing displacements at the end of construction (EoC) for different back-to-back interaction distances (D_i), overlapping length reinforcement distances (L_R), and single reinforcement layers attached between both opposite facing walls ($W = L = 0.7H$). As expected, the greater the overlapping distance ($L_R = 0.6H$), the smaller the outward wall displacement. However, when D_i was decreased from $0.6H$ to $L_R = 0.6H$, the permanent displacement decreased more than 50%. For brevity, the influence of the equivalent road pavement surcharge pressure (about 4 kPa) and live load (LL) surcharge application ($q = 12$ kPa) are shown for the base case $D_i = 0.6H$ only. The influence of other interaction distances (D_i) and overlapping distance (L_R) can be estimated by interpolation. For the case of $D_i = 0$, whether or not the reinforcement layers were connected did not make a practical difference on wall displacements due to the self-weight loading conditions (uniform loading) used in the models.

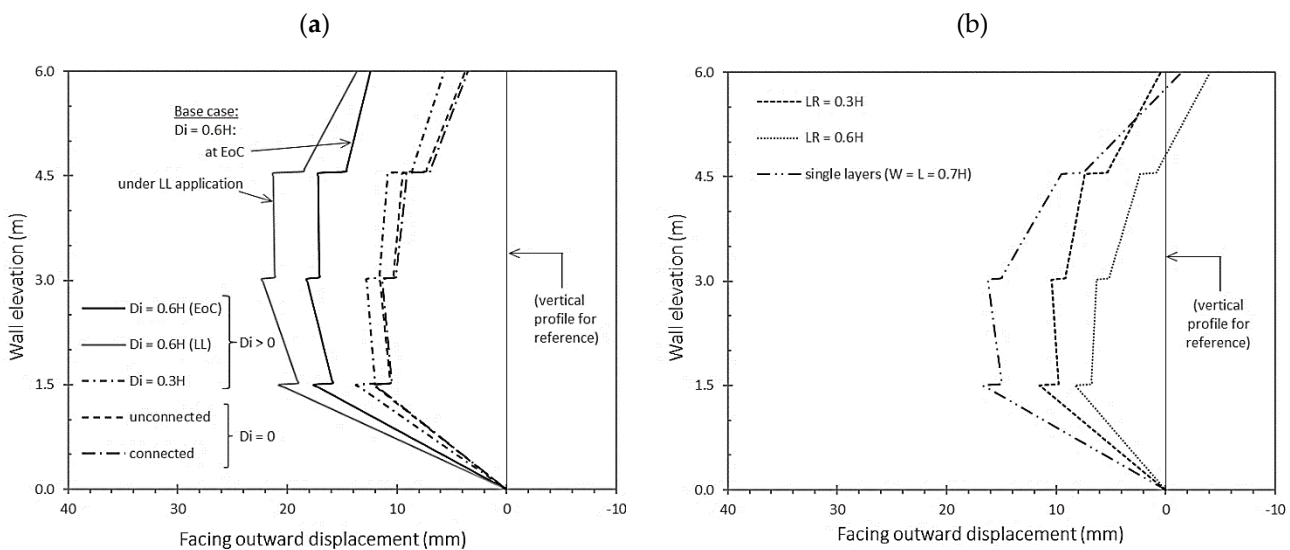


Figure 3.7. Facing displacements at the end of construction (EoC) for different interaction distances (D_i) between the back of the reinforced soil zone for opposite walls: (a) $D_i > 0$ and $D_i = 0$, and (b) $D_i < 0$.

Contour plots of shear strains achieved at the end of the construction are shown in Figure 3.8 for back-to-back wall interaction distances of $D_i = 0$ (connected and unconnected strip), $0.3H$ and $0.6H$, and with overlapping length reinforcement distances of $L_R = 0.3H$ and $L_R = 0.6H$, in addition to single strip connected to both of the facing walls ($W = L = 0.7H$). The internal soil shear zones fall within the 0–1% strain range (i.e., working stress conditions for polymeric strip reinforced soil systems by Miyata et al., 2018). Relatively high shear strains can be seen to propagate from the toe of the walls. While there were some isolated shear strains, even greater than those shown in Figure 2.15, they were not contiguous which is consistent with the notion of end-of-construction working stress conditions assumed in this study. The shear strain fields for $D_i = 0.3H$ and $D_i = 0.6H$ cases are similar. However, soil shear strains were attenuated to almost zero to below the upper third of the height of the wall for $D_i = 0$ to $L_R = 0.6H$ cases due to the presence of the reinforcement layers, but regarding the single layer case ($W = L = 0.7H$), the soil shear strain return increased to less than the upper third of the wall height (from $H/3$ to $H/1.14$). This is due to the reduction in the reinforcements layers (single not double).

Figure 3.9 shows the shear strains achieved at failure with the ϕ - c reduction method at the end of construction for back-to-back walls with different interaction distances (D_i), from 0–1% deformation. Relatively high shear strains can be seen to propagate from the toe to the top of the walls. As shown, the shear strain within back-to-back walls in both cases, $D_i = 0.6H$ and $0.3H$, intercept each other from two sides; more interactions occur as the interaction distance (D_i) decreases. The interaction distance (D_i) based on the FHWA design guideline can be determined using Equation (1.44), which is equal $0.42H$. In other words, when the interaction distance D_i is greater than $H \tan(45^\circ - \phi/2)$ ($0.42H$ assumed in this case study) the back-to-back wall should perform independently, but when the interaction distance D_i is lower than $H \tan(45^\circ - \phi/2)$, it should not perform independently. However, Figure 3.9 shows that the back-to-back walls still interact with each other when $D_i = 0.6H$. Thus, this assumption in the FHWA design guideline is apparently not supported by the obtained numerical results. However, the FHWA assumption provides more conservative results. For the case $D_i = 0$ with unconnected and connected layers as demonstrated in Figure 3.9, the shear strain in the two opposing walls enter the reinforced zone from another side, as the area of entrance increases when the layers are connected. For the overlapping cases $L_R = 0.3H$, $0.6H$ and single layers case ($W = L = 0.7H$), it can be seen, in general, that the interaction distance between the opposite facing walls have a signifying influence in the development of shear strain which expands from the top to bottom until reaching a clear base-failure at the toe of the structure. In addition, the shear strain zone is located at the end of the overlapping reinforcements. The factor of safety (FoS) increases about 130% from $D_i = 0.6H$ to $L_R = 0.6H$ case. On the other hand, the factor of safety (FoS) increases just 3% from $D_i = 0.6H$ to the single layers case ($W = L = 0.7H$).

Contour plots of plastic (failure) points for walls with different interaction distances (D_i) at the end of construction and at failure with the ϕ - c reduction method are presented in Figures 3.10 and 3.11, respectively. At the end of construction (EoC), the interaction distance

reduction (i.e., from $D_i = 0.6H$ to $L_R = 0.6H$ case) allows a tensile crack to develop at the wall top (from 0.375 m to 1.9 m), but regarding the single layers case ($W = L = 0.7H$), the tensile crack development occurs just at about 0.5 m depth from the top of the wall. As the interaction distance decreases, the failure points become swollen forming a slope approximately 65° from the facing element. At failure, the mass of plastic points becomes larger as the interaction distance between the back-to-back reinforced soil wall decreases (i.e., from $D_i = 0.6H$ to $L_R = 0.6H$ case, and also the single layer case, $W = L = 0.7H$).

Numerical results for horizontal pressures at different cross-section plane distances from facing panels, and calculated values of total horizontal stress from the Rankine coefficient of active earth pressure (K_a) and the coefficient of earth pressure at rest (K_o), at facing, at 1 m from facing, and behind the reinforcements (i.e., at L-distance from facing), are plotted in Figures 3.12–3.14, respectively. It is noted that the numerical results for lateral earth pressure at facing (Figure 3.12) are lower than the analytical ones. The closest agreement is obtained with the active Rankine lateral earth pressure when the interaction distance is large (i.e., $D_i = 0.6H$ and $D_i = 0.3H$) except for the upper half-height for single layers case (where a less yielding structural scenario closer to the at-rest stress state (K_o) is generated; see Figure 3.12d) and the base of the wall for cases from $D_i = 0.6H$ to $L_R = 0.3H$ and single layers ($W = L = 0.7H$) (due to the restraint imposed at the base of the walls by the toe embedment, as also observed by wall displacements). Similar observations have been made from full-scale walls (Won and Kim 2007; Huang et al., 2010). However, when the interaction distance (D_i) decreases from $0.6H$ to 0 and the overlapping L_R increases from $0.3H$ to $0.6H$, the lateral earth pressure decreases. For the case $D_i = 0$ with unconnected or connected layers, the lateral pressures in both were almost the same. As for the single layers case ($W = L = 0.7H$), higher values of lateral earth pressure are obtained compared with the other cases. For lateral earth pressure at 1 m from facing (Figure 3.13), there is an over predicted horizontal pressure for all cases compared with the lateral earth pressure acting as the facing. Behind the reinforced zone cases for $D_i > 0$ and $D_i = 0$ (Figure 3.14), an increase in lateral earth pressure was recorded compared with the results obtained at other distances from the facing. However, a decrease in lateral earth pressure is obtained at the bottom for all cases compared with the results obtained at 1 m distance from facing. As is shown, for $D_i = 0$ cases (both connected and unconnected layer scenarios) the lateral earth pressure is generated behind the reinforced zone. However, the FHWA guidelines suggested that the lateral earth pressure for external analysis should be ignored if $D_i = 0$. This suggestion would yield an unsafe design. However, FHWA guidelines indicate that the active thrust is reduced when there is a decrease in D_i (i.e., $D_i = 0.6H$ to $D_i = 0.3H$), which is confirmed by the FEM method.

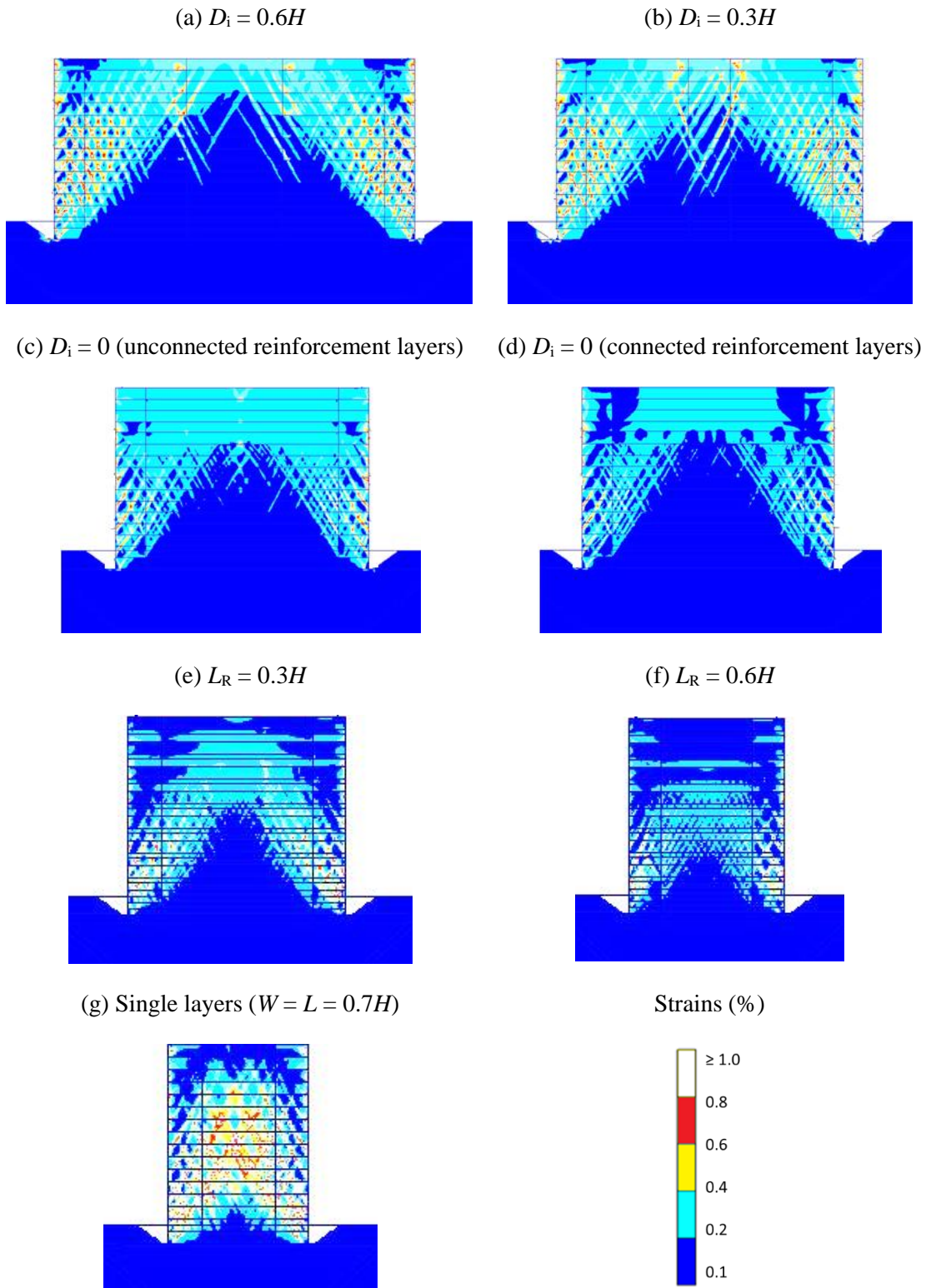


Figure 3.8. Shear strain contours at end of construction (EoC) for walls with different interaction distance (D_i) between the back of the reinforced soil zones for opposite walls. Note: results ranging from 0 to 1%.

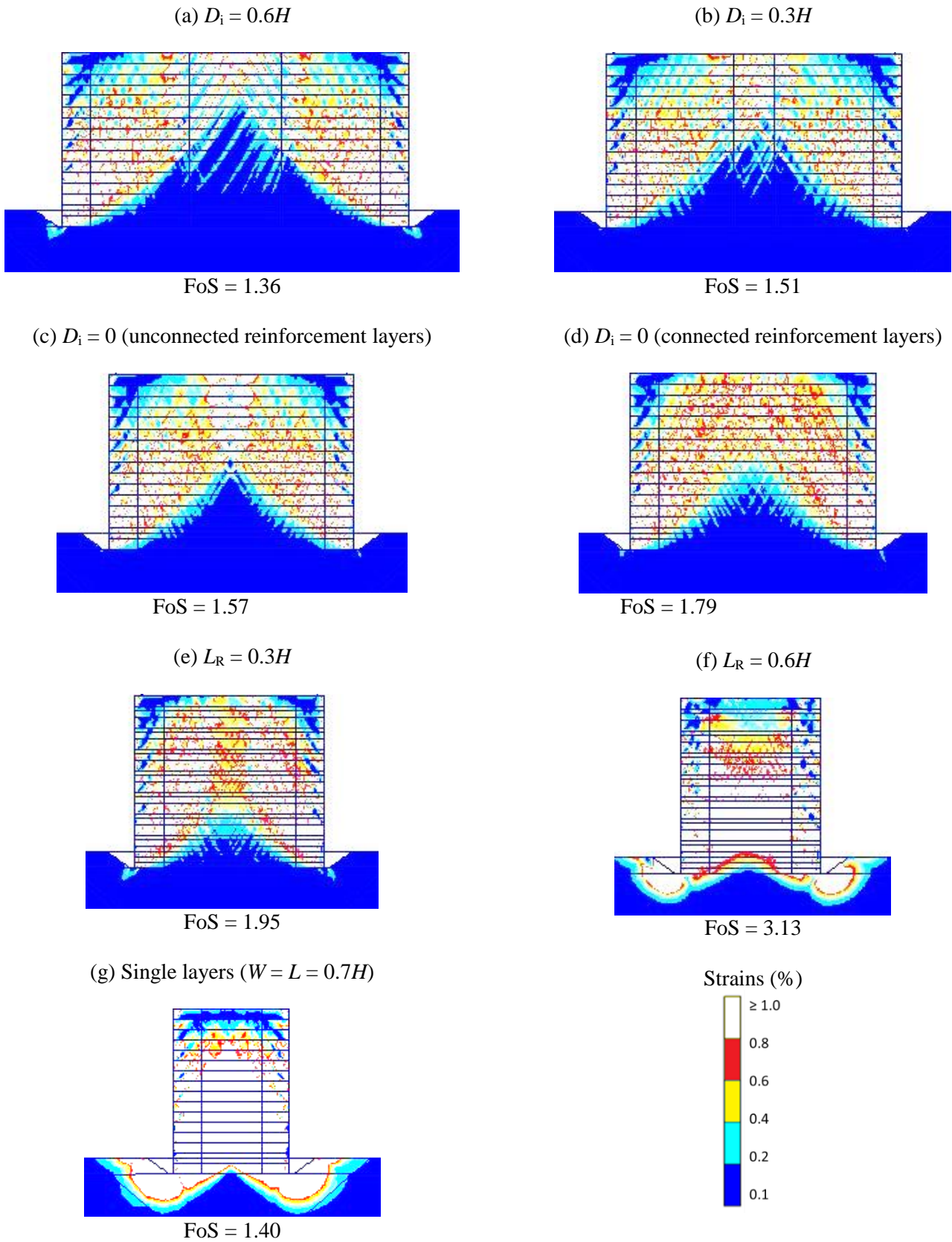


Figure 3.9. Shear strain contours at failure with ϕ - c reduction at end of construction (EoC) for walls with different interaction distance (D_i) between the back of the reinforced soil zones for opposite walls. Note: results ranging from 0 to 1%.

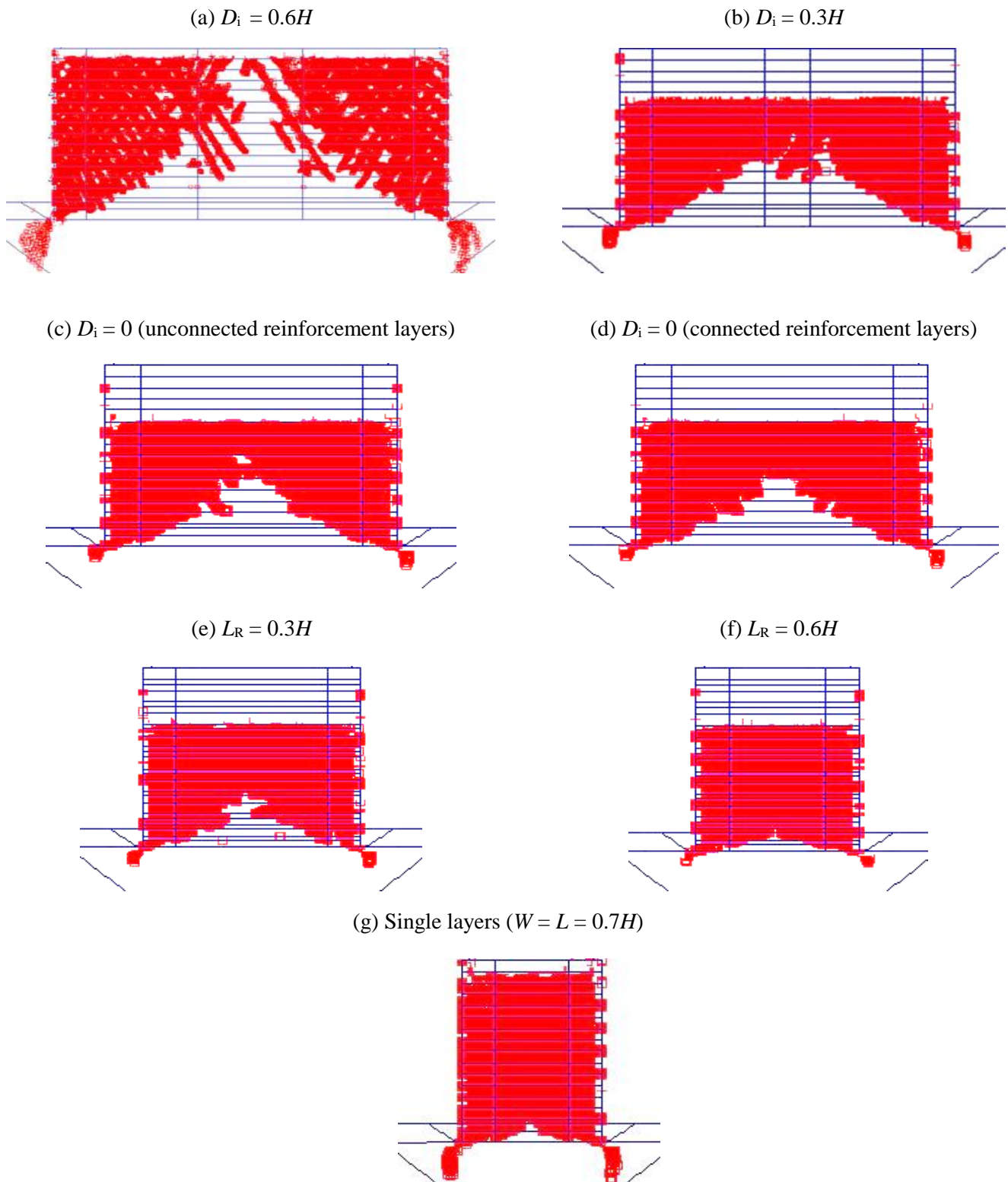


Figure 3.10. Plastic zones (Mohr–Coulomb points) in the soil at the end of construction (EoC) for walls with different interaction distances. (D_i) between the back of the reinforced soil zones for opposite walls. (Note: white zones on top of the models represent the location of tension cut-off points).

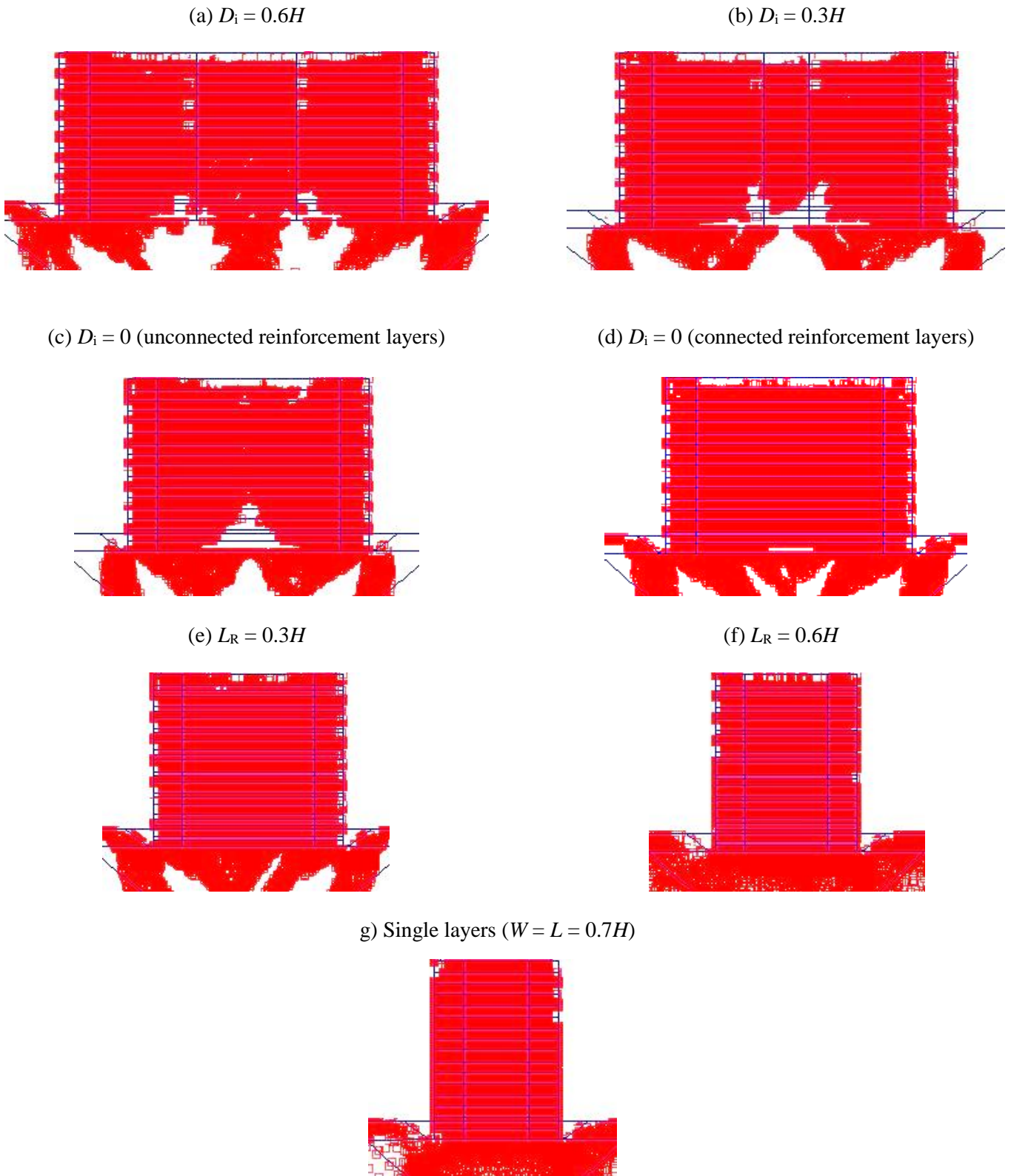


Figure 3.11. Plastic zones (Mohr–Coulomb points) in the soil at failure with the ϕ - c reduction method at end of construction (EoC) for walls with different interaction distance (D_i) between the back of the reinforced soil zones for opposite walls. (Note: white zones on top of the models represent the location of tension cut-off points).

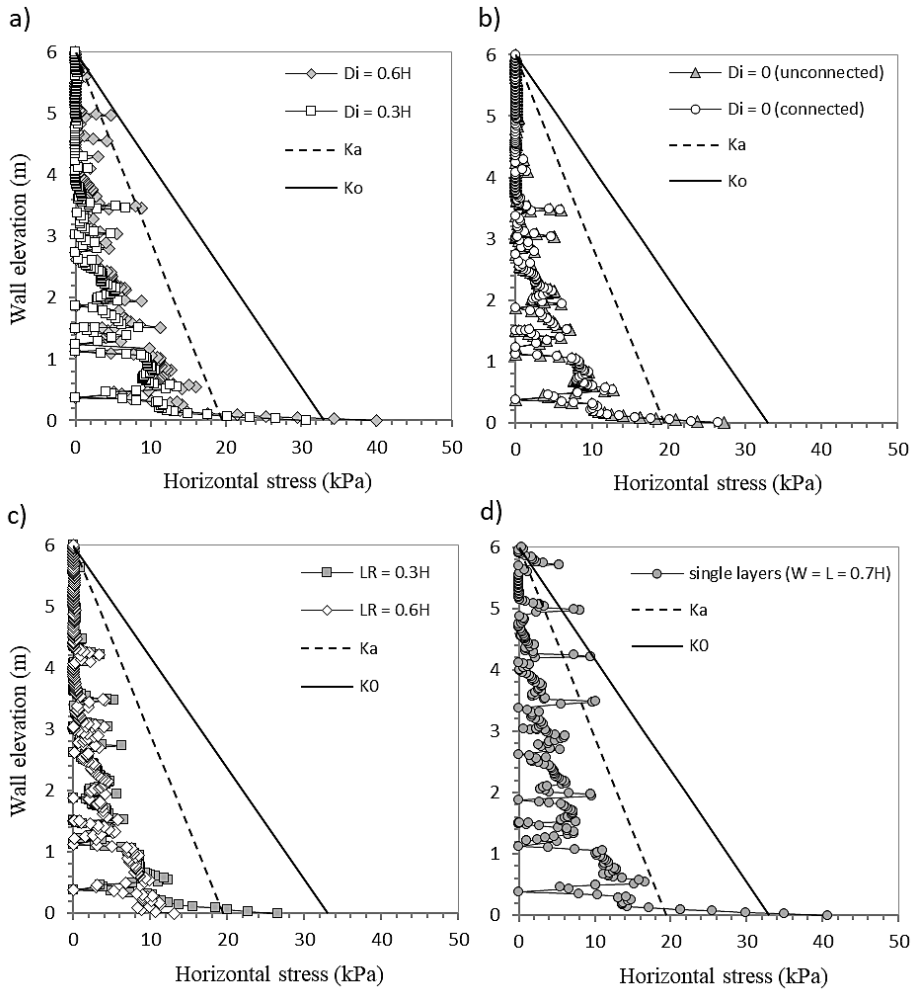
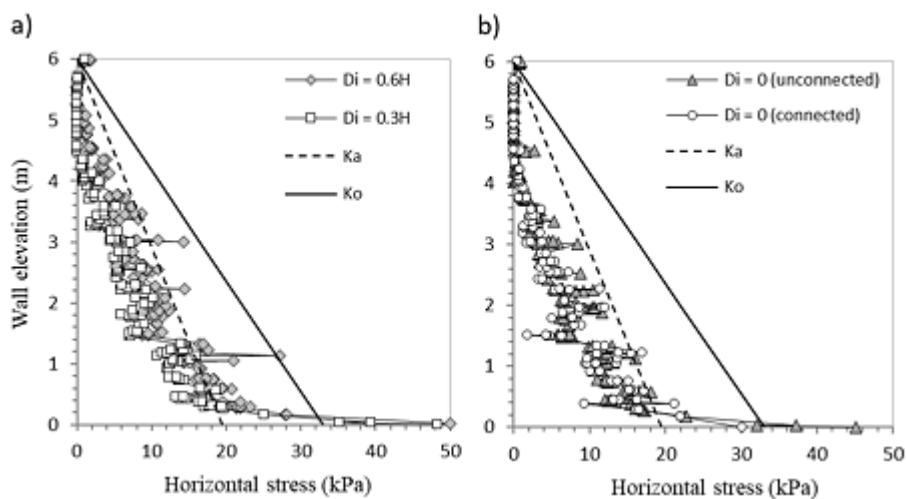


Figure 3.12. Lateral earth pressure at the facing at the end of construction (EoC) for different interaction distances (D_i) between back-to-back reinforced soil walls: (a) $D_i > 0$, (b) $D_i = 0$, and (c,d) $D_i < 0$.



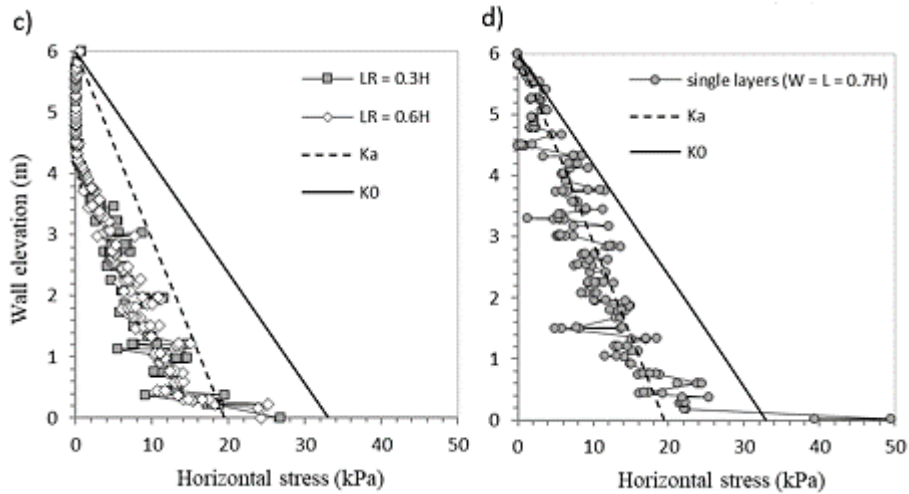


Figure 3.13. Lateral earth pressure at 1 m from the back of the facing at the end of construction (EoC) for different interaction distances (D_i) between back-to-back reinforced soil walls: (a) $D_i > 0$, (b) $D_i = 0$, and (c,d) $D_i < 0$.

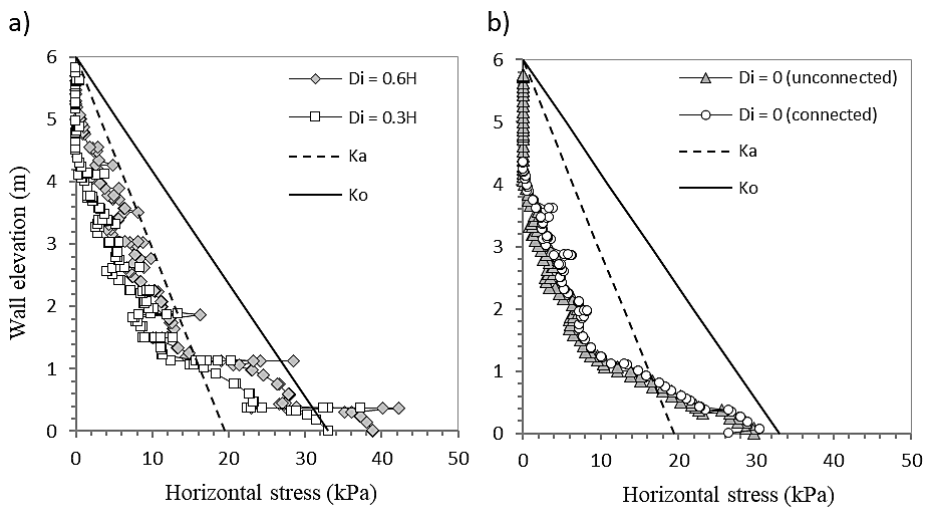


Figure 3.14. Lateral earth pressure behind the reinforcements (i.e., at L-distance from facing) at the end of construction (EoC) for different interaction distances (D_i) between back-to-back reinforced soil walls: (a) $D_i > 0$ and (b) $D_i = 0$.

The total soil pressure for all the cases discussed above and recorded at different distances from the facing are presented in Figure 3.15. The analytical linear trends from the active Rankine (K_a) and the at-rest lateral earth pressure (K_o) were based on the analyses of one side wall, therefore, no interaction of two opposite back-to-back walls was considered. A decrease in the interaction distance between the opposing walls from $D_i = 0.6H$ to $L_R = 0.6H$ decreases the lateral thrust at facing and at 1 m from facing, and from $D_i = 0.6H$ to $D_i = 0$ behind the reinforced zone. This trend of reduction in the lateral thrust is qualitatively in agreement with FHWA.

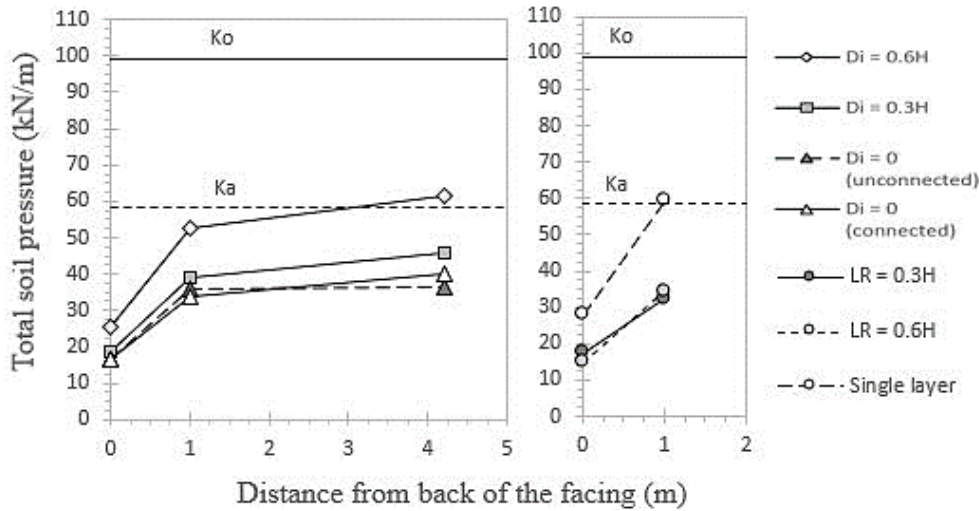
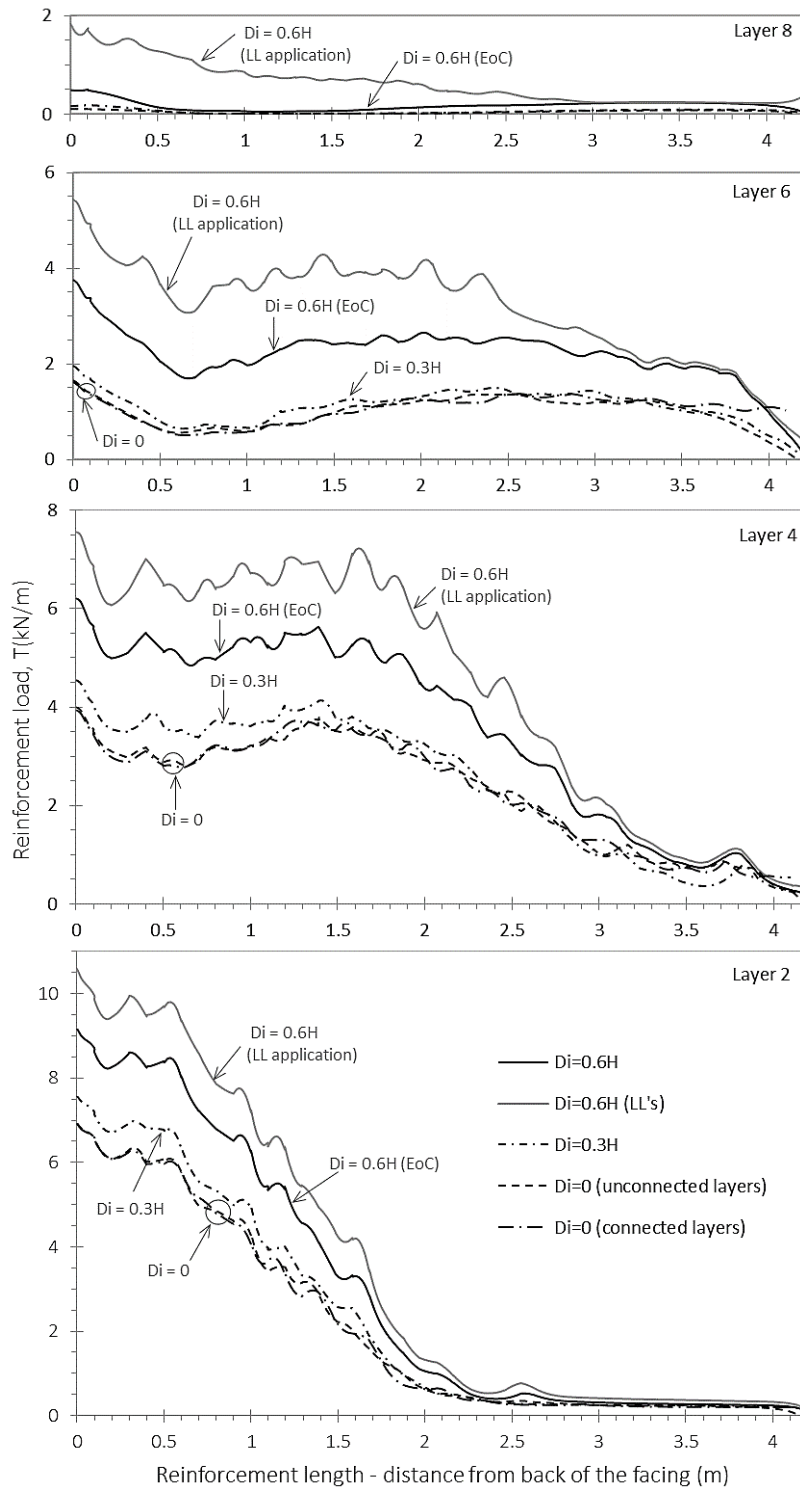


Figure 3.15. Total earth pressure at the facing, at 1 m from the facing, and behind the reinforcements (i.e., at L-distance from the facing) at the end of construction (EoC) for different interaction distances (D_i) between back-to-back reinforced soil walls.

Figure 3.16 presents reinforcement load distributions along the length of selected reinforcement layers. As D_i becomes smaller, the magnitude of tensile loads becomes smaller. However, from a practical point of view, the tensile load magnitudes and distributions are similar for $D_i = 0.6H$ and $D_i = 0.3H$ cases. The figure plots also show much less tensile load is generated for the $D_i = 0$ cases over the bottom half of the wall height and there are negligible differences for unconnected and connected cases. However, when the reinforcement layers extend as single strips from wall to wall (connected case) there is a small tensile load that is generated at the mid-point between walls. The influence of the pavement layer plus equivalent live load surcharge are shown in Figure 3.16 for the base case $D_i = 0.6H$ only. The influence of these surface loadings on tensile loads are detectable but judged to be negligible from a practical point of view. The cases of the overlapping $L_R = 0.3H$ and $L_R = 0.6H$ show a very slight and disparate decrease in tensile loads, respectively, compared with the other cases. However, for the $L_R = 0.6H$ there is an increase in the last two meters of reinforcements for the lower half height of the wall. Regarding the single layers, the figure shows an increase in reinforcement load in the middle of reinforcements below the mid-height of the wall.

(a)



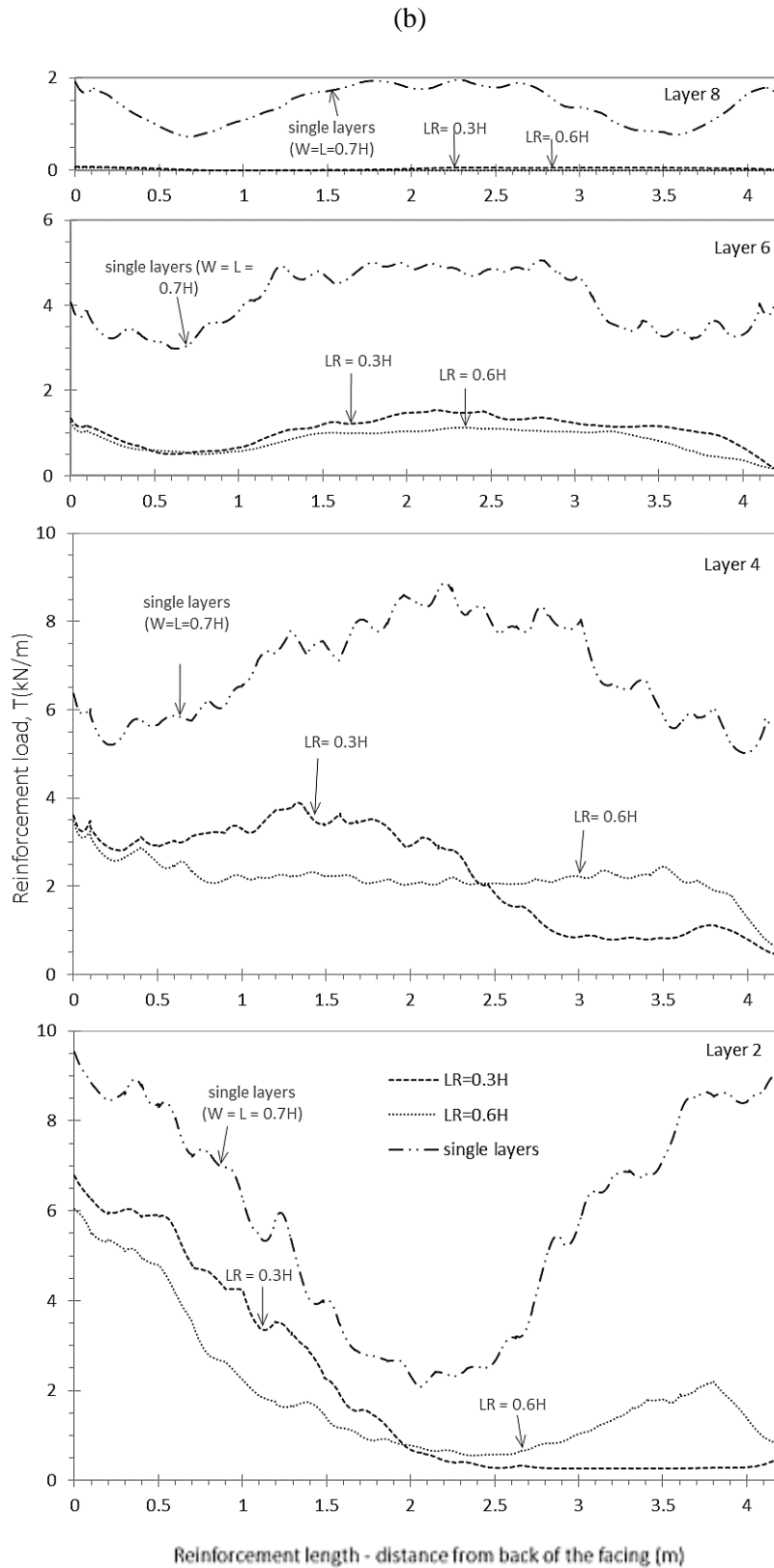


Figure 3.16. Reinforcement loads at end of construction (EoC) for walls with different interaction distances (D_i) between the back of the reinforced soil zones for opposite walls: (a) $D_i > 0$ and $D_i = 0$, and (b) $D_i < 0$.

Figure 3.17 presents the maximum numerically computed tensile loads and loads computed using the closed-form analytical methods recommended in the American (AASHTO Simplified Method and AASHTO Stiffness Method) and French (NF Coherent Gravity Method; NF P94-270) design codes, respectively. As expected from previous results, the tensile loads become less with decreasing interaction distance D_i . Differences in numerical results for $D_i = 0$ cases with and without connected reinforcement layers are negligible from a practical point of view. The single layers case produced higher maximum tensile loads values compared to other cases because the lesser yielding structural scenario is generated. The two design methods (AASHTO Simplified Method and NF P94-270 Coherent Gravity Method) give excessively conservative tensile loads that increase in value and conservativeness with depth. The AASHTO Simplified Stiffness Method provides a small improvement in the magnitude and distribution of T_{maximum} predictions than the other design methods, but remain non-conservative with depth for the single layers cases.

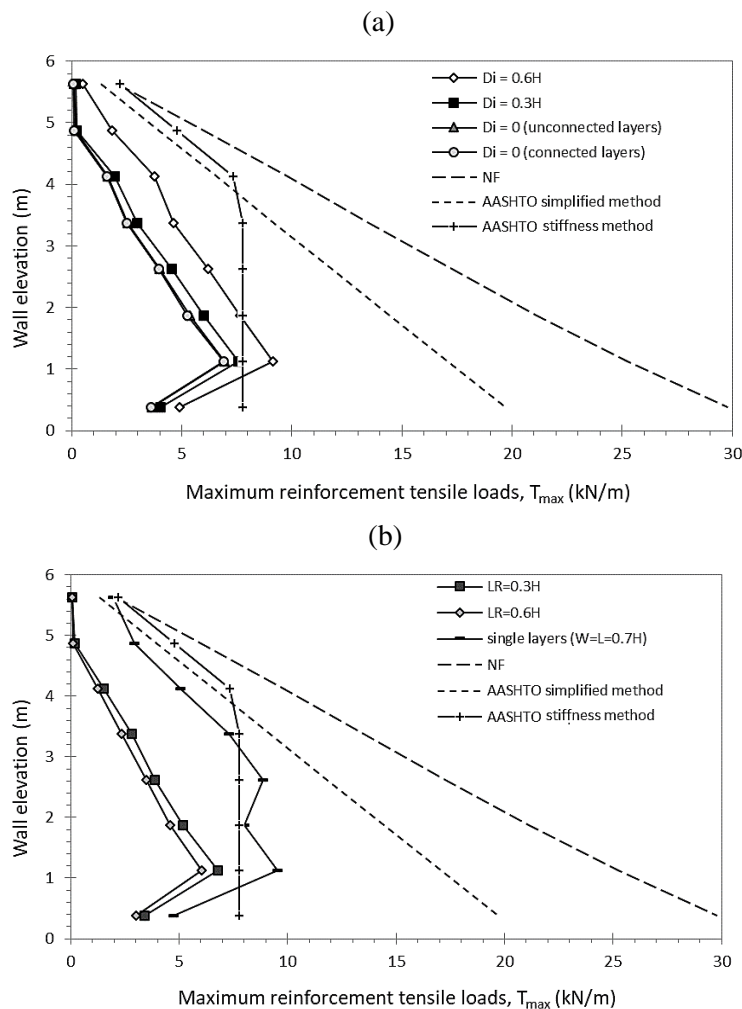


Figure 3.17. Numerical maximum tensile load for walls with different interaction distances (D_i) between the back of the reinforced soil zones for opposite walls: (a) $D_i > 0$ and $D_i = 0$, and (b) $D_i < 0$, and both cases compared with maximum tensile loads computed using AASHTO ($\times 2$) and NF design codes.

3.4.3. Effect of the pre-tensioning (T_i)

Figure 3.18 presents the computed facing displacements at the end of construction for the different pre-tension load cases. The plots show that the wall displacements decrease more than 50% when increasing the pre-tension load. A practical observation from these plots is that it may be possible to achieve an almost vertical facing alignment by applying a pre-tension load in the range of $T_i = 0.5$ kN/strip (i.e., 2 kN/m in the model) and 1 kN/strip (i.e., 4 kN/m in the model) for all reinforcement layers, assuming all other factors including method and good quality of construction remain the same.

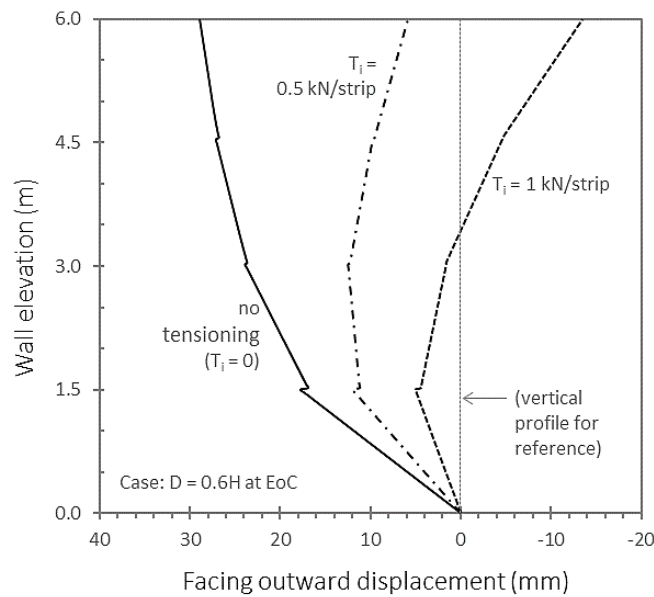


Figure 3.18. Facing displacements for $D_i = 0.6H$ case at the end of construction (EoC) and different pre-tensioning scenarios.

Figure 3.19 presents the contour plots of shear strain development and plastic (failure) zones generation for the $D_i = 0.6H$ case at EoC with and without pre-tensioning. The achieved internal soil shear zones fall within the 0–1% strain range. As shown, there is a reduction in shear strains and zones of plasticity in the reinforced soil zone with higher pre-tensioning load (i.e., tension points somehow overlap plastic points). The shear strain plots show that load transfer between the soil and reinforcement extends to the tail of the reinforcement layers for the pre-tension cases which is not the case for the no-tension case (see Figure 3.8a).

Horizontal earth pressures acting at the back of the facing are presented in Figure 3.20. Sharp jumps can be observed in the pressure profiles against the facing with higher pre-tensioning load at the top of the wall and the opposite occurred at the bottom of the wall.

Figure 3.21 shows the computed reinforcement tensile loads for the $D_i = 0.6H$ base case at the end of construction. A reinforcement tensile loads redistribution was generated due to strip pre-tensioning. For the top third of the structure (see layers 6 and 8), the pre-tension

load of 1 kN/strip exceeds the load that is naturally developed in the case of no-tension at all locations along the strips, whereas the no-tension case resulted in a higher connection load over the bottom half of the structure.

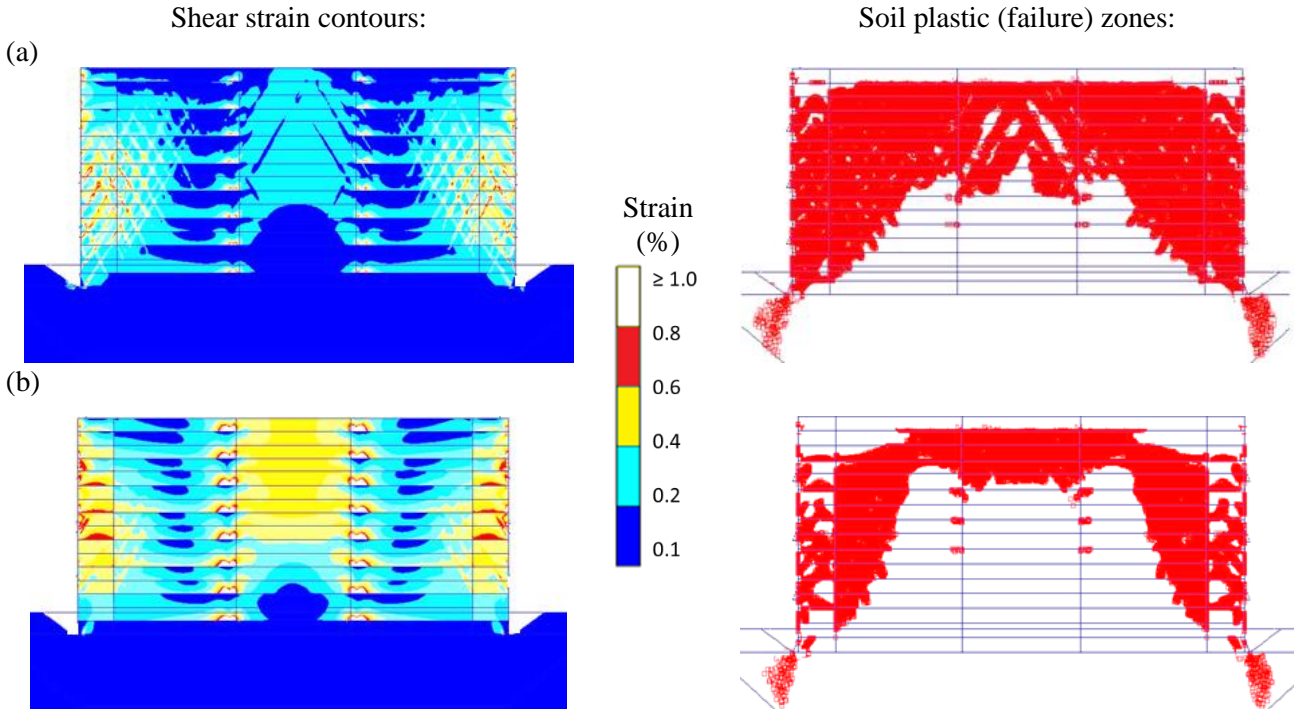


Figure 3.19. Shear strain contours and plastic (failure) zones in the soil at the end of construction for the $D_1 = 0.6H$ case. Strip pre-tension loads: (a) $T_i = 0.5$ kN/strip and (b) 1 kN/strip. Note: results range from 0–1% for shear strain contours, and white zones on top of the models represent the location of tension cut-off points for soil plastic zones).

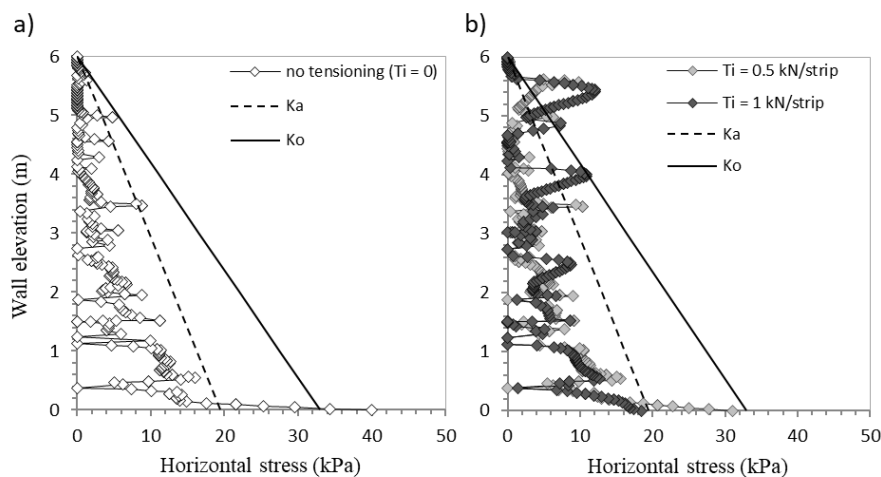


Figure 3.20. Horizontal earth pressure at the facing for the $D_1 = 0.6H$ case at the end of construction (EoC): (a) no tension case and (b) different pre-tensioning loads.

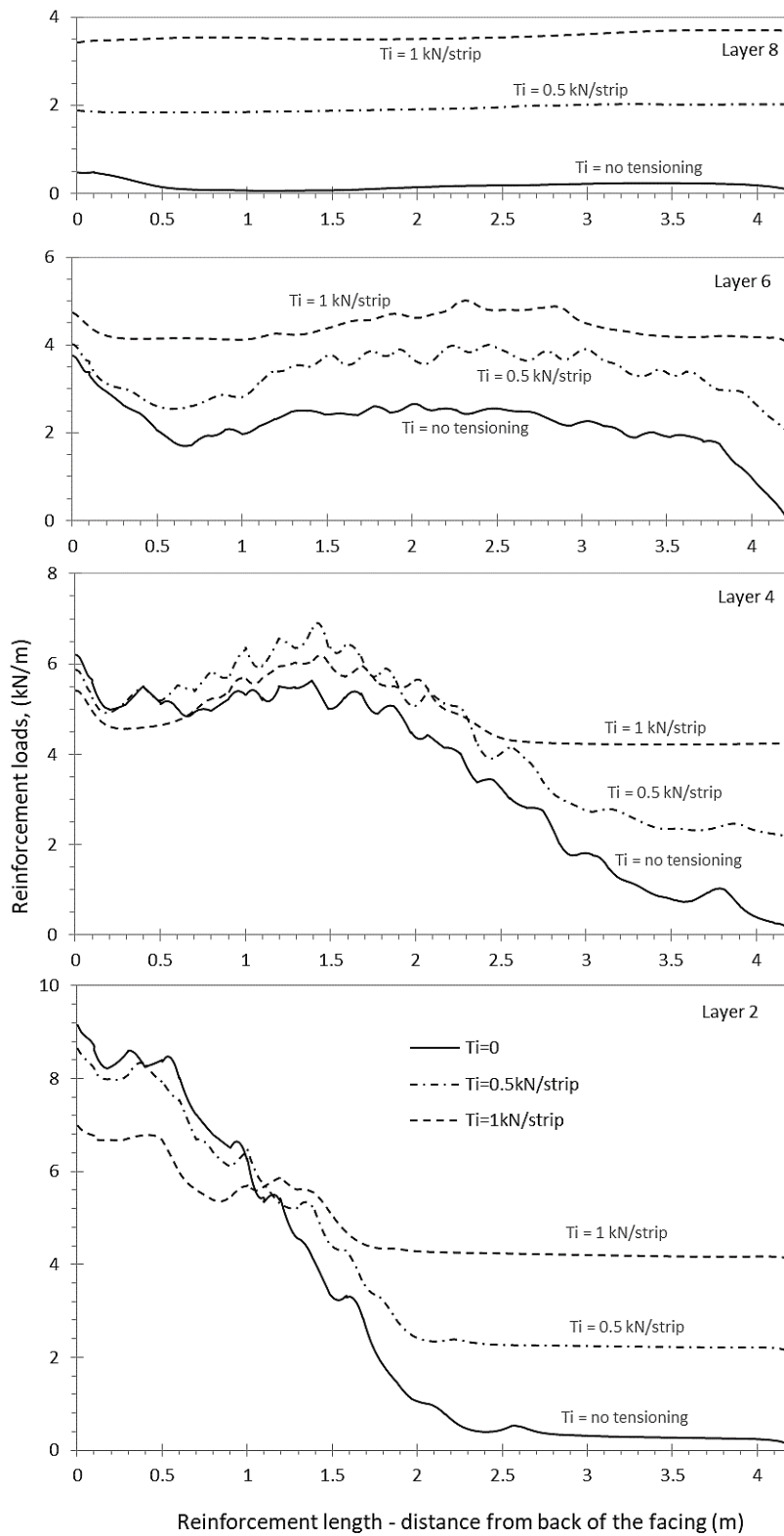


Figure 3.21. Reinforcement loads for $D_1 = 0.6H$ case at the end of construction (EoC) and different pre-tensioning loads.

3.4.4. Effect of the soil-polymeric interaction (R_i)

Numerical results assuming a variable and significantly higher soil–polymeric strength and stiffness interaction than for cases investigated thus far are shown in Figure 3.22. The data plots show that facing displacements are up to about 30% less when perforated reinforcement strips are used.

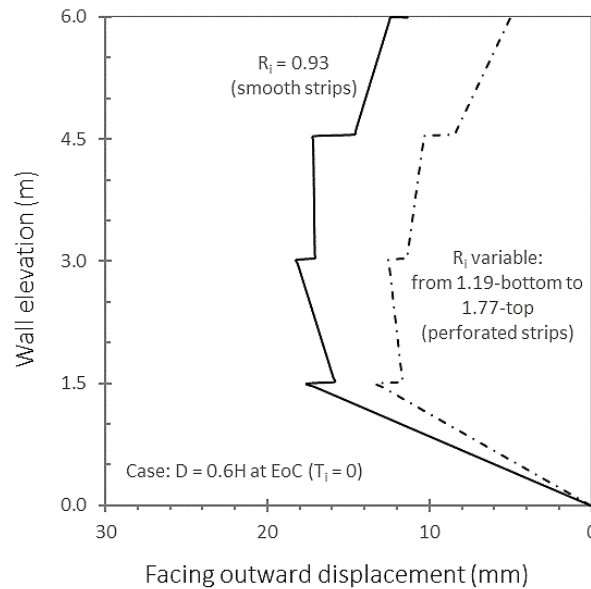


Figure 3.22. Facing displacements computed at the end of construction (EoC) using different polymeric–soil interface strengths and stiffness (R_i -factor) for the $D_i = 0.6H$ case with no pre-tensioning.

The computed plastic (failure) zones at the end of construction are presented in Figure 3.23. There is a detectable reduction in the size of the plastic zones for the case with larger R_i values (i.e., greater interface of polymeric–soil strength and stiffness) compared with small and constant R_i values (see Figure 3.23a).

(a) $R_i = 0.93$ (constant)

(b) $R_i =$ from 1.19 to 1.77 (variable)

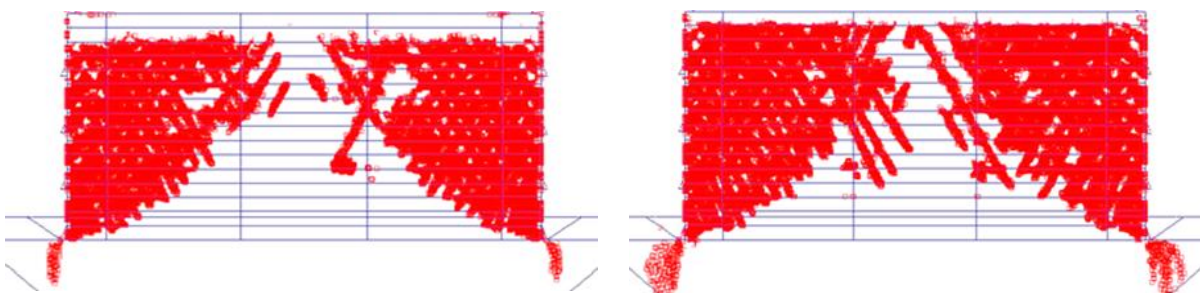


Figure 3.23. Plastic zones (Mohr-Coulomb points) at end of construction for $D_i = 0.6H$ case with no pre-tensioning and polymeric–soil interface factor assumptions: (a) $R_i = 0.93$ (constant), and (b) $R_i =$ from 1.19 to 1.77 (variable). (Note: white zones on top of the models represent tension cut-off points location).

The horizontal earth pressure generated from the facings is presented in Figure 3.24. Record low values were observed when the perforated polymeric strips were used compared with the smooth strips case. Small but detectable reductions in reinforcement loads were also detectable for the perforated strips as shown in Figure 3.25 with the exception of the top layer where soil confining pressure is least. The computed maximum strain for both cases is about 1%, which is a typical maximum value observed in instrumented and monitored field walls under operational (EoC) conditions by Miyata et al. 2018.

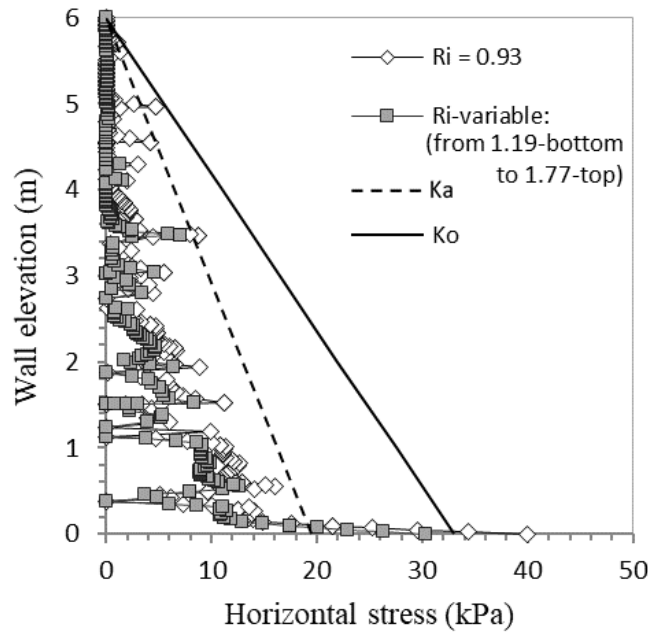
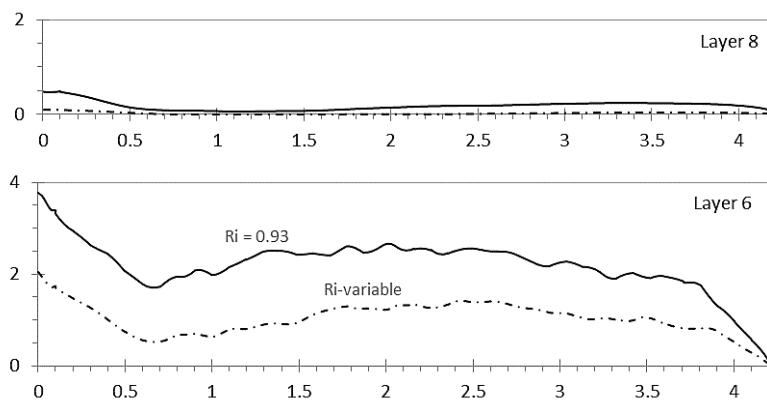


Figure 3.24. Horizontal earth pressure at the facing for the $D_i = 0.6H$ case at the end of construction (EoC) using different polymeric–soil interface strengths and stiffness (R_i -factor) for the $D_i = 0.6H$ case with no pre-tensioning.



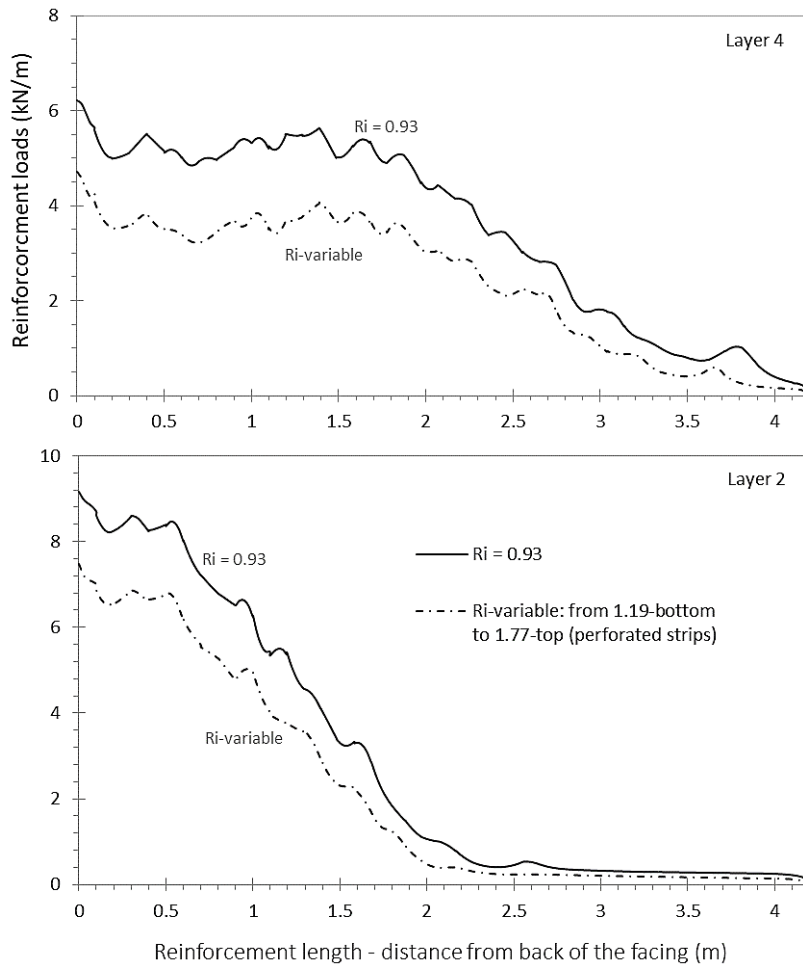


Figure 3.25. Reinforcement loads at end of construction (EoC) using different polymeric–soil interface strengths and stiffness (R_i -factor) for the $D_i = 0.6H$ case with no pre-tensioning.

3.5. Conclusions

Numerical simulations of a pair of idealized 6 m high back-to-back reinforced soil walls constructed with polymeric reinforcement strips are reported. The results of the simulation show that back-to-back reinforced soil walls behave jointly when they are far apart, and also interact with each other when they are close and overlapping. The FEM results demonstrate that the length of the reinforcement ($L = 0.7H$) in the overlapping case ($L_R > 0.3H$) complies with what is recommended by FHWA ($L \geq 0.6H$). Back-to-back reinforced soil walls with single layers of reinforcements that are connected to both wall facings produce a lesser yielding structural scenario, resulting in much higher reinforcement tensions than the other cases. This is conceptually consistent with those of FHWA design guideline, but without achieving in the modelled cases with polymeric strip reinforcements any global at-rest stress state. The average lateral pressure at the facing of the reinforced zone is close to the theoretical active Rankine lateral thrust when the interaction distance (D_i) is large except for the special case with the single layers. The interaction distance will change the location and

shape of the critical failure surface, and the distribution of plastic points. The comparison of the T_{maximum} for each method shows that the AASHTO Simplified Method is the most conservative (i.e., safest for design), the FEM Method and AASHTO Stiffness Method are similar and the least conservative, and the results of the NF P94-270 fall generally between the results using these three methods.

The polymeric strip installation procedure according to the pre-tension load applied to polymeric strips during construction as well as the continuous strip installation from one face to the other opposite face can have a significant effect on the quantitative behavior of these walls at end-of-construction (working stress) conditions. For example, very modest pre-tensioning loads may assist to maintain a target vertical or near-vertical facing panels alignment.

Compared with the no-pretension cases, pre-tensioning of strip reinforcements did generate larger tensile loads in the reinforcement layers and a redistribution of tensile loads particularly at the back of the layers. In order to achieve improvements in wall performance due to pre-tensioning at the time of construction, it may be necessary to use a tensioning device that can measure, control, and apply uniform or properly distributed initial tension load to all reinforcement layers at the back anchorage point.

Compared with smooth strips, polymeric strips with relatively higher interface friction reduced facing displacements by up to about 30% and reinforcement loads by small but detectable amounts. While not investigated in the current study, there is evidence that pull-out capacity is enhanced using the perforated polymeric strips. This has the practical benefit of improving the margin of safety for the pull-out limit state in conventional design practice.

Hence, the effect of the pre-tensioning and soil-reinforcement interaction provides a support for the basic point which is the distance between the back of the reinforced soil zones for the two opposing walls. This procedure can be utilized under the guidance of the designers of back-to-back reinforced soil walls to improve the behaviour of these structures.

CHAPTER FOUR

3D Finite Element Analysis

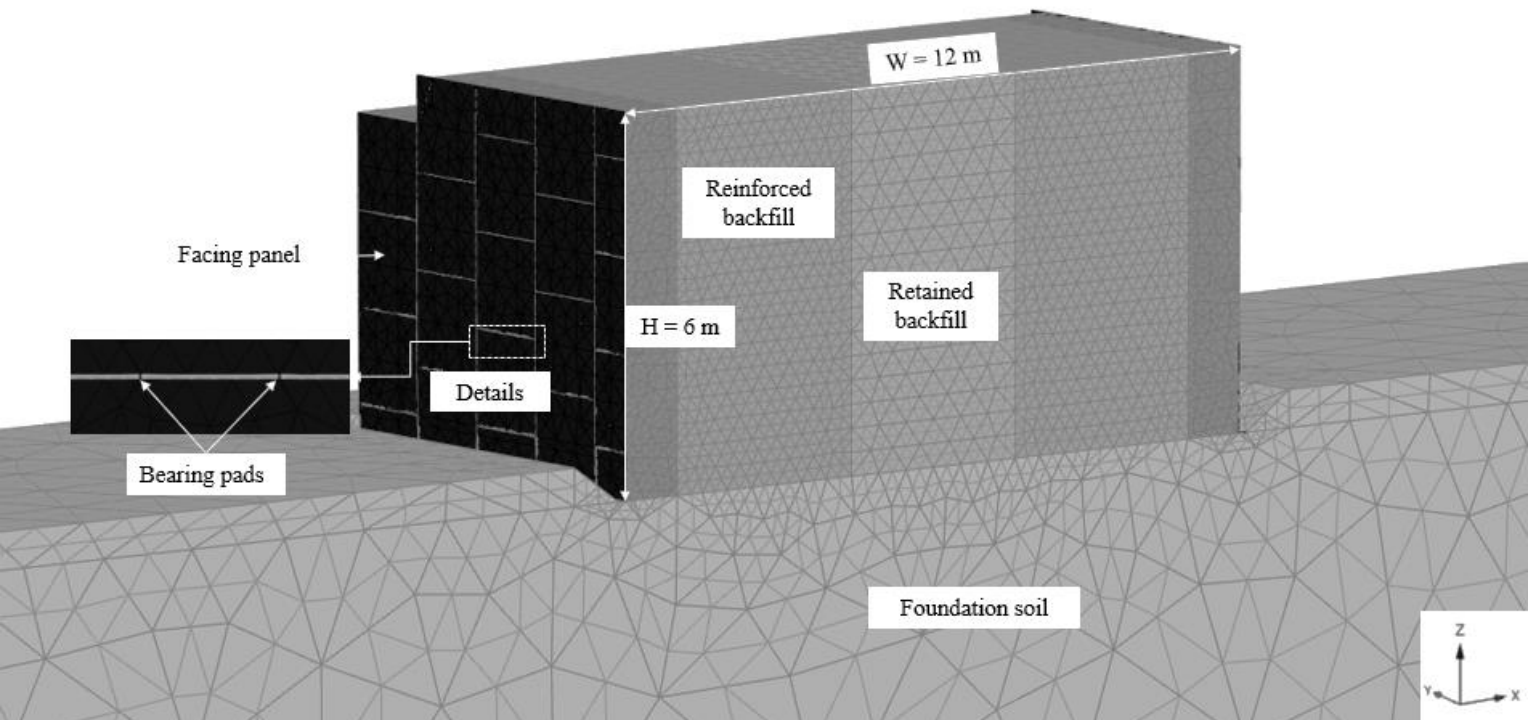
4.1. Introduction

The more realistic three-dimensional (3D) condition is frequently considered rather than the two-dimensional (2D) plane-strain condition. The 2D is usually by the transformation of the structural components width dimensions and the actual amount per width of any discrete component to equivalent 1 m-width components, as the main stress-strain directions of this kind of structures is quite well localized due to the slice symmetry assumed along the running direction of the wall. On the other hand, the 2D condition is unrepresentative and unjustified when the reinforced soil structure's alignment changes suddenly, contains a corners (Hung et al., 2021) and/or shows localized loadings. In this chapter, is to study the behaviour of back-to-back walls connected to the bridge abutment wall at end of construction (EoC) and under bridge load application that has not yet been well studied before, by comparing the predicted results of the 3D analysis with the previous results of the 2D analysis presented in the chapter Three, under static loading by wall displacement, lateral soil stress, reinforcement loads, and potential failure surface.

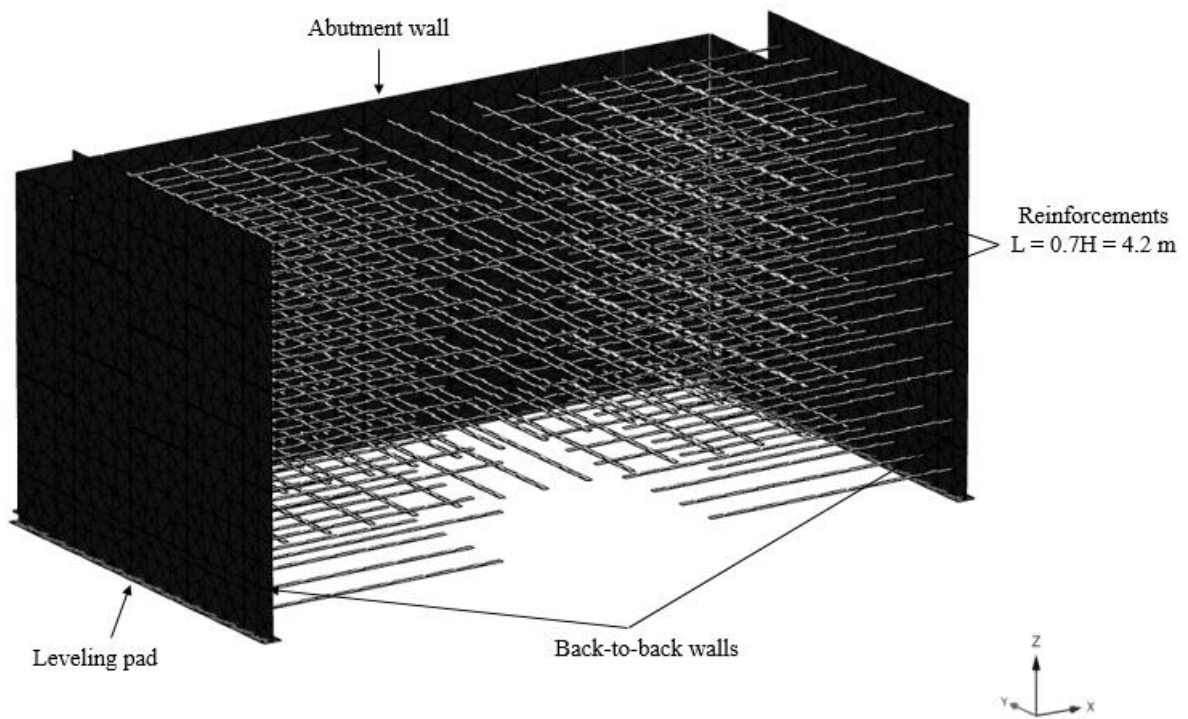
4.2. FE Numerical Modelling

The 3D model was created using the same geometry conditions, staged construction, and material parameters as with the 2D base case model ($D_i = 0.6H$) described in Chapter Three. A three dimensional (3D) analysis with 10-node tetrahedral elements. Considering the computational accuracy and efficiency, a total of 77,421 elements and 141,202 nodes was selected for the 3D numerical model, with mesh elements shown in Figure 4.1. The base width of the bridge support spread footing (bank seat), $b_f = 1.35$ m, and the location of the toe of the footing with respect to the back face of the abutment wall panels, $c_f = 0.15$ m according to FHWA. The height of the bank seat in top of the abutment, h , were selected to be 0.75 m. The span simulated by a load of 216 kPa applied along the bank seat which is corresponding a length of 36.6 m (Abu-Farsakh et al., 2019). The first course of the opposite sides walls facing (back-to-back walls facing) was placed and levelled, and then the abutment wall facing panels on the thin foundation layer (60 cm thick) to avoided direct contact between the longitudinal and transverse reinforcement layers. The vertical spacing between the reinforcement layer of back-to-back walls and the reinforcement of abutment wall is 10 cm.

(a)



(b)



(c)

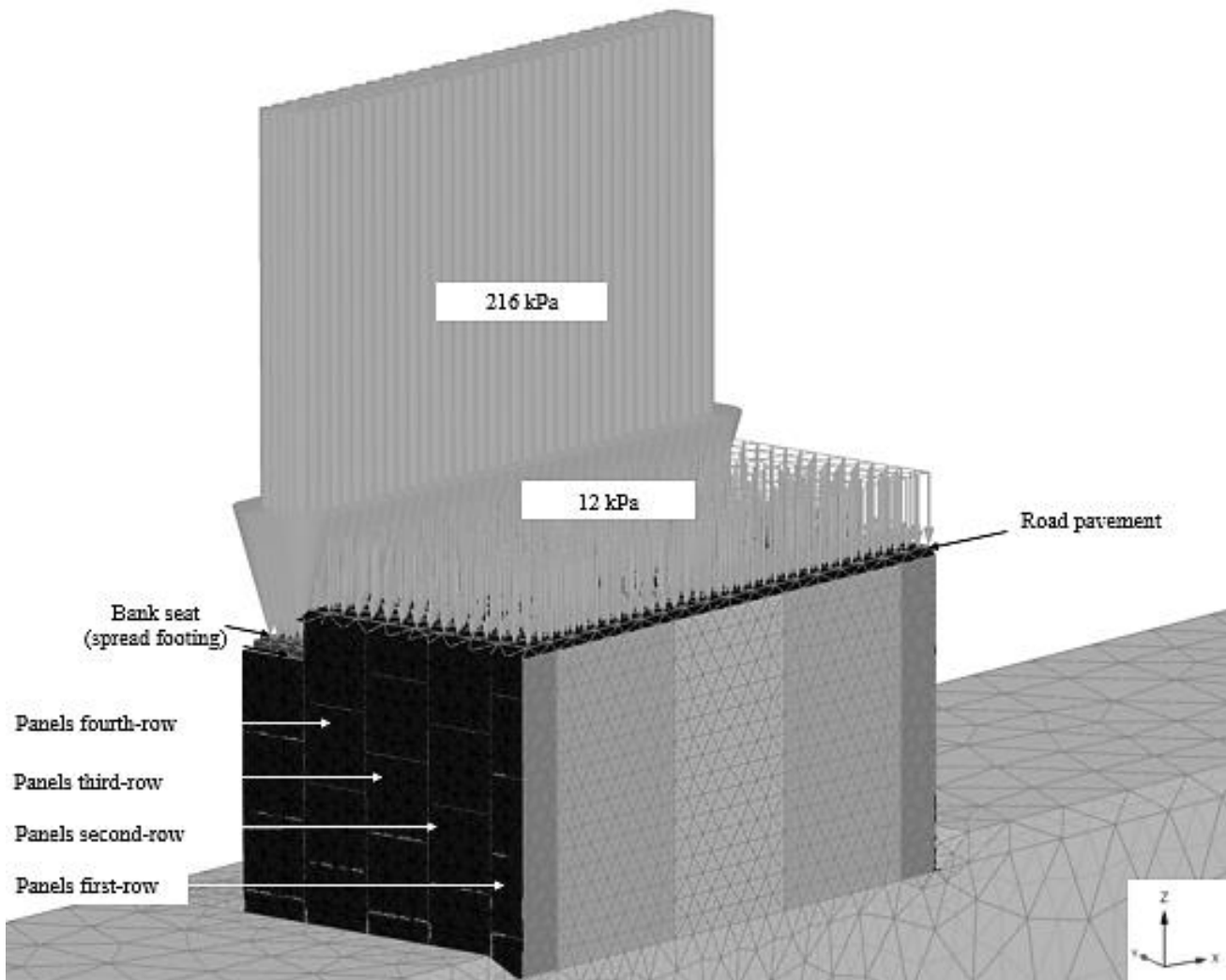


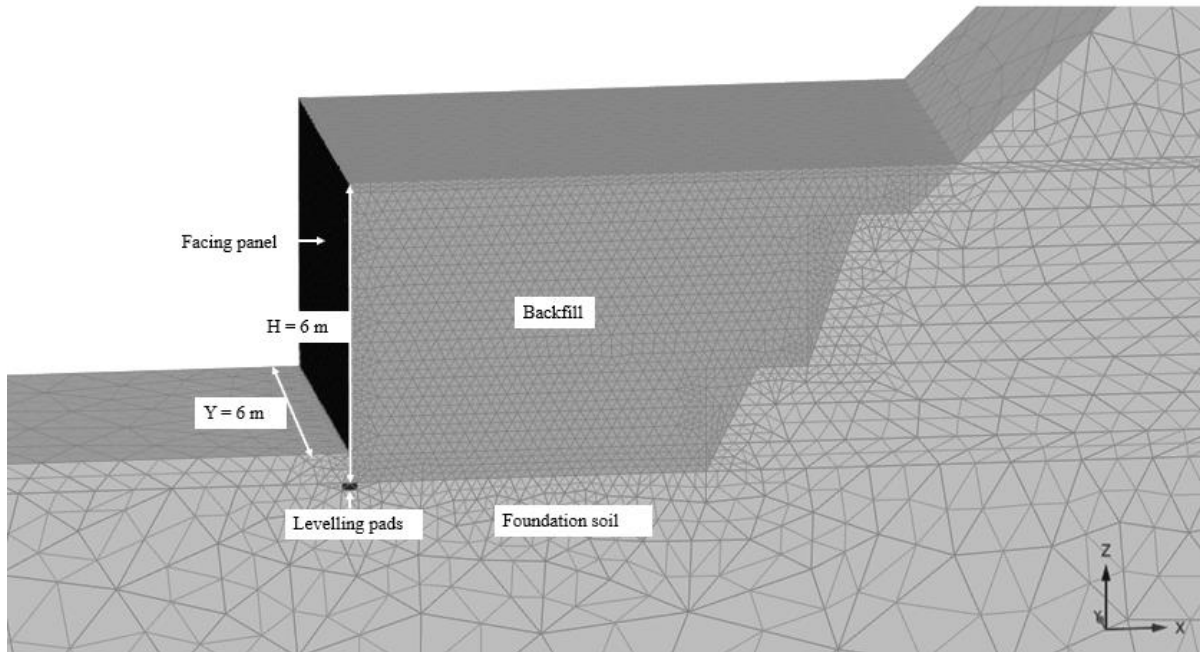
Figure 4.1. FE mesh of back-to-back MSE walls connected bridge abutment baseline case ($D_i = 0.6H$): 3D-FE mesh at EoC (a), Details of the reinforcements arrangement (b) and 3D-FE mesh under surface loading (c).

4.3. Verification on FE model

A full-scale test of random reinforced soil wall was considered to validate the 3D-FE model of this study because there are no experimental studies of back-to-back reinforced earth walls under static loading in the literature. Detailed information of the field instrumentation can be found in Jayakrishnan (2013) and in Chapter Three. Figure 4.2. shows the numerical model and mesh details for 3D-FE model simulations of Jayakrishnan (2013). Therefore, 3D-FE model in this study was validated by comparing the results from this study with those from measured results reported by Jayakrishnan (2013) and 2D results in chapter Three. The maximum loads for each layer of reinforcements located at the centerline of the 3D

reinforced soil wall model were extracted. Results of the axial reinforcement force at end of construction in Figure 4.3 show reasonable agreement between 2D, 3D-FE and experimental results. Maximum reinforcement axial force results in Figure 4.4 show close agreement between numerical and experimental results where the convergence recorded between 3D and the measured more than the 2D results, which verifies the reliability of the modelling technique using PLAXIS 3D.

(a)



(b)

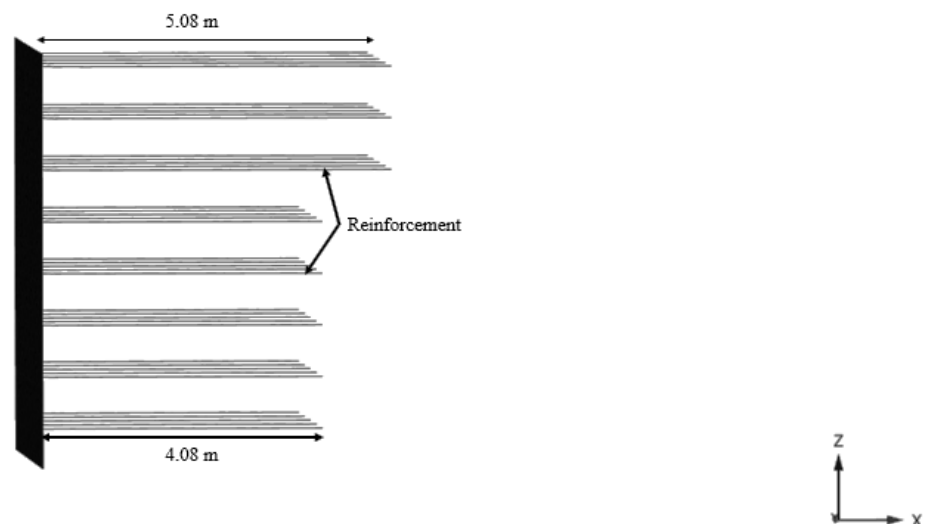


Figure 4.2. Numerical model geometry for 3D FE model simulations: 3D-FE mesh (a), Details of the reinforcements arrangement in 3D-FE model.

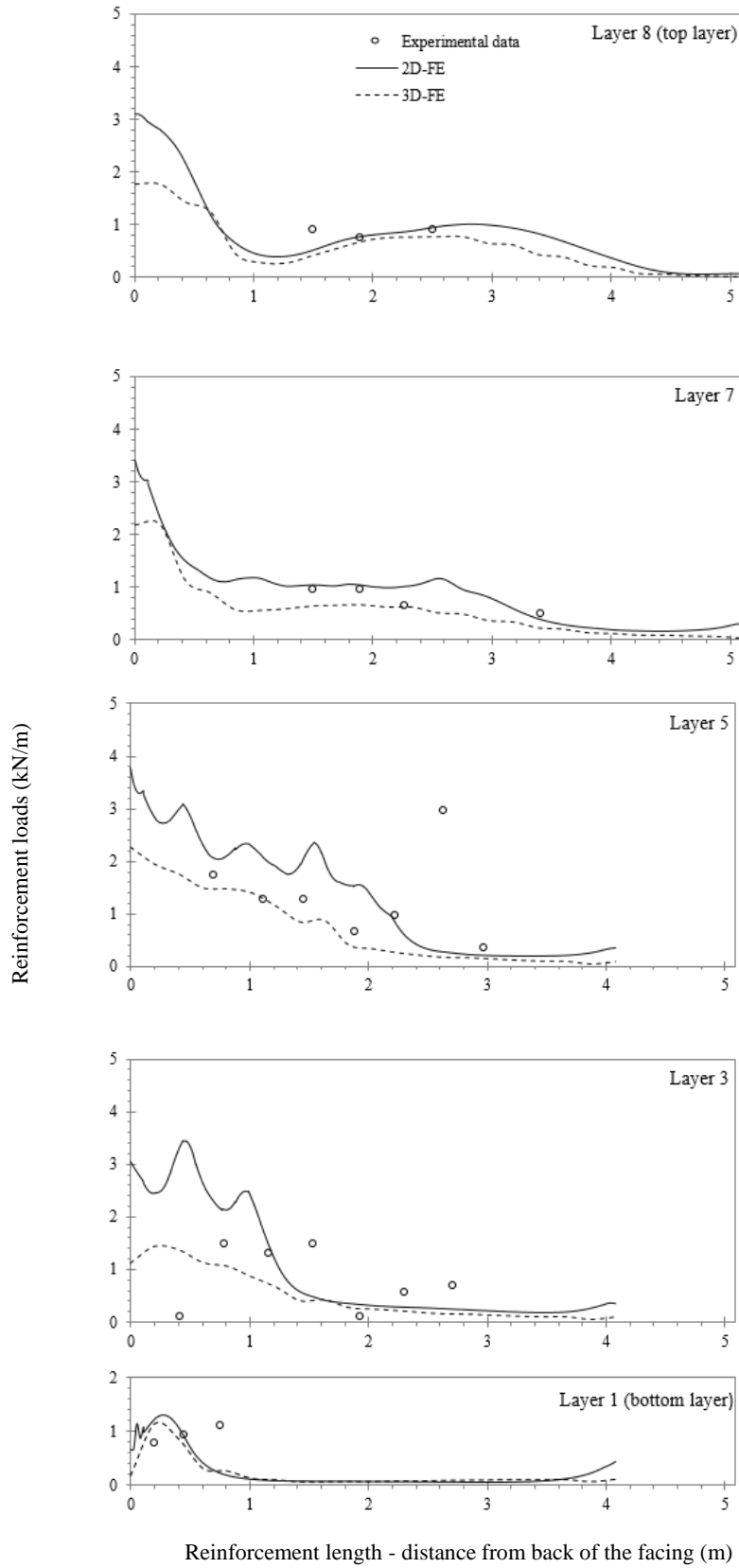


Figure 4.3. Comparison of experimental data and numerical results of distribution of axial force along reinforcement strips.

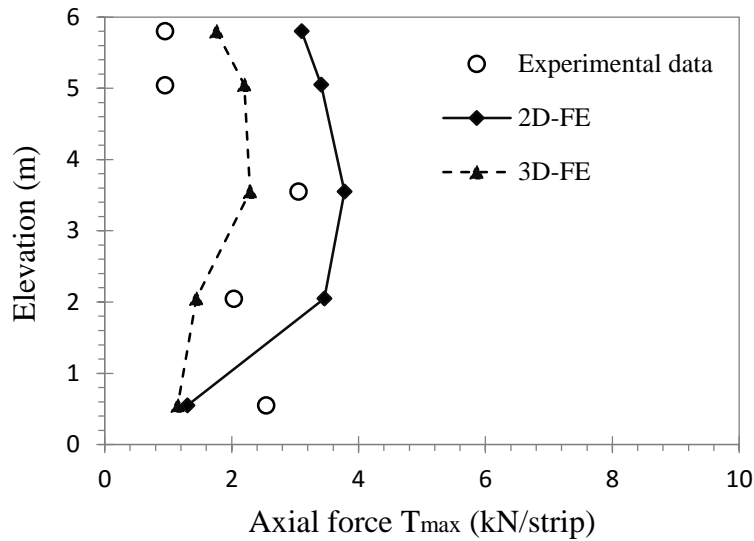


Figure 4.4. Comparison of experimental data and numerical results of maximum reinforcement axial force per strip.

4.3. Results of Analyses

4.3.1. General

In this section, a comprehensive FE analyses in terms of wall horizontal displacement, lateral earth pressure, reinforcement loads, and potential failure surface was carried out to evaluate the performance of the back-to-back wall connected bridge abutment wall system. The results of 3D-FE analyses were compared with 2D-FE analyses. Two different loading conditions were considered in this study: at the end of construction of the back-to-back walls and abutment wall, which is equal the self-weight of the structure; bridge load application, which is equal to the dead load (bank seat and bridge span load) plus the equivalent live traffic load.

4.3.2. Wall displacement

Figure 4.5 shows outward displacement profiles determined using the 3D-FE of four panels-rows and 2D-FE analysis at the end of construction (EoC) of back-to-back walls connected abutment wall, and under bridge loading. At end of construction (EoC), it can be seen that the prediction results by 3D-FE analyses are somehow close to 2D-FE whenever go from the corner to end of wall (from panels fourth-rows to panels first-row), this due to the influence of the turning corner (Hung et al 2021), also the more convergence with elevation (H). The difference in the shape and values of the displacement of panels first-row and third-row compared to other panels rows and 2D-FE because of the effect of the vertical facing stiffness (i.e., changing the number of horizontal joints along the facing height of the wall) which reported by Damians et al. 2013b. Under bridge loading application, there is an almost perfect convergence between 2D and 3D also whenever go from the corner to end of wall,

high values were recorded at the corner and this due the dead load effect (i.e., bank seat and bridge span load).

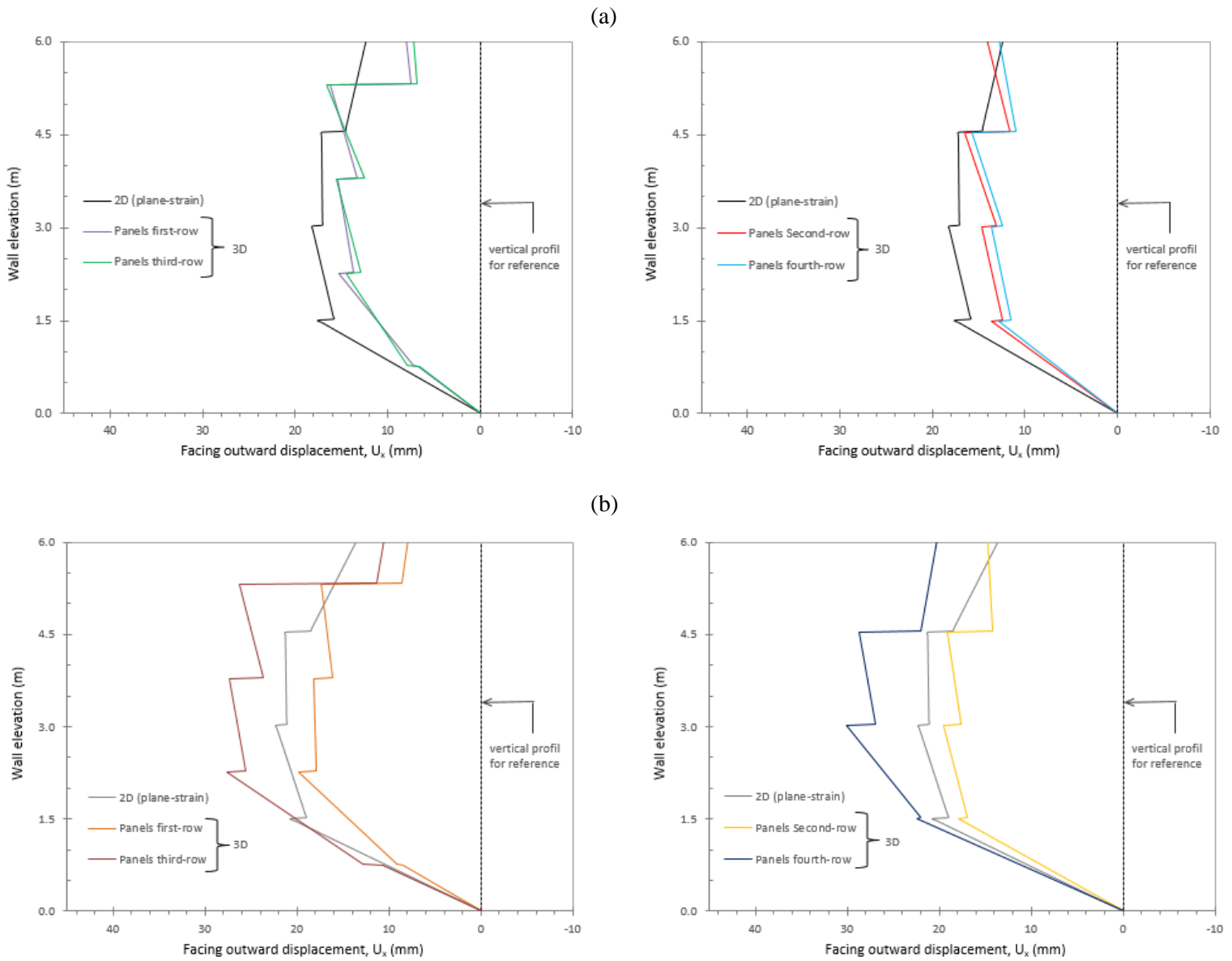


Figure 4.5. Lateral facing displacement comparison of 2D and 3D-FE analysis at EoC (a) and under service loading (b).

4.3.3. Lateral earth pressure

Figure 4.6 presents the lateral pressures predicted using the 3D-FE at the middle of each panels at different sections from the facing (i.e., at facing, at 1-m from the facing and behind the reinforced zone) at EoC compared with 2D-FE analyses, along with calculated values of total horizontal stress from the Rankine coefficient of active earth pressure (K_a) and the coefficient of earth pressure at rest (K_o). Almost perfect match between the lateral pressure of 3D-FE analysis and 2D-FE when the distance from the facing is increased. Figure 4.7

shows the lateral pressures predicted using the 3D-FE at the middle of each panels at different sections from the facing under the bridge load application compared with 2D-FE, here is a clear discrepancy between the results of 3D and 2D, where the 3D are more than the 2D simulations with increasing distance from the facing in the longitudinal direction and nearing the abutment wall in the transversal direction. The lateral earth pressure increase with nearing to the abutment wall due the dead load application of the spread footing (i.e., bridge seat) and bridge deck. At behind the reinforced zone, recorded an increase of about 80% at the middle of the panels fourth-rows (near to the abutment wall) and in the same time recording a decrease of 60% behind the reinforced zone at the middle of the panels first-rows (away from the abutment wall) compared to the 2D results.

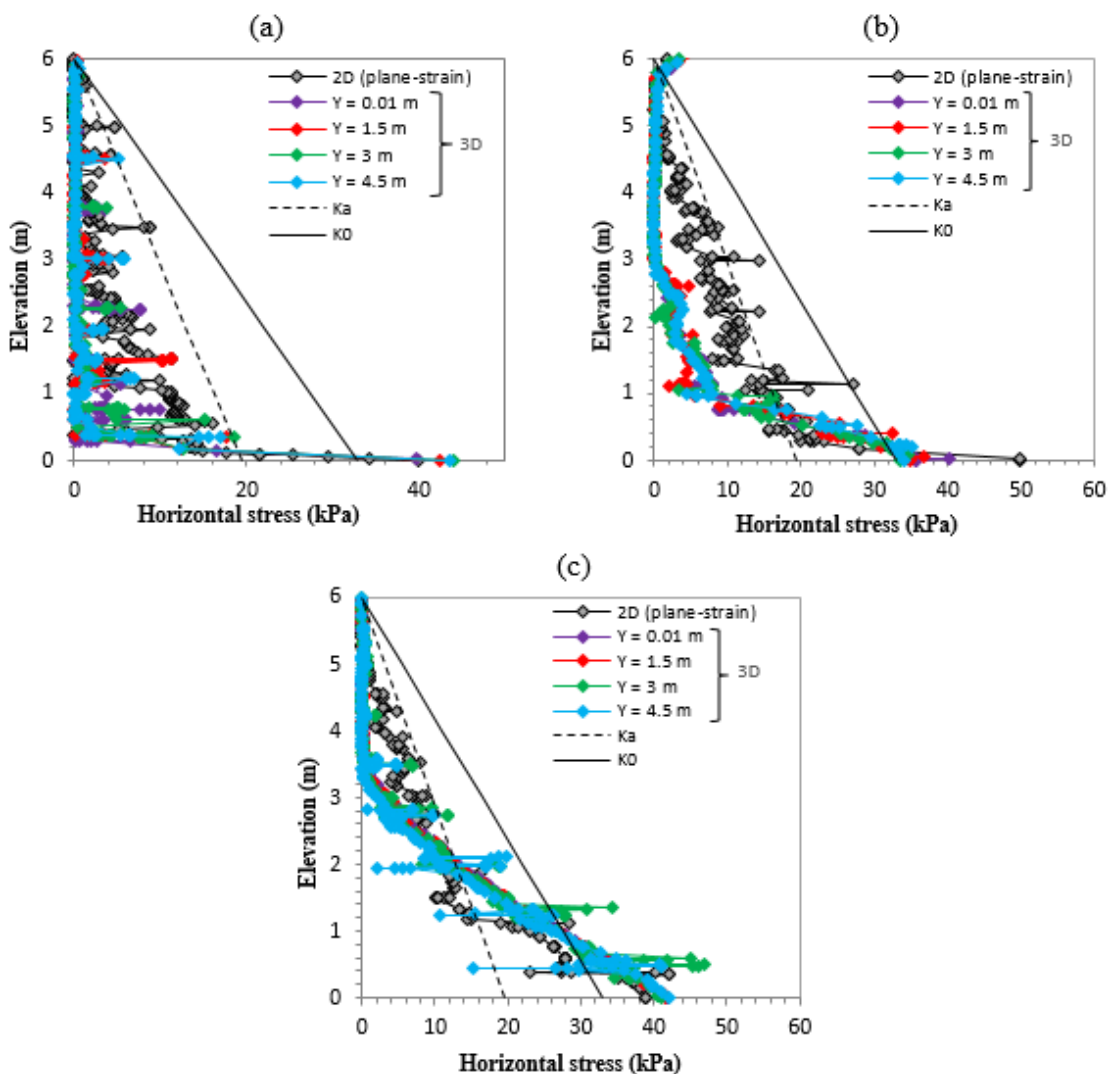


Figure 4.6. Lateral earth pressure at the facing (a), at 1 m from the facing (b), and behind the reinforcements (c) at the end of construction (EoC) by 2D & 3D simulation.

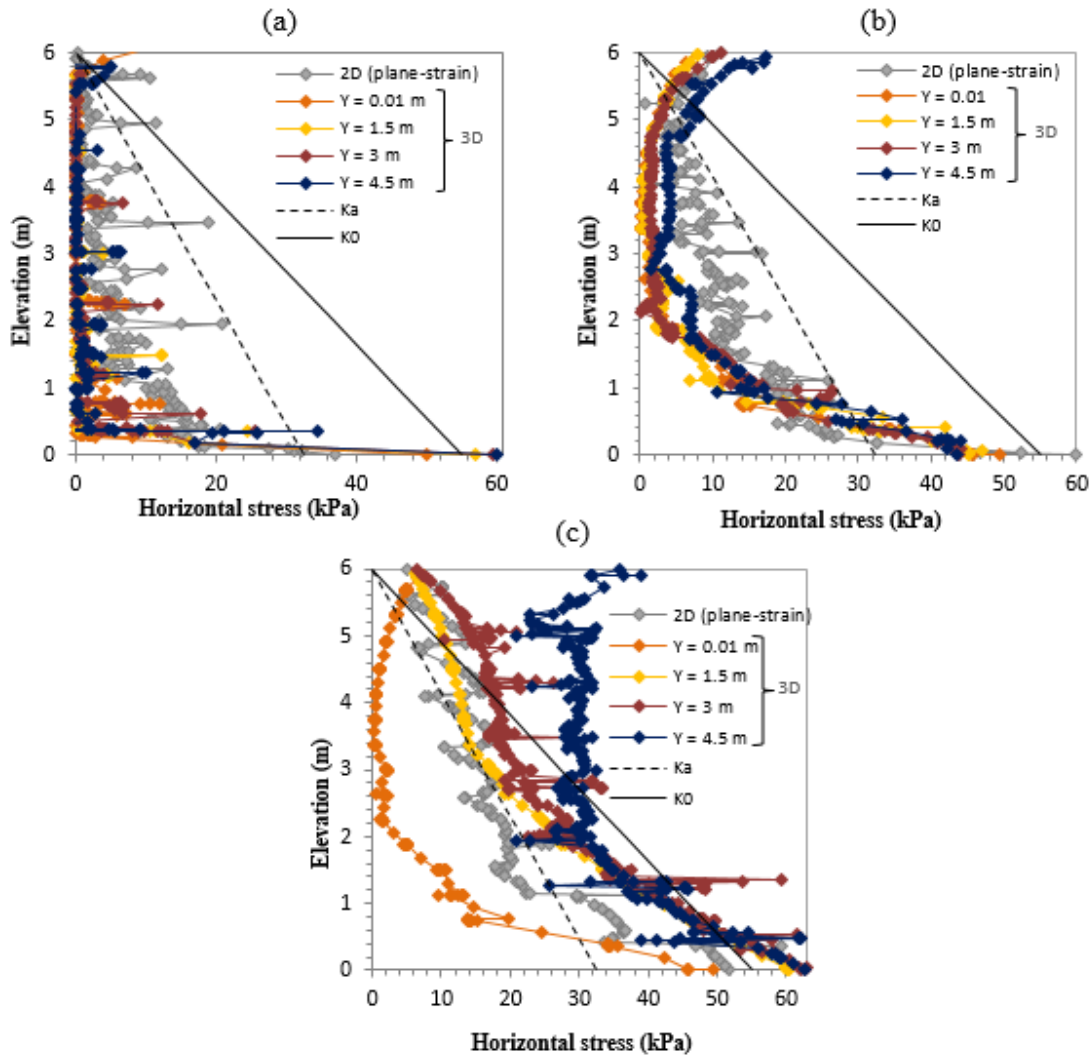


Figure 4.7. Lateral earth pressure at the facing (a), at 1 m from the facing (b), and behind the reinforcements (c) under bridge loads application (EoC) by 2D & 3D simulation.

4.3.4. Reinforcement loads

Distributions of reinforcement tensile loads of each reinforcement located at a different position (Y-direction) of 3D analysis compared to 2D analysis at EoC are shown in Figure 4.8. Full agreement between 3D and 2D analysis results regarding to the top layer except for the second half of the reinforcement length. Tensile loads for the 3D simulation are greater than for the 2D simulated values especially near the facing connections for mid-height layers (i.e., layer 6 & 4) to become all 3D analysis results smaller than 2D analysis (i.e., layer 2). As usual, lower values are recorded for the reinforcements that are located near the abutment wall (the corner) compared to the rest as well the 2D simulation results. Figure 4.9 shows reinforcement load distributions along the length of selected reinforcement layers of 3D & 2D analysis under bridge loading. The same as in the case of EoC but the larger values are

recorded for the reinforcements near the abutment walls compared to the rest and this is due to the effect of the dead loads.

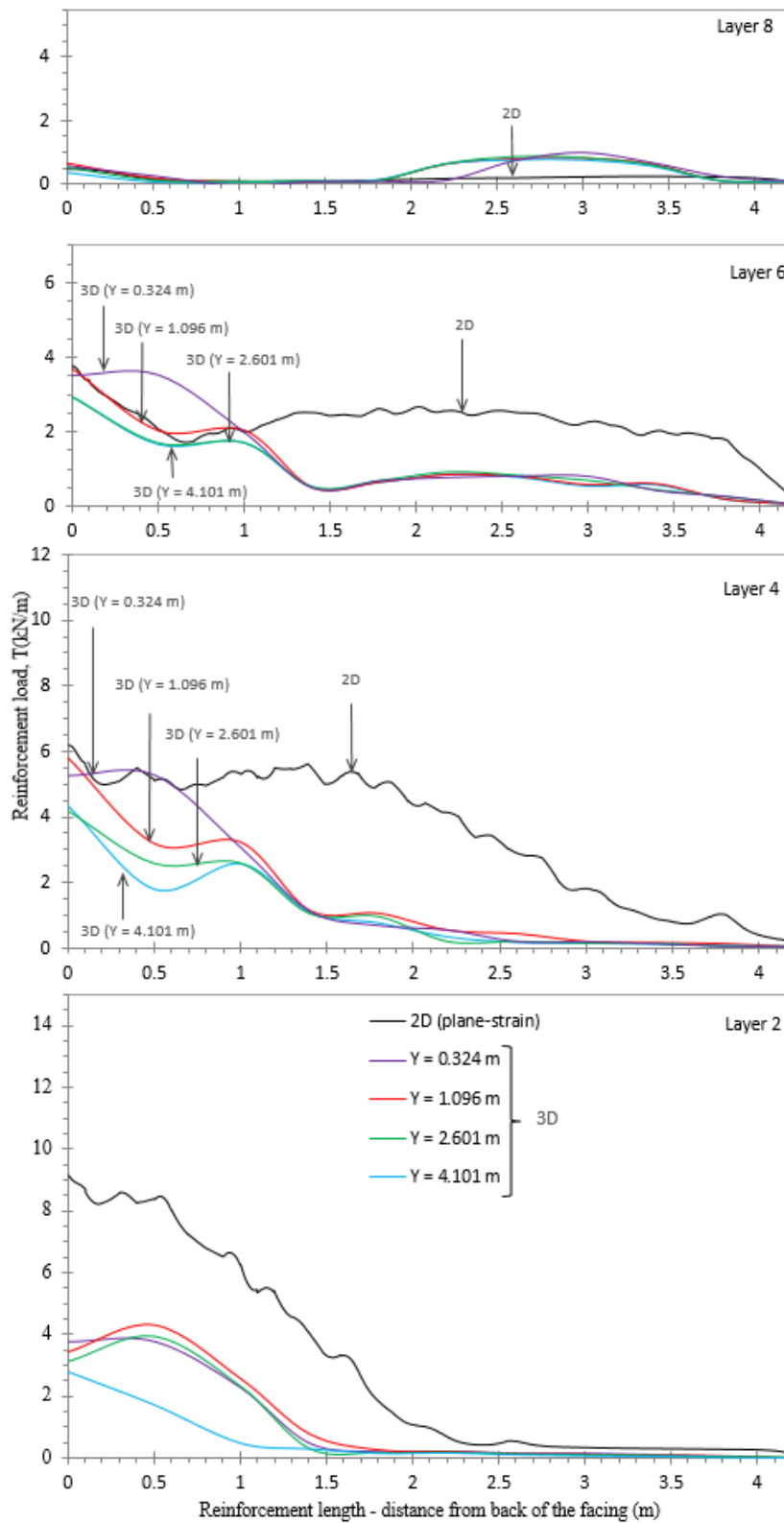


Figure 4.8. Tensile reinforcement loads in selected reinforcement layers of 2D and 3D analysis at EoC.

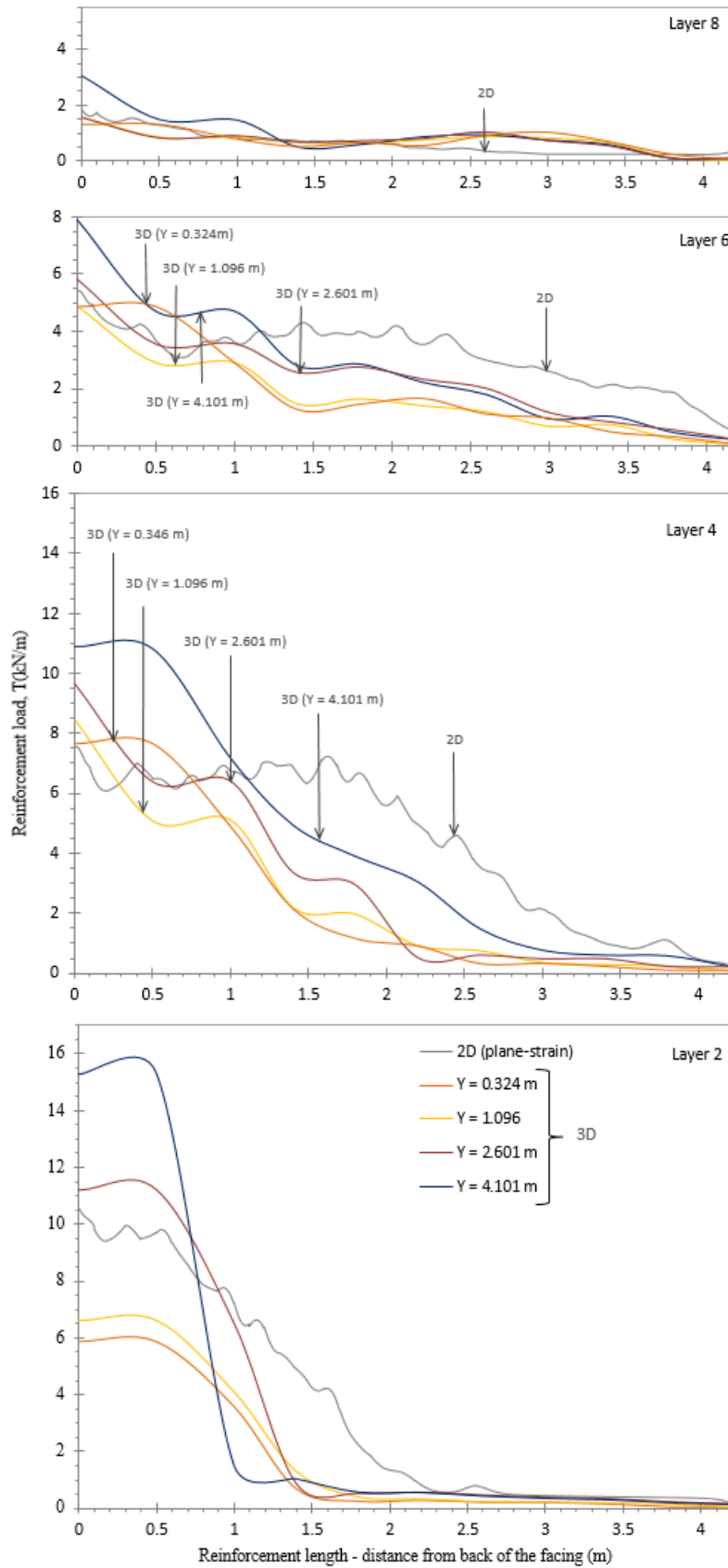


Figure 4.9. Tensile reinforcement loads in selected reinforcement layers of 2D and 3D analysis under bridge loading.

The distribution of the maximum tensile loads in the reinforcements (T_{max}) at a different position (Y-direction) of 3D analysis compared to 2D analysis at EoC and under bridge load application (see Figure 4.10) compared to Meyerhof classical analytical calculation, the Simplified and Stiffness Method given by NF P94-270 standards and AASHTO, respectively, where the distribution of T_{max} is linear with depth from the top of the wall for NF P94-270, AASHTO Simplified Method and bilinear for AASHTO Stiffness Method. At EoC, 3D maximum tensile forces are nearest to the 2D simulated from the reinforcement layer located away from the abutment wall ($Y = 0.324$ m) to the abutment wall ($Y = 4.101$ m) in the two-thirds of the top of the wall and then decrease speedily toward the bottom. Under loading, happens the opposite.

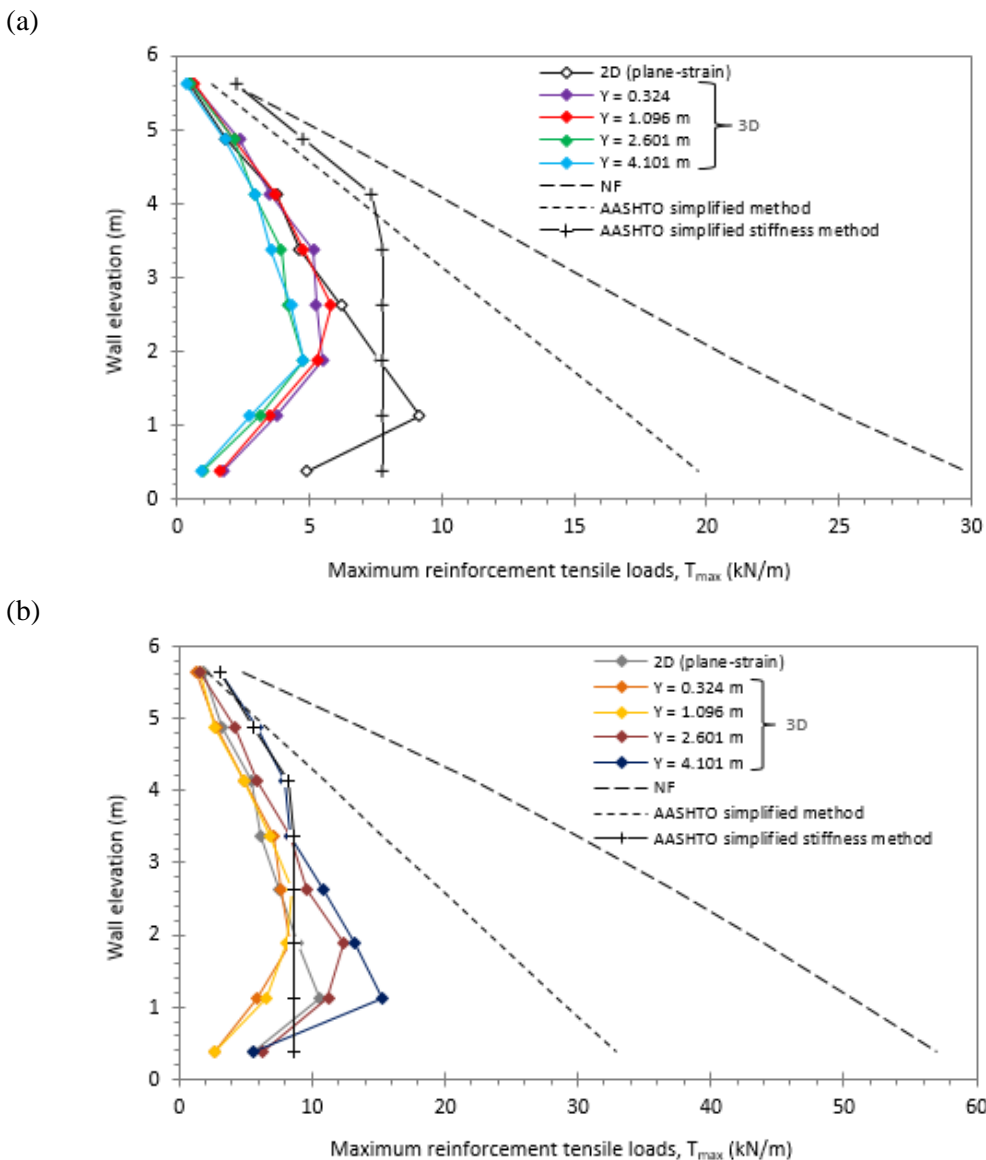


Figure 4.10. Maximum reinforcement loads at end of construction (a) and under bridge loading (b) by 2D and 3D analysis comparison with maximum tensile loads computed using AASHTO Simplified and Stiffness Method, and NF design codes.

4.3.5. Potential failure surface

The potential failure surfaces at failure at the end of construction of the back-to-back walls connected bridge abutment and under bridge load application by 2D and 3D-FE (i.e., Front-view) analysis are presented in Figure 4.11. There is a big different in the locations of critical failure surfaces between 2D & 3D simulation, where in 3D simulation shows that the critical failure surfaces in two opposing walls do not intercept each other, this assumption in the FHWA design guideline is apparently supported by the obtained 3D analysis results contrary to 2D analysis results.

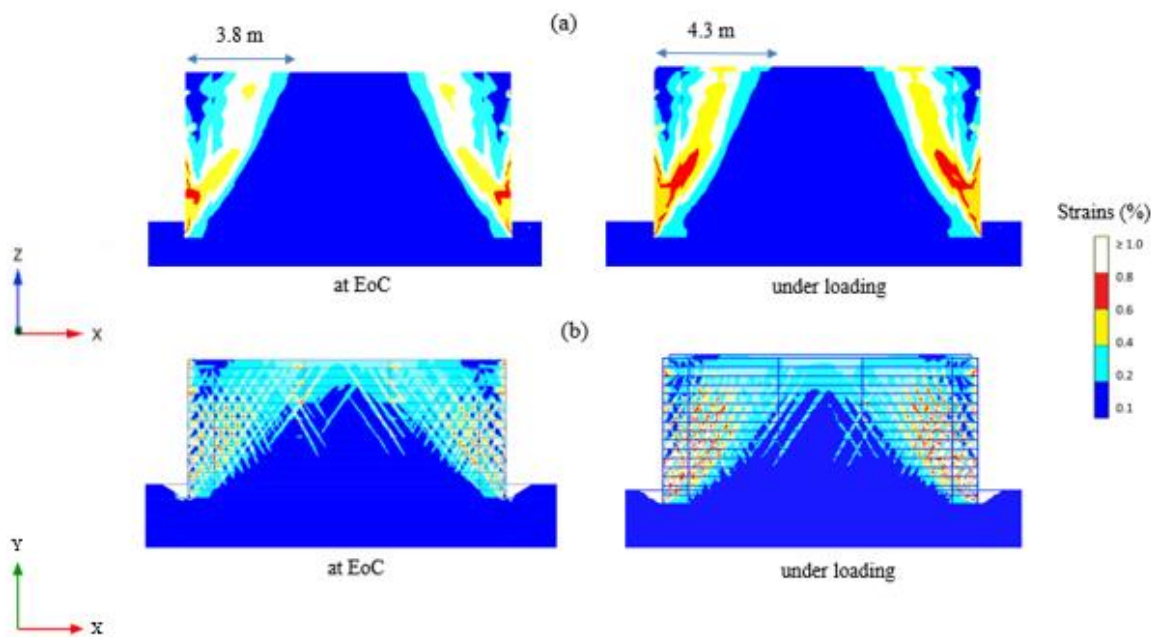


Figure 4.11. Potential failure surface at end of construction (EoC) and under bridge loading by 3D analysis (a) and 2D analysis (b).

Note: take front view for 3D models.

4.4. Conclusions

A 2D-FE and 3D-FE investigation to evaluate the performance of back-to-back reinforced soil walls connected abutment at EoC and under bridge load application. Based on the results of this study, the following conclusions can be drawn:

1. Rapprochement of the 3D lateral displacement to the 2D analysis in case away from the abutment walls at end of construction and under the bridge loading application.

2. A clear difference between the results of 3D & 2D simulation under bridge load application regarding the lateral earth pressure behind the reinforced zone an increase of 80% near the abutment wall and a decrease of 60% away from the abutment wall compared to the 2D simulation results.
3. Convergence of maximum 3D reinforcement loads for 2D analysis in the case of far away from abutment walls at the end of construction except the bottom layers and happens the opposite in case under the bridge loading.
4. The two NF, AASHTO Simplified Method are more conservative than the numerical results contrary to the stiffness method.
5. 3D shear strain zone is slightly propagate than the 2D simulation in the two cases at EoC and under bridge load application.

CONCLUSIONS

The research work presented in this thesis was developed within the laboratory Numerical Modelling and Soil-Structure Instrumentation (MN2I2S) of the University of Biskra and Department of Civil and Environmental Engineering (DCEE) of the Universitat Politècnica de Catalunya (UPC-BarcelonaTech). The objective is to analyse the behaviour of Back-to-Back Reinforced Soil Walls by 2D & 3D analysis using the PLAXIS geotechnical finite element software, with polymeric strips under the effect of static loadings.

This thesis consists two main part:

The first part is dedicated to the literature review on the design methods for reinforced soil walls and the studies on back-to-back reinforced soil walls, has highlighted the following points:

- The calculation method according to the French standard (NF P 094-270) is complicated and laborious, whereas the British standard (BS 8006) and LRFD Bridge Design Specifications (AASHTO) is quick and simple;
- Recognition a new method is called the simplified stiffness technique, which introduced in the new edition of AASHTO 2020, emphasizes the impact of reinforcement stiffness on reinforcing loads, rather than strength, as in the previous AASHTO 2014, but it is rather complicated.
- Only the American guidelines (i.e., FHWA) which proposes a method for dimensioning of back-to-back reinforced soil walls
- All umerical studies of this type of structure are recent (i.e., beganing of 2010 by Han and Leshchinsky) . The experimental studies are very limited on back-to-back walls.

The second part consists the analysis of the PLAXIS 2D simulation results of three effect on the behaviour of back-to-back walls (i.e., geometry, pre-tensioning & soil-reinforcement interaction), has allowed us to to conclude :

- When back-to-back reinforced soil walls are far away, they behave together at a certain distance of interaction and when they are near and overlapping, they interact.
- Back-to-back reinforced soil walls with single layers of reinforcements attached to both wall facings have a lower yielding structural situation, resulting in much larger reinforcement tensions than the other scenarios.
- The FHWA design guide underestimates the lateral earth pressure when back-to-back walls interact with each other.
- The Tmaximum for each approach shows that the AASHTO Simplified Method is the most conservative (i.e., safest for design), the FEM Method and AASHTO

Stiffness Method are comparable and the least conservative, and the NF P94-270 findings are roughly in the middle of the three.

- The process for installing polymeric strips based on the pre-tension load given to the strips during construction as well as the insertion of a continuous strip from one face to the opposite face can have a big impact on the quantitative behavior of these walls at the end of the construction (operational conditions). Small pre-tensioning loads, for example, may help maintain a goal vertical or near-vertical facing panel alignment.
- Polymeric strips with increased interface friction reduced facing displacements by up to 30% and reinforcement loads by a modest but noticeable amount when compared to smooth strips.

The analysis of the PLAXIS 3D simulation results of back-to-back walls connected to bridge abutment wall by confrontation with the 2D simulation results, has allowed us to conclude that there are two main factors to the variance of results between 2D & 3D simulation:

- The influence of the corner because 2D plane-strain analysis is incapable of highlighted it.
- The influence of the dead load (i.e., bridge seat & deck) , also because 2D plane-strain analysis is incapable of highlighted it.

Unfortunately, experimental data on real or full-scale structures are insufficient to have a thorough understanding of this type of structure, as well as numerical modeling, although in the last ten years there has been somewhat increased studies on back-to-back walls . However, it seems useful to ensure the continuity of this work under static and seismic loading.

REFERENCES

AASHTO, 2014. LRFD Bridge Design Specifications (7th edition). American Association of State Highway and Transportation Officials (AASHTO), Washington, DC, USA.

AASHTO, 2020. LRFD Bridge Design Specifications (9th edition). American Association of State Highway and Transportation Officials (AASHTO), Washington, DC, USA.

Abu-Farsakh, M.Y., Ardah, A., Voyiadjis, G. Z., 2019. Numerical parametric study to evaluate the performance of a Geosynthetic Reinforced Soil–Integrated Bridge System (GRS-IBS) under service loading. *Transportation Geotechnics* 20.

Allen, T.M. and Bathurst, R.J., 2015. Improved simplified method for prediction of loads in reinforced soil walls. *ASCE Journal of Geotechnical and Geoenvironmental Engineering* 141(11): 04015049

Allen, T.M. and Bathurst, R.J., 2018. Application of the Simplified Stiffness Method to Design of Reinforced Soil Walls. *ASCE Journal of Geotechnical and Geoenvironmental Engineering* 144 (5): 04018024

ASTM D2487, 2011. Standard Practice for Classification of Soils for Engineering Purposes (Unified Soil Classification System). American Society for Testing Materials (ASTM International), West Conshohocken, PA, USA.

Anderson, P.L., Gladstone, R.A., Brabant, K. and Sankey, J., 2018. Back-to-Back MSE Walls–A Comprehensive Understanding. In *Innovations in Geotechnical Engineering* pp 431-447

Benmebarek, S., Attalaoui, S., Benmebarek, N., 2016. Interaction analysis of back-to-back mechanically stabilized earth walls. *Journal Rock Mechanics and Geotechnics Engineering* 8(5):697–702

Benmebarek, S., Djabri M., 2018. FEM to investigate the effect of overlapping reinforcement on the performance of back-to-back embankment bridge approaches under self-weight. *Transportation Geotechnics* 11:17-26

Benmebarek, S.; Djabri, M., 2018. FE Analysis of Back-to-Back Mechanically Stabilized Earth Walls Under Cyclic Harmonic Loading. *Indian Geotechnical Journal* 48: p498–509.

Berg, R.R., Christopher, B.R., and Samtani, N.C., 2009. Design and construction of mechanically stabilized earth walls and reinforced soil slopes, Volume I (FHWA NHI-10-024) and Volume II (FHWA NHI-10-025), National Highway Institute, Federal Highway Administration. U.S. Department of Transportation, Washington, DC, USA.

Chapter based on Brouthen, A., Houhou, M.N., Damians, I.P., 2022. Numerical Study of the Influence of the Interaction Distance, the Polymeric Strips Pre-Tensioning, and the Soil–Polymeric Interaction on the Performance of Back-to-Back Reinforced Soil Walls. *Infrastructures* 7(2).

Brouthen, A., Damians, I.P., Bathurst, R.J., Houhou, M.N., 2022. FE analysis of the effect of soil-reinforcement interaction and reinforcement pre-tensioning on the behaviour of back-to-back polymeric strip reinforced soil walls. *Proceedings of the 7th European Geosynthetics Conference (EuroGeo7)*, Warsaw, Poland.

BSI, 2010. *Code of Practice for Strengthened/Reinforced Soil and Other Fills*, British Standards Institution (BSI), Milton Keynes, UK.

Capilleri, P.P.; Ferraiolo, F.; Motta, E.; Scotto, M.; Todaro, M., 2019. Static and dynamic analysis of two mechanically stabilized earth walls. *Geosynthetics International* 26:26–41.

Coulomb C.A., 1776. *Essai sur une application des règles des maximis et minimis à quelques problèmes de statique relatifs à l'architecture*. *Mémoires de l'Académie Royale des Sciences présentés par des savants*, vol. 7, pp 343-382

Damians, I.P., Bathurst, R.J., Josa, A., Lloret, A., and Albuquerque, P.J.R., 2013a. Vertical facing loads in steel reinforced soil walls. *ASCE Journal of Geotechnical and Geoenvironmental Engineering*, 139(9): 1419-1432.

Damians, I.P., Lloret, A., Josa, A., and Bathurst, R.J., 2013b. Influence of facing vertical stiffness on reinforced soil wall design, *Proceedings of the 18th International Conference on Soil Mechanics and Geotechnical Engineering*, Paris, France, 4p.

Damians, I.P., Bathurst, R.J., Josa, A., and Lloret, A., 2014. Numerical study of the influence of foundation compressibility and reinforcement stiffness on the behavior of reinforced soil walls. *International Journal of Geotechnical Engineering* 8(3): 247-259.

Damians, I.P., Bathurst, R.J., Lima, J.; Lloret, A., Josa, A., 2015a. Numerical study of the use of actively-tensioned polymeric strips for reinforced soil walls. In *Proceedings of the XVI European Conference on Soil Mechanics and Geotechnical Engineering, Geotechnical Engineering for Infrastructure and Development*, Edinburgh, UK, 13–17 September 2015; pp. 3834–3838.

Damians, I.P., Bathurst, R.J., Josa, A., and Lloret, A., 2015b. Numerical analysis of an instrumented steel-reinforced soil wall. *ASCE International Journal of Geomechanics* 15(1):04014037.

Damians, I.P., Bathurst, R.J., Josa, A. and Lloret, A.; 2016. Vertical facing panel-joint gap analysis for steel-reinforced soil walls. *ASCE International Journal of Geomechanics* 16, 04015103.

- Damians, I.P., 2016. Mechanical performance and sustainability assessment of reinforced soil walls. PhD thesis, UPC BarcelonaTech 383 p.
- Damians, I.P.; Bathurst, R.J.; Adroguer, E.; Josa, A.; Lloret, A., 2018. Sustainability assessment of earth retaining wall structures. *ICE Environmental Geotechnics* 5:187–203.
- Djabri, M., Benmebarek, S., 2016. FEM Analysis of Back-to-Back Geosynthetic-Reinforced Soil Retaining Walls. *International Journal of Geosynthetics and Ground Engineering* 2 (26).
- Dram, A., Balunaini, U., Benmebarek, S., Mouli, S., 2021. Earthquake response of connected and unconnected back-to-back geosynthetic reinforced soil walls. *ASCE International Journal of Geomechanics* 21, 04021223.
- Elias, V., Christopher, B.R., Berg, R.R., 2001. Mechanically Stabilized Earth Walls and Reinforced Soil Slopes Design and Construction Guidelines Publication No. FHWA-NHI-00-043.
- El-Sherbiny, R., Ibrahim, E., Salem, A., 2013. Stability of back-to-back mechanically stabilized earth walls. In *Geo-Congress Stability and Performance of Slopes and Embankments III*; American Society of Civil Engineers (ASCE): Reston, VA, USA, 2013; pp. 555–565.
- EN 14475, 2006. Execution of Special Geotechnical Works—Reinforced Fill; European Committee for Standardization (CEN): Brussels, Belgium.
- GECO Industrial Co. Ltd. Available online: <http://gecoind.com/en/product/fasten.php>
- Han, J., Leshchinsky, D., 2010. Analysis of back-to-back mechanically stabilized earth. *Geotextile Geomembrane* 28: 262–267.
- Hausmann, M., & Lee, I. K., 1976. Strength characteristics of a reinforced soil. In *Proceedings, International Symposium on New Horizons in Construction Materials*, Lehigh.
- Huang, B., Bathurst, R.J., Hatami, K., Allen, T.M., 2010. Influence of toe restraint on reinforced soil segmental walls. *Canadian Geotechnical Journal* 47: 885–904.
- Hung, C., Liu, C.H., Liu, H., 2021. Three-dimensional finite element analysis of geosynthetic-reinforced soil walls with turning corners. *Geotextiles and Geomembranes* 49(3): 629-645.
- Jacquelin, M., 2006. Conception et calcul des murs de soutènement en terre armée, Ed .Institut supérieur du bâtiment et des travaux publics.
- Jayakrishnan, P.V., 2013. Report on Full Scale Instrumented MacRes Wall at Jundiai-Brazil; Officine Maccaferri S.p.A.: Bologna, Italy.
- Kramer, S.L., 1996. Geotechnical earthquake engineering, Prentice-Hall, New Jersey, pp 466- 505.

- McKittrick, D.P., 1978. Reinforced Earth: Application of Theory and Research to Practice, keynote paper, Symposium on Soil Reinforcing and Stabilizing Techniques, Sydney, Australia.
- Ministry of Transport, 1979. Reinforced Earth Structures, Recommendations and Rules of the Art, Direction of Roads and Road Transport, (English Translation) Paris, France 1-194.
- Miyata, Y., Bathurst, R.J., Allen, T.M., 2018. Evaluation of tensile load model accuracy for PET strap MSE walls. *Geosynthetics International* 25:656–671.
- NF P 94-270, 2009. Calcul Géotechnique: Ouvrages de Soutènement. Remblais Renforcés et Massifs en Soil Cloué; Norme française, Association Française de Normalisation (AFNOR): La Plaine Saint-Denis, France.
- PLAXIS, 2008. PLAXIS 2D Reference Manual Version 9, PLAXIS; Delft University of Technology: Delft, The Netherlands.
- PLAXIS, 2017. PLAXIS 3D Reference Manual Version 2017, PLAXIS; Delft University of Technology: Delft, Netherlands.
- Rajagopal, G., Thiyyakkandi, S., 2020. Numerical evaluation of the performance of back-to-back MSE walls with hybrid select-marginal fill zones. *Transportation and Geotechnics* 26.
- Rankine, W., 1857. On the stability of loose earth. *Philosophical Transactions of the Royal Society of London*, vol. 147.
- Runser, D.J., Fox, P.J., Bourdeau, P.L., 2001. Field performance of a 17 m-high reinforced soil retaining wall. *Geosynthetics International* 8:367–391.
- Samee, A.A., Yazdandoust, M., Ghalandarzadesh, A., 2021a. Performance of back-to-back MSE walls reinforced with steel strips under seismic conditions. *Transportation Geotechnics* 30.
- Samee, A.A., Yazdandoust, M., Ghalandarzadesh, A., 2021b. Effect of reinforcement arrangement on dynamic behaviour of back-to-back mechanically stabilised earth walls. *International Journal of Physical Modelling in Geotechnics* 21.
- Sarvanam, S. M., Balunaini, U., Madhira, R. M., 2016. Reinforcement tensile forces in back-to-back retaining walls. Indian Geotechnical Conference IGC2016 15-17, December 2016, IIT Madras, Chennai, India.
- Saravanam, S. M., Balunaini, U., Madhira, R. M., 2019. Behavior and Design of Back to Back Walls Considering Compaction and Surcharge Loads. *International Journal of Geosynthetics and Ground Engineering* 5 (31).

- Sraavanam, S. M., Balunaini, U., Madhira, R. M., 2020a. Behavior of Connected and Unconnected Back-to-Back Walls for Bridge Approaches. *International Journal of Geomechanics* 20 (7).
- Saravanam, S. M., Balunaini, U., Madhira, R. M., 2020b. Analysis of single and back-to-back MSE walls with full-length panel facia. *Geotechnical and Geological Engineering* 38:6281-6293.
- Schlosser, F., & Long, N.T., 1969. Comportement de la Terre Armee a liAppareil Triaxial", Activity Report, Laboratoire Central des Ponts et Chaussees.
- SETRA-LCPC., 1979. Les ouvrages en terre armée : recommandations et règles de l'art. Laboratoire Central des Ponts et Chaussées, Guides techniques.
- Soletanche Freyssinet © .Availibale online: www.soletanchefreyssinet.com
- Vidal, H., 1966. La Terre Armée, un Matériau Nouveau Pour les Travaux Publics. *Annales de l'I.T.B.T.P.*, Paris, France, 223/224: 887-936.
- VSL Construction Systems—VSoL® Retained Earth System. Available online: www.vsl.com
- Won, M.S., Kim, Y.S., 2007. Internal deformation behavior of geosynthetic-reinforced soil walls. *Geotextiles and Geomembranes* 25:10–22.
- Yang, G., Zhao, Y., Wang, H., Wang, Z., Liu, W., 2020a. Study on the Mutual Influence of Back-to-back Geogrid Reinforced Soil Wall by Finite Element Method. *Dynamic Systems and Applications* 29 (7).
- Yang, G., Zhao, Y., Wang, H., Wang, Z., Liu, W., 2020b. Performance of a Back-to-back Geogrid Reinforced Soil Retaining Walls for Passenger-dedicated Railway during Service: Case study. *Solid State Technology* 63(1).
- Yazdandoust, M.; Samee, A.A.; Ghalandarzadesh, A., 2022. Assessment of seismic behavior of back-to-back mechanically stabilized earth walls using 1g shaking table tests. *Soil Dynamics and Earthquake Engineering* 155.
- Yu, Y., Bathurst, R.J., Miyata, Y., 2015. Numerical analysis of a mechanically stabilized earth wall reinforced with steel strips. *Soils and Foundations* 55:536–547.
- Xu, P., Yang, G., Li, T., Hatami, K., 2021. Finite element limit analysis of bearing capacity of footing on back-to-back reinforced soil retaining walls. *Transportation Geotechnics* 30.
- Zheng, Y., Guo, W., Fox, P.J. and McCartney, J.S., 2022. 2D and 3D simulations of static response of a geosynthetic reinforced soil bridge abutment. *Gesosynthetics International* 29.